FINAL REPORT

Development of Methodologies for Evaluating Emissions from Metal-Containing Explosives and Propellants

SERDP Project WP-2611

February 2018

Kevin L. McNesby, Ph.D.
US ARMY RESEARCH LABORATOR
Brian K. Gullett, Ph.D.
US ENVIRONMENTAL PROTECTION AGENCY

SERDP SEED PROJECT (WP-2611) – FINAL REPORT

Development of Methodologies for Evaluating Emissions from Metal-Containing Explosives and Propellants

February 2018

Authors:

US Army Research Laboratory: Kevin McNesby*, Mike Nusca, Mike McQuaid, Chiung-Chu Chen, Richard Benjamin, Ronnie Thompson, Will Sickels, Gene Summers, Ray Sparks

US Environmental Protection Agency, Office of Research and Development: Brian Gullett*, Amara Holder

University of Dayton Research Institute: Johanna Aurell

***Co-Principal Investigator**

REPORT DOCUMENTATION PAGE

Form Approved
OMB No. 0704-0188

1. REPORT DATE *(DD-MM-YYYY)*	2. REPORT TYPE	3. DATES COVERED *(From - To)*
11-15-2017	SERDP Final Report	DEC 2015 – Dec 2016

4. TITLE AND SUBTITLE

Development of Methodologies Evaluating Emissions from Metal-Containing Explosives and Propellants

5a. CONTRACT NUMBER

5b. GRANT NUMBER

5c. PROGRAM ELEMENT NUMBER

6. AUTHOR(S)

US Army Research Laboratory: Kevin McNesby, Mike Nusca, Mike McQuaid, Chiung-Chu Chen, Richard Benjamin, Ronnie Thompson, Will Sickels, Gene Summers, Ray Sparks

US Environmental Protection Agency, Office of Research and Development: Brian Gullett, Amara Holder

University of Dayton Research Institute: Johanna Aurell

5d. PROJECT NUMBER WP-2611

5e. TASK NUMBER

5f. WORK UNIT NUMBER

7. PERFORMING ORGANIZATION NAME(S) AND ADDRESS(ES)

US Army Research Laboratory
RDRL-WML-C
Aberdeen Proving Ground, MD 21005-5066

8. PERFORMING ORGANIZATION REPORT NUMBER
WP-2611

9. SPONSORING / MONITORING AGENCY NAME(S) AND ADDRESS(ES)

SERDP & ESTCP Program Offices
901 North Stuart Street, Suite 303
Arlington, VA 22203-1853

10. SPONSOR/MONITOR'S ACRONYM(S)
SERDP

11. SPONSOR/MONITOR'S REPORT NUMBER(S) WP-2611

12. DISTRIBUTION / AVAILABILITY STATEMENT

Approved for Public Release; Distribution is Unlimited

13. SUPPLEMENTARY NOTES

14. ABSTRACT

Experiments were performed to develop methodologies that will allow determination of pollutant emission factors for gases and particles produced by exploding metal-containing energetic materials. Materials studied included M855 ammunition (nitrocellulose ($(C_6H_7(NO_2)_3O_5)_n$) /nitroglycerin ($C_3H_5N_3O_9$) propellant, Cu-jacketed lead projectile) fired using an M4 carbine shoulder-fired weapon; medium-sized (660 grams) charges of neat TNT (trinitrotoluene, $C_7H_5N_3O_6$); and medium-sized (660 grams total weight) charges of TNT (80% by weight)/Mg (magnesium powder, 325 mesh, 4% by weight)/B (boron powder, 0.8 micrometer, 16% by weight). Although not included here, the analysis methods described will be directly applicable to the study of pyrotechnics.

15. SUBJECT TERMS
Explosives, Propellants, Metal-containing, Pollutant Emissions, Emission Factors, Modifed Combustion Efficiency, TNT, M855

16. SECURITY CLASSIFICATION OF:			17. LIMITATION OF ABSTRACT	18. NUMBER OF PAGES	19a. NAME OF RESPONSIBLE PERSON
a. REPORT	b. ABSTRACT	c. THIS PAGE			Kevin L. McNesby
Unclassified	Unclassified	Unclassified	Unclassified Unlimited	131	19b. TELEPHONE NUMBER *(include area code)* 410-306-1383

Table of Contents

List of Tables

List of Figures

List of Acronyms

ANOVA	Single factor one-way analysis of variance
APG	Aberdeen Proving Ground
ARL	Army Research Laboratory
B	Boron
C_2	flame radical
CBP	combustion by-product
CE	Combustion Efficiency
CFD	Computational Flow Dynamics
CH	flame radical
CHEETAH	Computational program to predict explosive and propellant performance
CHEMKIN	Computational program to predict combustion parameters
C-J point	Chapman-Jouguet point
CO	Carbon Monoxide
CO_2	Carbon Dioxide
Comp-b	Explosive formulation Composition B, 60% RDX, 40% TNT
EBW	Exploding Bridgewire
ED-XRF	Energy Dispersive X-ray Fluorescence
ELPI	Electrical Low Pressure Impactor
EPA	US Environmental Protection Agency
F_C	Carbon Fraction
FID	Flame Ionization Detector
Fps	frames per second
GC	Gas Chromatography
GC/LRMS	Gas Chromatography / Low Resolution Mass Spectrometry
GC-MS	Gas Chromatography / Mass Spectrometry
GPa	Giga Pascal
GRI	Gas Research Institute
HCN	Hydrogen Cyanide
IB	Interior Ballistics
IC	Internal Combustion
LI-COR	Equipment Manufacturer
LLNL	Lawrence Livermore National Laboratory
M4	Shoulder fired rifle (carbine)
M855	The type of round fired by the M4 carbine
MCE	Modified Combustion Efficiency
Mg	Magnesium
ms	millisecond
NASA	National Aeronautics and Space Administration
NC	nitrocellulose
ND	Not Detected
NDIR	Non-Dispersive Infra-red
NEW	Net Explosive Weight
NG	nitroglycerin
NMOC	Non-methane organic carbon

NO	Nitric Oxide
OD	Open Detonation
OD	Outer Diameter
PAH	Poly-aromatic Hydrocarbons
PC	Particulate Carbon
PETN	explosive Pentaerythritol tetranitrate
PM	Particulate Matter
PM_{10}	Particulate matter with an average diameter less than 10 micrometers
$PM_{2.5}$	Particulate matter with an average diameter less than 2.5 micrometers
PMMA	polymethyl methacrylate (“plexiglas”)
Psia	pounds per square inch above ambient
PUF	polyurethane foam
RH	Relative Humidity
RPD	Residual percent deviation
RSD	Residual standard deviation
SIM	Selective ion monitoring
SMP 842	gun propellant formulation manufactured by St. Mark’s Powder
SNL	Sandia National Laboratories
SUMMA	genericized trademark that refers to electropolished, passivated stainless steel vacuum sampling canisters
TEF	Toxic Equivalent Factor
TNT	explosive Trinitrotoluene
XAD	highly absorbent resins used to sample organic materials

Acknowledgements

The authors would like to thank the following:

US Army Research Laboratory**:** Dr. John Schmidt, Dr. Rose Pesce-Rodriguez, Dr. Joe South

Abstract

Objective: This work is intended to address a FY16 SERDP SEED call for "Methods for Characterizing Near-Field Emissions From Metal-Based Energetics and Pyrotechnics WPSEED-16-01". We had originally intended to develop methods to predict and quantify emissions of gases and particles produced by functioning (i.e., exploding) metal-containing solid explosives, gun propellants, and pyrotechnics. Early on in our work, it became apparent that the inclusion of pyrotechnics would carry us beyond our 1-year performance schedule, so the work was focused on metal-containing explosives and gun propellants. We believe the approach described in what follows is directly applicable to pyrotechnics.

Technical Approach: Materials studied included **M855 ammunition** (nitrocellulose ($(C_6H_7(NO_2)_3O_5)_n$) /nitroglycerin ($C_3H_5N_3O_9$) propellant, Cu-jacketed lead projectile) fired using an M4 weapon; medium-sized (660 grams) charges of **neat TNT** (trinitrotoluene, $C_7H_5N_3O_6$); and medium-sized (660 grams) charges of **TNT:Mg:B** [by weight 80% TNT : 4% magnesium powder, 325 mesh : 16% boron powder, 0.8 micrometer]. Gun firings and explosions were conducted at the US Army Research Laboratory (**ARL**) at Aberdeen Proving Ground, MD. Emissions of gases and particles were measured using a mobile lab operated by the US Environmental Protection Agency (**EPA**), with chemical analysis by the EPA and the University of Dayton Research Center (**UDRI**). Predictions of emissions were performed at the ARL, and were based on the observed stages of energy release for each event.

Results: For the gun firings metal species produced by the event were found in particles. Carbon species produced by the event were found in gases and particles. The metal detected in highest concentration following the M4 carbine firing is copper (in the range of 50 grams per kilogram of propellant) which originates from the bullet casing rather than the propellant. Lead is detected for all

tests, at approximately 1/3 the level of Cu. The source of the lead is believed to be the No. 41 primer used to initiate the propellant. The measured "modified combustion efficiency" (MCE), an indicator of the extent of carbon oxidation, is between 0.44 and 0.5 for all ammunition tested, indicating that the total initial carbon is under-oxidized (a MCE of 1 is full oxidation). This results in higher than expected concentrations of emitted CO gas. This is in contrast to simulations, which predict approximately 25% higher level of carbon oxidation. As with the gun firings, metals in the explosive formulations are found after testing in the emitted particles, and carbon is found in the emitted gases and particles. Metals detected in highest concentration following detonation/explosion of "neat" (i.e., pure) TNT are iron (Fe) and aluminum (Al), likely from fixtures in the test environment and the blast chamber walls. For detonation/explosion of the TNT:Mg:B formulation, B and Mg are the metals detected at highest concentration after explosion, with measured particle masses approaching 300 grams per kilogram of explosive formulation. The experimental MCE for all detonations/explosions of "neat" and metallized TNT is near 0.98, indicating most of the carbon measured following explosion is fully oxidized. Simulations of the MCE for each material are within 25% of experiment.

Benefits: Overall, we believe the main area for improvement in the gun emissions work is in the area of simulation of soot and particle production during interior ballistics, and in simulation of particle combustion during exterior ballistics. Of particular concern is the high level of CO gas measured following firing of the M4 carbine. For simulation and measurement of exploding metal-containing energetics, the main area for improvement is in prediction of particle combustion during the second stage of energy release, and eventual incorporation of heterogeneous reaction chemistry into fluid dynamic modeling. We believe a follow-on effort should incorporate refinements in these areas, as well as others improvements detailed in the conclusions and recommendations section of the full report.

Executive Summary

Objective

This document is the final report of a 1-year effort to demonstrate prediction and measurement of emissions from explosions and combustion events produced by metal-based energetic formulations, based upon observed stages of energy release. The work described here compares simulation to experiment for a series of gun firings (M4 carbine shoulder-fired weapon) and explosions (detonation of metal-containing TNT formulations). The simulations predict solid and gaseous chemical species produced by explosive events. The experimental work measured gases and particles emitted during testing of these materials, and imaged each event. The original Call for Proposals included a request for analysis of pyrotechnics in addition to explosives. Although not included here, the analysis methods described will be directly applicable to the study of pyrotechnics.

Facilities

The simulation and experimental work summarized in this report was conducted at the US Army Research Laboratory (ARL) Detonation Science Facility located at the Aberdeen Proving Ground, MD. Testing at this site occurred in a medium-scale (up to 25 kilograms net explosive weight - NEW) indoor blast facility, employing particle and chemical species diagnostic equipment developed by the EPA Office of Research and Development. This equipment was designed by the EPA to allow for field use (to include aerostat and drone deployment [Aurell, 2011]), in a setting that attempted to bridge the gap between laboratory and field-scale. Each explosive event measured using EPA instrumentation was imaged using ARL high speed cameras and spectrographs. An overall goal of this work was to develop a predictive methodology for toxic chemical species produced during explosions

of metal-containing energetic materials, using simulation tools available to most explosives researchers [LLNL, 2010], building upon previous efforts such as POLU13 (Navy), MERLIN (Army), PCAD (El Dorado, Inc.), and ADORA (Blaze Tech, Inc.) [O'Brien, 2003].

EPA and ARL Instrumentation

Products of energy release for each material tested were measured using a suite of fielded analytical chemical instrumentation developed by the US EPA Office of Research and Development for measuring particles and chemical species during testing of munitions [Aurell, 2011]. The instruments employed included extractive particle analyzers (2 micrometers (μm) to 100 μm), and extractive mass spectral detection of permanent chemical species to 450 atomic mass units (amu). Metal and soot particles were collected as residues on filters and analyzed using x-ray fluorescence (XRF) techniques. Permanent gases and volatile organic compounds were analyzed continuously and via canister grab samples [AMCCOM, 1992]. All explosive events were recorded using the ARL Detonation Science Facility suite of high speed imaging instrumentation. Gun firings were imaged using an Edgerton shadowgraphy system. Explosive events were imaged using a high-speed, high-definition framing camera with and without external illumination. Outdoor tests for air-shock velocity measurements were imaged using a laser-synchronized low-parallax high brightness imaging rig. The imaging instrumentation has been summarized elsewhere [McNesby, 2016].

Qualitative Approach

Observed stages of energy release for each energetic material tested were similar. In each test, a solid material (explosive or propellant) is rapidly (anaerobically) converted to an under-oxidized dense gas/particle cloud. This first stage (burning of the propellant in the gun barrel or detonation of the solid

explosive) is responsible for most of the observed energy release. The second stage of energy release in each test involves air oxidation of the under-oxidized products of the first stage [McNesby, 2010]. For gun firings employing propellants this second stage is mostly associated with muzzle flash, while for detonations of energetics the second stage is responsible for the explosive fireball. These stages of energy release were verified for all materials tested, prior to chemical emissions measurement, using high speed digital imaging and synchronized laser illumination, and are reported here.

The analytical approach used here is that the final chemical emissions from the energy release of all materials tested are dependent upon sequential processes. The simulation effort mimicked each observed stage of energy release using equilibrium thermodynamic and chemical kinetic tools developed specifically for explosive and combustion events. For predicting chemical species emission during the first stage of energy release, the NASA-Lewis (or NASA-Glenn) equilibrium thermochemical simulation computer code was used for gun firings [Gordan, 1994]; the equilibrium thermochemical simulation computer code CHEETAH was employed for detonations [LLNL, 2010]. For the second stage of energy release, flow dynamics coupled to NASA-Lewis equilibrium calculations [Nusca, 2011] or finite rate chemical kinetic calculations (CHEMKIN combustion simulator, Reaction Design, Inc.) were used to predict final emissions for gun firings. For solid explosives, the CHEMKIN combustion simulator was used to predict species present in the fireball following detonation [[Kotlar, 1992], [LLNL, 2010], [McNesby, 2010]].

Gun Firing Results

In general, for the gun firings, metal species produced by the event were found in particles. Carbon species produced by the event were found in gases and particles. The metal detected in highest

concentration following the M4 carbine firing is copper (in the range of 50 grams per kilogram of propellant), which originates from the bullet casing rather than the propellant. Lead is detected for all tests, at approximately 1/3 the level of Cu. The source of the lead is believed to be in the propellant ignition train – it is present in the No. 41 primer used to initiate the propellant, and in the bullet core (cased in a copper jacket). The sensitivity of the EPA detection methods is illustrated by the measurement of potassium (K) in the "salted" rounds, at about ½ the detected level of copper (K is added as a combustion-radical scavenger to suppress muzzle flash [Glassman, 1987]), and not in the "unsalted" rounds. The measured particles were distributed approximately evenly between $PM_{2.5}$ and PM_{10} (emitted total particles approximately 57 grams per kilogram "salted" propellant, approximately 32 grams per kilogram "unsalted" propellant) , at levels similar to previous studies [Wingfors, 2014]. Unsalted (no potassium (K) flash suppressant) and legacy (Viet Nam-era) M855 rounds exhibited similar particle emissions, while the salted rounds exhibited higher particle concentrations, likely caused by suppression of second-stage combustion by the added K.

For all gun firings, carbon present in the double base propellant (nitrocellulose (83% by weight)/nitroglycerin (13% by weight)) is distributed between particles and gaseous CO and CO_2. However, the measured "modified combustion efficiency", an indicator of the extent of carbon oxidation, (MCE, [Sinha, 2003]) is near 0.44 (legacy) and 0.5 (salted and unsalted), indicating that at the EPA sensor position, the total initial carbon is under-oxidized. Total measured gaseous carbon emitted for all gun firings was around 500 grams per kilogram of propellant (see Section 13 for details) with CO_2 measured concentrations slightly higher than CO. HCN gas was not tested here, although it is expected to be present for firings of all rounds tested here at an emission factor near 1 milligram per gram of propellant consumed [Kirchner, 1993].

This is in slight contrast to the gun simulations, which predict gun-emitted gaseous carbon to be present at the sensor position mostly as CO_2 and as CH_4. Two simulations were performed. The main effort used a modified NASA-Lewis thermochemical code coupled to computational flow dynamics (CFD) to estimate gases at the muzzle exit and at the EPA sensor position (approximately 15 centimeters from the muzzle of the M4 carbine) [Nusca, 2011]. This simulation predicted most gaseous carbon at the sensor position present as CO_2, with about one third as much CH_4, and trace amounts of CO, yielding a predicted MCE near 0.73. This modified NASA-Lewis simulation was used because it allows for varying levels of soot production during the interior ballistic cycle, and accurately depicts the time-delay as muzzle gases diffuse to the EPA sensors. A second effort, described briefly in Appendix 2, used a combination of CHEETAH gun calculations coupled to the chemical kinetic simulation computer code CHEMKIN [LLNL, 2010]. This simulation predicted full carbon oxidation and a MCE of 0.997. Both methods of simulation over-predict carbon oxidation, relative to measurement, with the NASA-Lewis/CFD giving results much closer to measurement. This discrepancy is discussed in detail in this report.

Overall, we believe the main area for improvement in the gun effort is in the area of simulation of soot and particle production during interior ballistics, and in simulation of particle combustion during exterior ballistics. Additionally, it is worth emphasizing that simulations do not account for metal particle combustion during the second phase of energy release.

Detonations of Solid Explosives Results

For studies of chemical emissions following detonation of solid chemical explosives, TNT was selected as the base explosive, because it is extremely well-characterized, it's stages of energy release form the basis for the approach used in this study, and because particles of graphitic carbon are predicted as a major species (mole fraction) following detonation (luminescence from condensed C is responsible for the yellow color of the TNT fireball) [McNesby, 2016]. The Mg/B additive was selected because it is a metal additive designed to overcome thermodynamic limitations on realizing full-combustion enthalpy for boron on detonation time-scales [Kuo. 2012]. The TNT/Mg/B ("hot mill alloy", 80:4:16 by weight, stoichiometry approximately MgB_2) formulation therefore allows study of pollutant emission by explosions that produce carbonaceous particles, study of metal additives known to combust when formulated in explosives (Mg), and study of metal additives (B) for which full explosive performance has yet to be realized. The loading level (20% metal by weight) was selected because it is similar to the loading level of the aluminum-containing fielded explosive formulation Tritonal (80% TNT, 20% Al powder) [Meyer, 2007].

As with the gun firings, metals in the explosive formulations are found after testing in the emitted particles, and carbon is found in the emitted gases and particles. Metals detected in highest concentration following detonation/explosion of "neat" (i.e., pure) TNT within the blast chamber are iron (Fe) and aluminum (Al), at less than 20 grams per kilogram of explosive formulation, likely from fixtures in the test environment and the blast chamber walls. B and Mg are detected at trace levels (as are all other tested metals) following detonation of "neat" TNT. The experimental modified combustion efficiency (MCE) for all detonations/explosions of "neat" TNT is near 0.98, indicating most of the carbon measured following explosion is fully oxidized. For detonation/explosion of the

TNT/Mg/B formulation, B and Mg are the metals detected at highest concentration after explosion, with measured particle masses approaching 300 grams per kilogram of explosive formulation. The full elemental analysis of the B- and Mg-containing particles was not available at time of this writing. The measured MCE for the TNT/Mg/B formulations was near 0.98, indicating initial carbon was fully oxidized.

It is expected that during explosion, anaerobic (first stage energy release) reaction of metals in metal-containing explosive formulations will decrease available oxygen, increasing the level of carbonaceous soot/particles [McNesby, 2010]. This is seen in experiment, and in simulation. For the detonation/explosion simulations, the CHEETAH simulation of the first stage of energy release allows the choice of the boron additive to be inert (inactive) or reactive (active). Mg is always active. In the CHEMKIN simulation of the second stage of energy release (afterburn or fireball), particle combustion is ignored, and the simulation approximates the afterburn as occurring in a homogeneous (single phase, well-mixed) reactor. For all simulations, the calculated MCE (0.86 for neat TNT, approaching 0.76 for metallized formulations) was in reasonable agreement (within 15% to 25%) with experiment.

It is worth noting that for detonations within the ARL blast chamber, shock reflections from the interior walls stir the detonation product gases, promoting afterburn. Additionally, because the CHEETAH simulation predicts condensed products for the first stage energy release, the calculated emission factors (CHEETAH + CHEMKIN) neglect particle combustion, yielding values less than measured by experiment.

Summary

Overall, we believe the main area for improvement in the gun effort is in the area of simulation of soot and particle production during interior ballistics, and in simulation of particle combustion during exterior ballistics. Of particular concern is the high level of CO gas measured following firing of the M4 carbine. For measurements and simulation of metal-containing explosives, the main area for improvement is in prediction of particle combustion during the second stage of energy release, and eventual incorporation of heterogeneous reaction chemistry into fluid dynamic modeling. The methodology of using computer simulation to predict emissions of sequential stages of energy release is well known and provides the ability to estimate emissions over a wide range of gun firing and detonative conditions, from firing within an enclosed position, to open air firing, to detonation within closed volumes, to open detonations (OD). Other shortcomings of this work are mostly on the simulation side, and include the lack of predictive ability for most PAH's, and the general need for reduced chemical kinetic mechanisms that are amenable to insertion into computational flow dynamics.

Small-Caliber Gun Propulsion

1. Background- Prediction of Product Species for Small-caliber Gun Firings.

A gun is similar in essence to a piston-type internal combustion (IC) engine. The gun function is similar to the power stroke of a 4-cycle engine, with the expansion of hot gases driving a projectile instead of a piston. When the propelling charge (made up of propellant "grains") behind the projectile (bullet) is ignited, gases are evolved from the surface of the burning propellant grains, and the pressure in the temporarily sealed chamber (breach – sealed gun barrel) increases rapidly. Resistance to initial motion of the projectile is high, and relatively high chamber pressures are attained before motion of the projectile occurs. The chemistry and physics within the sealed chamber volume, prior to bullet "uncorking", are considered part of the topic of gun interior ballistics. As the projectile begins to move within the gun barrel, the chamber volume is increased, and the rate of burning of the solid propelling charge increases. The net effect is a rapid increase in the pressure within the chamber until the point of maximum pressure is reached. This usually occurs at a relatively short distance from the origin of barrel rifling. Beyond that point, the pressure drops and prior to bullet exit reaches a value from 10% to 30% of maximum, depending upon the weapon design and propellant type. This pressure at muzzle exit continues to act on the projectile for a short distance beyond the muzzle, accelerating the projectile beyond the muzzle [Jones, 1965].

As the projectile exits the gun barrel, hot, dense, fuel rich propellant gases and particles (usually soot) push into surrounding air, creating an air shock wave. These propellant product gases are typically fuel rich (under-oxidized). If the gases and particles are hot enough, they may incandesce, producing a light with a grey-body emission signature near the muzzle exit. As the gases expand and

mix with air, they may also combust, emitting light which is a combination of incandescence and discrete emission from flame-propagation combustion radicals, such as CH and C_2 [McNesby, 2016]. The light emission from hot particles at muzzle exit and combustion of fuel rich propelling particles and gases after mixing with air is responsible for the muzzle "flash" seen for most firings of small caliber guns (for the discussion here, bullet diameter of 12.5 mm and below). Within a few to tens of centimeters after bullet exit from the gun barrel, aerodynamic drag causes the expelled gases and particles to lose much of their forward velocity, and the bullet emerges from the propellant gases and moves downrange. The chemistry and physics of the gases and particles after projectile exit from the gun barrel, and the disposition of the projectile after barrel exit, are considered part of the topic of gun exterior ballistics.

For the shoulder-fired M4 carbine, firing M855 ammunition (5.56-mm diameter bullet), the bullet velocity is near 890 meters per second (m/s). Figure 1-1a) shows an M4 carbine in a rig designed to allow remote firing of the weapon during high-speed imaging. Figure 1-1b is a series of shadowgraphs showing bullet exit from the M4 carbine, and expansion of the propelling gases as the bullet travels down range.

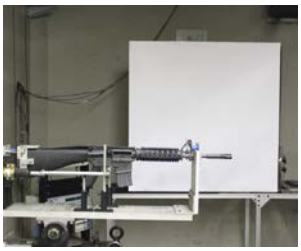

M4 weapon (5.56 mm diameter bullet) in testing rig

Edgerton shadowgraphy during weapon firing

Figure 1-1: a) *The M4 carbine shoulder- fired weapon in an experimental fixture;* ***b)*** *Sequential Edgerton shadowgraphy images of bullet "uncorking" and propellant gas expansion.*

As described above, prediction of chemical species (gases and particles) from firing of small-caliber guns must take into account chemical and physical processes occurring in the domains of interior and exterior ballistics. For firing of the M4 carbine using a double base propellant (NC (nitrocellulose) and NG (nitroglycerin)), chemical species are produced during the sequential stages of energy release. The first stage is the anaerobic propellant burning (deflagration) and gas expansion within the gun barrel. The second stage is the reaction of the deflagration products with the ambient air.

The approach we employ to predict final products of detonations/explosions attempts to simulate, and link, the two stages of energy release described above. For gun firings we use equilibrium chemical calculations to predict anaerobic deflagration product species (first stage) followed by flow dynamics coupled to equilibrium thermochemistry to calculate air combustion of these detonation products (second stage). The initial chemical species produced during detonation and anaerobic expansion and their relative amounts, density, and temperature are predicted by the NASA-Lewis (NASA-Glenn) equilibrium simulation computer code [Gordan, 1994]. We approximate the end

of the first stage of energy release as the density and temperature at which chemical species stop changing (i.e., "freeze out"). For most energetic materials this occurs near a temperature of 1800K. These species are expanded into air to simulate second stage energy release and yield final products.

a. Converting from mass/mass Carbon to mass/mass initial source

The emission ratio of each analyte/species of interest was calculated from the ratio of background-corrected target analyte concentrations to background-corrected carbon dioxide (ΔCO_2) and carbon monoxide (ΔCO) concentrations. Emissions factors were calculated using these emissions ratios following the carbon balance method [Burling, 2010], and presented as mass pollutant per mass of charge weight. Equations 1-1 and 1-2 describe the method employed for calculation of emission factors for chemical species and elements, respectively.

$$EF_i = f_c \times \frac{Anlyte_i}{\sum C_j} \qquad \textbf{Eq. 1-1}$$

where:

EF_i = Emission factor of target analyte i in terms of mass pollutant per mass initial source

fc = mass fraction of carbon in the initial source

$Analyte_i$ = the mass emission ratio of species i,

ΣC_j = the background corrected mass concentration of carbon in major carbon emissions species j (carbon calculated from ΔCO_2 and ΔCO).

The majority of the carbon emissions were emitted as CO_2 and CO. With this assumption, CO_2 and CO are the only carbon-containing compound that was required to be measured at each measurement location.

$$EF_{Element_i} = EF_i \times \frac{1}{F_{Element}} \qquad \textbf{Eq. 1-2}$$

where:

$EF_{Element_i}$ = Emission factor of target analyte i in terms of mass metal per mass metal in initial source

EF_i = Emission factor of target analyte i in terms of mass pollutant per mass initial source

$F_{Element}$ = mass fraction of element in the initial source

Standard deviations, as well as the relative standard deviations (RSDs), were used for showing the measure of dispersion of three or more data values. The relative percent difference (RPD) was used as a quality indicator when only two data values (duplicate samples) were obtained. Single factor one-way analysis of variance (ANOVA) with a level of significance $\alpha = 0.05$ was used to determine any differences in emissions between 855-salt and 855/Legacy. To establish significant difference, the ANOVA-returned p value (significant value) has to be less than level of significance (0.05) and the $F=F/F_{crit}$ value has to be greater than 1.0.

b. **Modified Combustion Efficiency (MCE)**

Comparison of simulations with measurements of chemical species emissions from explosions and combustion events can be challenging. Simulations may often focus on estimation of concentrations of permanent gases (e.g., CO_2, NO_x, H_2O, CO, etc.) while measurements may focus on emissions of

gaseous and particle species in minute quantities or for which thermodynamic or kinetic parameters are incomplete (e.g., HCN, H_2S, polycyclic aromatics, etc.). A metric amenable to both simulation and measurement is the combustion efficiency [Sinha, 2003]. The combustion efficiency (CE) is the molar ratio of carbon (C) emitted as CO_2 from an explosion/combustion event to the total excess carbon emitted [Ward and Hardy, 1991]. The excess, given the symbol Δ and expressed as a mole fraction, is the concentration of a species above ambient concentration. The combustion efficiency is then given by:

$$CE = \Delta C_{CO2} / (\Delta C_{CO2} + \Delta C_{CO} + \Delta C_{CH4} + \Delta C_{NMOC} + \Delta C_{PC}) \quad \textbf{Eq. 1-3}$$

Where the subscripts NMOC and PC refer to non-methane organic carbon and particulate carbon, respectively. Equation 1-3 is often modified, depending on the difficulty of measuring NMOC and PC [Ward, 1993]. As used in this report, the modified combustion efficiency (MCE) is given by:

$$MCE = \Delta C_{CO2} / (\Delta C_{CO2} + \Delta C_{CO} + \Delta C_{CH4} + \Delta C_{PC}) \quad \textbf{Eq. 1-4}$$

It is worth noting that neglecting NMOC and PC in calculation of MCE has been reported to result in errors of less than a few percent, compared to calculations of CE [Sinha, 2003].

2. Materials - Small Caliber Gun Propulsion - M4 Carbine

a. Composition

Three types of ammunition rounds were used:

- Unsalted - X7468 M855 Non-salt-coated SMP842 with propellant weight equal to 26.4 grains (1.71 grams) per round (copper jacketed lead bullet, bullet is 5.56 mm in diameter, no additives in propellant for muzzle flash reduction).
- Salted - X7393 M855 SMP842 with propellant weight 26.1 grains (1.69 grams) per round. No additive in propellant to reduce muzzle flash.
- Legacy (Viet Nam-era ammunition, for comparison to modern issue). Same composition as unsalted round above, but approximately 30 years older. No additive in propellant to reduce muzzle flash.

The "Salted" rounds contained KNO_3 for improved ignition behavior and suppressed flash. All three round types contained a #41 primer. The composition percentage and carbon fraction for these rounds are found in Tables 2-1 and 2-2.

It must be pointed out that the M855 ammunition used in what is described here is not the currently fielded M855A1 "green" lead-free ammunition. The M855 ammo was used in these tests because a copper-jacketed lead projectile was desired for this study. Figure 2-1shows a photograph of an M855 round, together with a schematic showing the components of the round.

Table 2-1: *Carbon fraction (F_C) and metal fraction (e.g., antimony mass fraction is F_{Sb}) in each ammunition round, propellant and primer (N/A = not in the composition).*

Test Item	F_C	F_{Pb}	F_{Al}	F_{Ba}	F_{Sb}	F_S	F_{Bi}	F_K
855	0.31	0.0034	0.0010	0.0007	0.0046	0.0009	0.0020	N/A
855 Salted	0.31	0.0035	0.0014	0.0034	0.0022	0.0009	0.0020	0.0027
Legacy	0.31	0.0034	0.0010	0.0007	0.0046	0.0009	0.0020	N/A

Table 2-2: *Composition in each ammunition round, propellant and primer.*

Test Item		855 Salted mg/round	855 mg/round	Legacy mg/round
Propellant	Nitrocellulose	1,346.0	1,373.9	1,373.9
	Nitroglycerine	226.6	229.3	229.3
	Graphite	3.4	3.4	3.4
	Ethyl Centralite	65.9	66.7	66.7
	Diphenylamine	20.3	20.5	20.5
	Elemental Bismuth	3.4	3.4	3.4
	Potassium nitrate	11.8	N/A	N/A
Primer	Lead styphnate	13.0	13.0	13.0
	Pentaerythritol tetranitrate (PETN)	1.8	1.8	1.8
	Aluminum powder	2.5	2.5	2.5
	Barium nitrate	11.2	11.2	11.2
	Antimony sulfide	5.3	5.3	5.3
	Tetracene	1.4	1.4	1.4

N/A = not applicable (not in the composition).

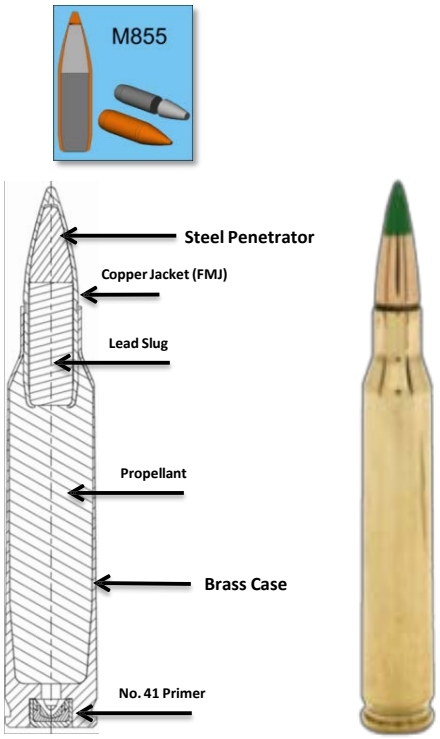

Figure 2-1: *A photograph of an M855 round, together with a schematic showing the components of the round.*

3. Methods - Small Caliber Gun Propulsion

a. Target Analytes and Collected Target Analytes

The target analytes for the M4 gun firings are listed in Table 3-1. CO_2 and CO were successfully measured continuously through all tests. The total number of target analyte samples collected for each type of ammunition are shown in Table 3-2. The aim was to obtain three replicates of each target compound for 855-salt and two replicates from each of 855 and Legacy since they consisted of the same composition. In order to obtain detectable levels of PAHs only replicate samples were collected.

Table 3-1: *Target Analytes for the M4 gun firings.*

Analyte	Instrument/Method	Frequency
CO_2	Non-dispersive infrared	Continuous
CO	Electrochemical cell	Continuous
$PM_{2.5}$[a]	Impactor, Teflon filter	Batch
PM_{10}[b]	Impactor, Teflon filter	Batch
Nitrocellulose	Glass fiber filter	Batch
Nitroaromatics	Glass fiber filter	Batch
PAHs	Glass fiber filter and PUF[c]	Batch
Elements	Teflon filter from $PM_{2.5}$ and PM_{10} batch filter	Batch
VOCs	SUMMA Canister	Batch
PM Size distribution	Electrical Low Pressure Impactor	Continuous & Batch
PM Composition/Size	Single Particle Soot Photometer	Continuous & Batch

[a]Fine particles in ambient air with diameters less than or equal to 2.5 µm.; [b]Fine particles in the ambient air with diameters less than or equal to 10 µm. ;[c]PUF – polyurethane foam

Table 3-2: *Collected Target Analytes from each type of ammunition.*

Analyte	855-Salt	855	Legacy	Total
$PM_{2.5}$	3	2	2	7
PM_{10}	3	2	2	7
Nitroaromatics	3	2	2	7
Elements	6	4	4	14
VOCs	3	2	1	6
PAHs	2	2	2	6
PM Size	6	4	7	17
PM Size/Composition	6	6	9	21

b. Samplers and Analytical

A remotely controlled sampling system, including a computer and control software, was used to sample for the target analytes shown in Table 3-1. The sampling system computer was connected to an external computer via an Ethernet cable enabling the samplers to be controlled outside of the gun room. All sensor data and flow rates were logged on the sampling system's computer.

CO_2 was continuously measured using a non-dispersive infrared (NDIR) instrument (LI-COR 820 model, LI-COR Biosciences, USA). This unit is configured with a 14 cm optical bench, giving it an analytical range of 0-20,000 ppm with an accuracy specification of less than 3% of reading. The LI-820 was calibrated in accordance with U.S. EPA Method 3A [EPA, 1989], undergoing a three point, zero, and calibration drift test. All gas cylinders used for calibration were certified by the suppliers to be National Institute of Standards and Technology (NIST) traceable standards. A precision dilution calibrator, Serinus Cal 2000 (American ECOTECH L.C., Warren, RI, USA), was used to dilute the high-level span gases to appropriate levels for the CO_2 LICOR calibration curves.

CO was continuously measured using an electrochemical gas sensor (e2V EC4-500-CO, SGX Sensortech, United Kingdom) which measures CO concentration by means of an electrochemical cell through CO oxidation and changing impedance. The E2v CO sensor has a detection range of 1-500 ppm with resolution of 1 ppm and sensitivity of 55-85 nA/ppm. The temperature and RH (relative humidity) operating range is -20 to +50°C and 15 to 90% RH, respectively. The response time is less than 30 seconds. Output is non-linear from 0 to 500 ppm. A calibration curve has been calculated in the EPA Metrology Laboratory at 0 to 100 ppm with ±2 ppm error using U.S. EPA Method 3A [EPA, 1989]. The sensor was calibrated for CO on a daily basis in accordance with U.S. EPA Method 3A

[EPA, 1989]. A post drift check was conducted after each test day. All gas cylinders used for calibration were certified by the suppliers that they are NIST traceable. A precision dilution calibrator, Serinus Cal 2000 (American ECOTECH L.C., Warren, RI, USA), was used to dilute the high-level span gases for acquiring the mid-point concentrations for the e2V EC4-500-CO calibration curves. During testing it was found that the CO levels inside the M4-carbine test enclosure exceeded the CO detection range of 500 ppm. A second CO and CO_2 inlet was added to the test chamber in which the gases from the test chamber were diluted with N_2 to a ratio of approximately 15:1.

$PM_{2.5}$ and PM_{10} were sampled with SKC impactors using 47 mm tared Teflon filters with a pore size of 2.0 µm via Leland Legacy sample pumps (SKC Inc., USA) with a constant airflow of 10 L/min. PM was measured gravimetrically following the procedures described in 40 CFR Part 50 [CFR App L, 2014]; CFR AppJ, 2014]. Particles larger than 10 µm in the PM_{10} impactor (or larger than 2.5 µm in the $PM_{2.5}$ impactor) were collected on an oiled 37 mm impaction disc. The Leland Legacy Sample pumps were calibrated with a Gilibrator Air Flow Calibration System (Sensidyne LP, USA).
The particulate matter collected on the Teflon filters was used to determine metal concentrations through analysis by energy dispersive x-ray fluorescence spectrometry (ED-XRF) according to U.S. EPA Compendium Method IO-3.3 [EPA-XRF, 1999]. Boron (B) was analyzed by inductively coupled plasma (ICP) using EPA Compendium Method IO-3.4 [EPA-ICP, 1999].

Volatile organic compounds were sampled via U.S. EPA Method TO-15 [EPA-GC/MS, 1999]. Sampling for VOCs was accomplished using laboratory-supplied 6 liter SUMMA Canisters. Each SUMMA was equipped with a manual valve, metal filter, orifice, pressure gauge, pressure transducer, and an electronic solenoid valve. The SUMMA's sampling rate through the orifice was approximately

0.5 L/min. The SUMMA valves were checked for leakage before sample collection by ensuring that the pressure gauge was not showing decreased pressure with time. The electronic solenoid valve sampling system is opened and closed based on operator-set CO_2 concentration set points using the sampling system's control software program. When the LI-820 measures elevated levels of CO_2, the software enables the solid state relay, opening the SUMMA's solenoid valve to start sampling. The SUMMA canisters were analyzed by ALS Environmental (Simi Valley, California, USA) using U.S. EPA Method TO-15 [EPA-GC/MS, 1999] using full scan mode gas chromatograph-low resolution mass spectrometer (GC/LRMS). The SUMMA canisters were also analyzed for CO_2, CO, and CH_4 by a GC/ flame ionization detector (FID) according to modified U.S. EPA Method 25C [EPA-25C, 2016].

Particle-bound and gas phase PAHs were sampled using a PUF/XAD-2/PUF sorbent (modified U.S EPA Method TO-9A [EPA-TO-9A]) preceded by a quartz microfiber filter with a sampling rate of 0.005 m^3/min (Leland Legacy pump). The PUF/XAD-2/PUF cartridge was purchased pre-cleaned from Supelco (USA). The glass cartridge is 2.2 cm in OD and 10 cm long with 1.5 g of XAD-2 sandwiched between two 3 cm PUFs. The Leland Legacy pump was calibrated with a Gilibrator Air Flow Calibration System (Sensidyne LP, USA). The target PAH compounds (naphthalene, acenaphthylene, acenaphthene, fluorene, phenanthrene, anthracene, fluoranthene, pyrene, benzo(a)anthracene, chrysene, benzo(b)fluoranthene, benzo(k)fluoranthene, benzo(a)pyrene, indeno(1,2,3-cd)pyrene, dibenz(a,h)anthracene, benzo(ghi)perylene) were analyzed using a modified EPA Method 8270D [Wingfors, 2014]. Labeled standards for PAHs were added to the XAD-2 traps before the samples were collected. The surrogate recoveries are measured relative to the internal standards and are a measure of the sampling cartridge collection efficiency. Internal standards were added before mass analysis. The filter, XAD, and PUF were combined in a Soxhlet extractor and spiked with quantitation internal

standards for PAHs. The extraction was conducted by toluene. After extraction, the extracts were concentrated with a three-ball Snyder column (no rotary evaporation). The three-ball Snyder setup is only able to concentrate down to 50-100 mL so the solution was filtered and transferred to a TurboVap device (Biotage, Sweden) for nitrogen blow-down concentration. The extract final volume was 1 mL. Prior to analysis, a recovery spike was added to determine the percent recovery of the internal standards through the extraction process. PAH analyses were conducted by GC/LRMS SIM. The target PAHs are the 16 PAH priorities of US EPA. PAH emission factors evaluated using toxic equivalent factors (TEFs) relative to benzon[a]-pyrene toxicity equivalent (B[a]]P-TEQs) [Larsen and Larsen, 1998].

Energetics, including nitroaromatics, nitrocellulose, and their byproducts, were sampled using a $PM_{2.5}$ impactor with a quartz fiber filter (Fisher Scientific). A Leland Legacy pump sampled at a constant flow rate of 10 L/min. The filters were analyzed by APPL Inc. (Clovis, CA, USA) following analytical methods U.S. EPA Method 8330b [EPA-HPLC, 2006] for nitroaromatics and possible degradation products and U.S EPA Method 353.2 [EPA-nitrate, 1993] for nitrocellulose by a nitrate-nitrite colorimetric method.

Continuous measurements of particle size distributions were sampled with a porous tube dilution probe and an eductor (DI500, Dekati Ltd.), with nitrogen as the diluent. The particle size distribution of the diluted emissions was measured with an Electrical Low Pressure Impactor (ELPI, Dekati Ltd.) continuously following gun firing at a two second time resolution. For some of the gun firings polycarbonate filters were placed on the ELPI impactor plates for a gravimetric measurement of the particle size distribution. A single particle soot photometer (SP2) also continuously measured the size distribution of particles that both incandesced and scattered light at 1064 nm at a one second time

resolution. The SP2 had a secondary dilution flow of nitrogen to further reduce the particle concentration to keep within the range of the instrument. The SP2 had two incandescence photomultiplier tube detectors, a ‘blue’ detector measuring incandescent light from 300 – 550 nm and a ‘red’ detector measuring incandescent light from 580 nm to 710 nm. The color ratio is the ratio of the signal from the two detectors and provides a measure of the temperature at which the particle incandesces and can be used to infer particles of different chemical composition.

c. Test Chamber

The testing rig for gun firings consisted of an M4 carbine shoulder-fired weapon firing M855 ammunition [Schmidt, 2009], a polymethylmetacrylate (PMMA, also referred to here as “plexiglass”) chamber (0.5 m high X 0.5 m wide X 1.0 m long, 3/8 inch wall thickness) into which the muzzle of the M4 weapon protruded, an extractive chemical / particle analyzer system and an Edgerton shadowgraphy system for imaging bullet flight and muzzle gases [McNesby, 2016]. The imaging system enabled verification of proper weapon function (e.g., no bullet fragmentation on launch, bullet launch velocity measurement) and verification of muzzle gases being confined within the sampling chamber. Figure 3-1 shows a schematic of the testing rig for gun firings.

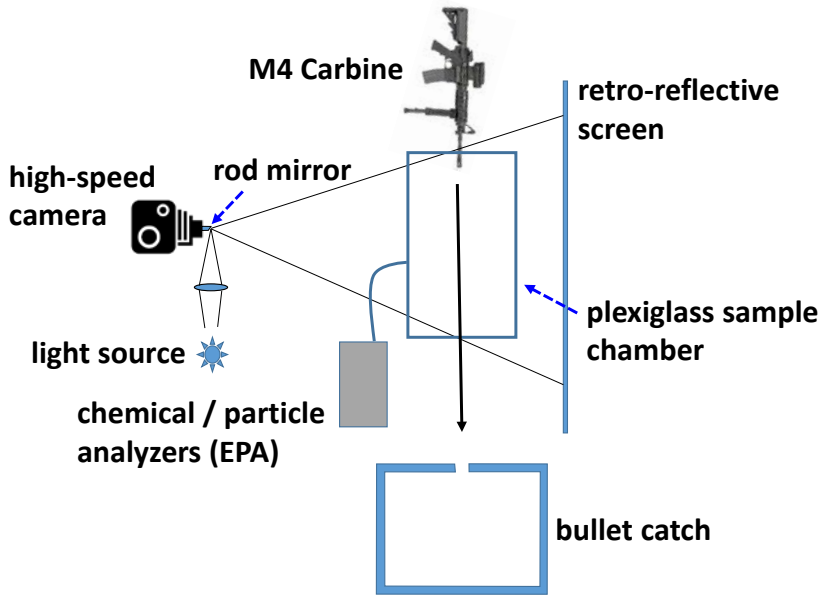

Fig 3-1: *A schematic of the testing apparatus used for emission measurements following firing of the M4 weapon (M855 ammunition). The PMMA sample chamber is referred to in the figure as "plexiglass".*

The PMMA enclosure surrounding the M4 carbine muzzle was built around the muzzle to allow for rapid sampling of the interior gases after firing. The side was removable for insertion of samplers, interior wipe samples, and cleaning of the wall surfaces between firings. The samplers within the box were the PM impactors and PAH cartridge. The sampling instruments were interfaced with the PMMA enclosure as depicted in Figure 3-2. Sampling lines penetrated the PMMA enclosure to the sampler heads. The impactor lines were lead to their respective pumps on the control system. The clear sides of the box facilitated the Edgerton shadowgraphy imaging measurements.

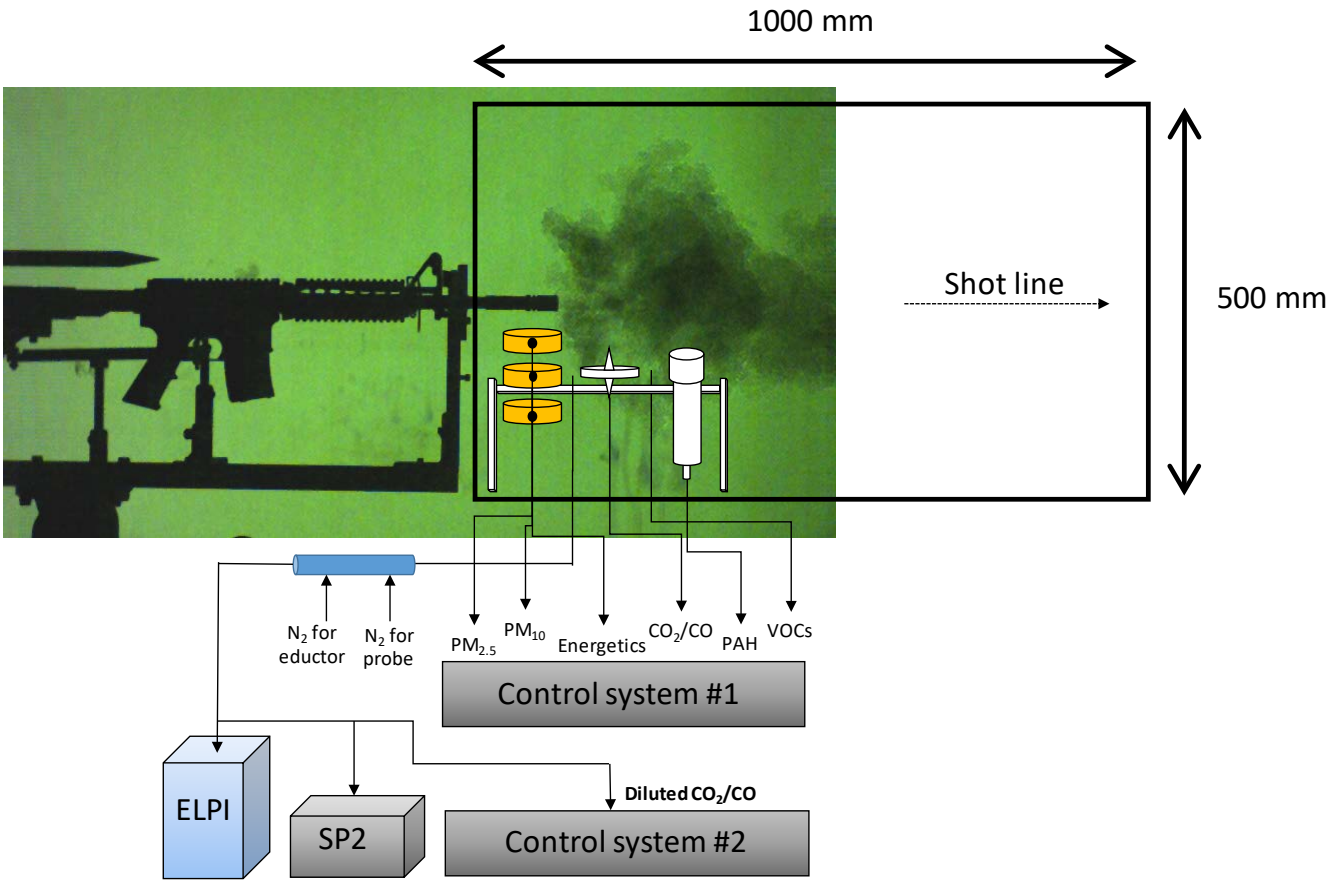

Figure 3-2: *A schematic of the extractive chemical and particle analysis system superimposed on a shadowgraph image of an M4 weapon firing. The PMMA enclosure is indicated by the heavy black lines in the figure.*

A photograph of the testing rig, taken from the vantage point of the imaging system, is shown in Figure 3-3. Figure 3-4 shows the particle and gas samplers within the PMMA enclosure. Figure 3-5 shows a series of images (times shown are time after initiation of trigger mechanism) during emissions test of the M4 weapon firing salted M855 ammunition.

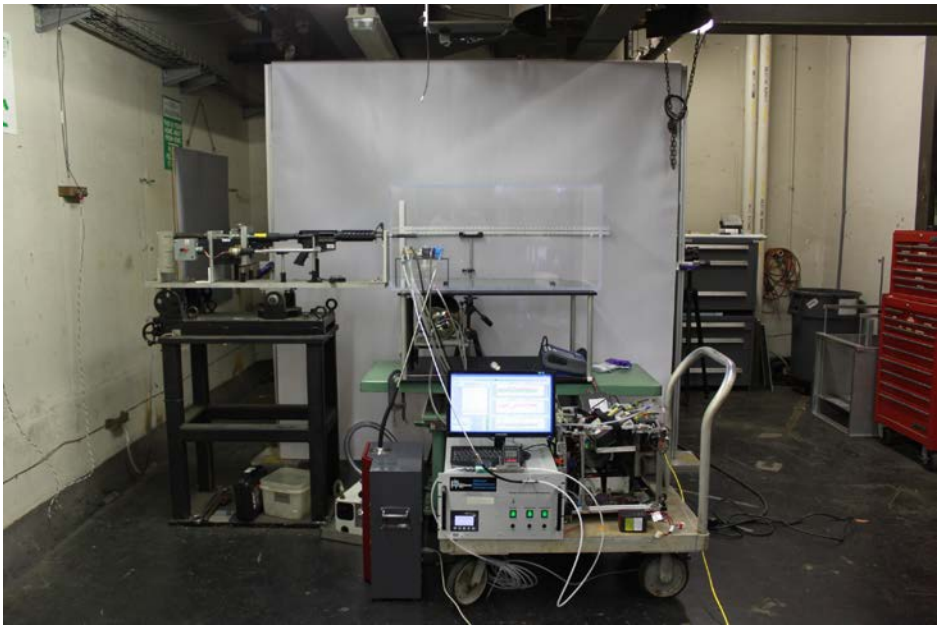

Figure 3-3: *A photograph of the sampling system used to measure emissions following firing of the M4 weapon. The processors for the in-chamber extractors are on the portable cart.*

Figure 3-4: *The particle and gas samplers within the PMMA enclosure. Note the proximity to the "birdcage".*

The birdcage is a slotted cylindrical structure at the end of the gun barrel, designed to suppress muzzle flash. It may be seen in Figure 3-4, near the EPA samplers.

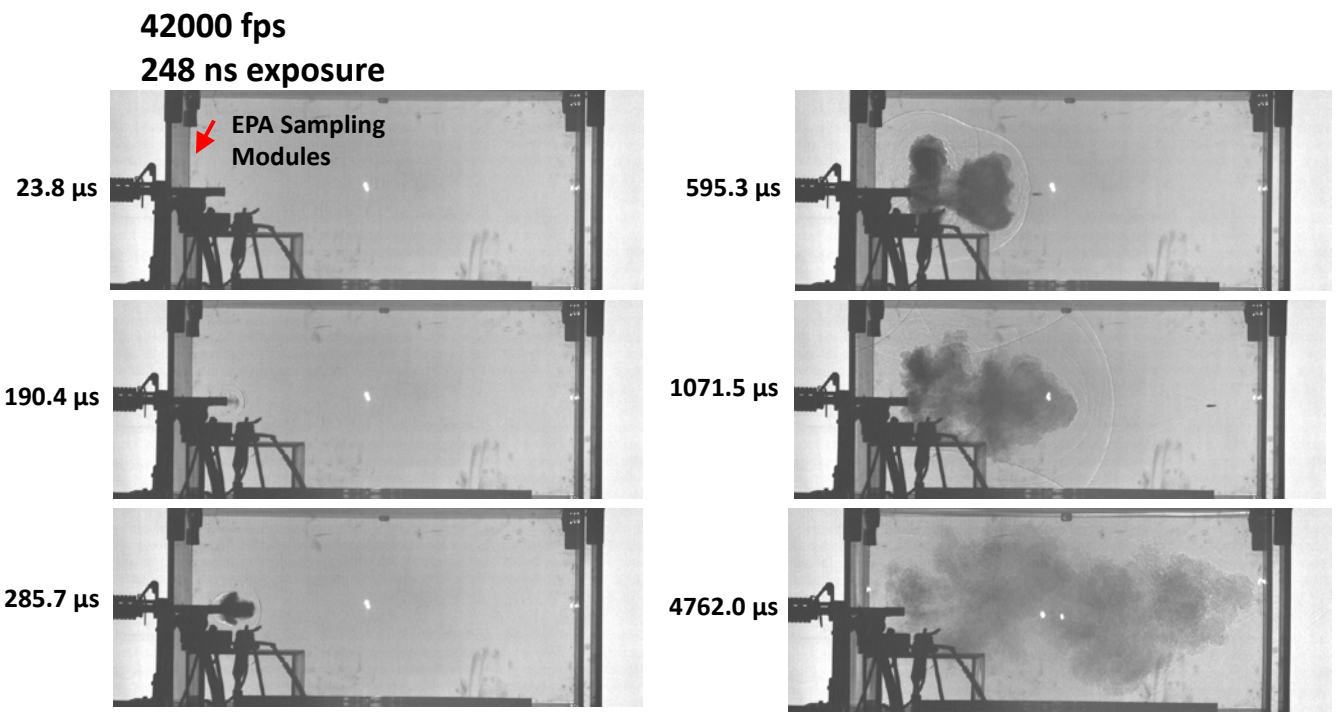

Figure 3-5: *A series of Edgerton shadowgraph images (times shown are time after initiation of trigger mechanism), measured through the PMMA enclosure, during emissions testing of the M4 weapon firing salted M855 ammunition. The images are part of an image sequence captured at 42000 frames per second (fps) using an exposure time of 248 nanoseconds (ns). Illumination was by arc lamp, camera was a Photron Camera Model SA-z monochrome.*

d. Cleaning of test chamber/box walls.

The test chamber enclosure was made up by poly(methyl methacrylate) (PMMA). The PMMA was cleaned between firings with a glass cleaner to obtain clear photographs. This glass cleaner contained volatile organic compounds (VOC's) shown in Table 3-3.

Table 3-3: *Glass cleaner ingredients [Windex, 2017].*

Glass cleaner ingredients	
2-hexaoxyehtanol	C9-11 pareth-3
Isopropanolamine	Citronellol
Lauryl dimenthyl amine oxide	Citrus aurantium dulcis peel oil
Sodium dodecylbenzene sulfonate	Dirpopylene glycol
Benzyl acetate	Ethoxydiglycol
Butylphenyl methylpropional	Hexyl cinnamal
Linlool	Terpineol

4. Results of Simulations - Small Caliber Gun Propulsion

The simulations used to predict gas and particle emissions from firing of the M4 carbine are based upon a sequence of steps that make up the firing process. When the trigger in the weapon is actuated, a primer adjacent to the propellant within the shell casing is initiated by the firing pin in the weapon. The propellant is ignited by hot gases and particles from the primer, and burns. The burning propellant gases expand and accelerate a projectile within the gun barrel. The projectile exits the gun barrel at the muzzle, followed by the high pressure and temperature gases and particles. The gases and particles mix with air, and combustion occurs (often incomplete), often producing a muzzle flash, and determining the final emission products of the event.

The US Army Research Laboratory (ARL) maintains a suite of gun interior ballistics (IB) models that range from a lumped-parameter (i.e., well-stirred mixture) representation to 1D/2-phase and 2D/2-phase models that utilize computational fluid dynamics techniques applicable to multi-phase flow [Horst, 2006]. These models have been successfully applied to weapons of the class used in the present study (i.e., 5.56mm, M855 small-caliber ammunition interior ballistics) [Schmidt, 2009; Nusca, 2011].

Although some of these IB models have the capability to simulate chemically reacting gas-phase flows (using a well-defined set of chemical kinetics based on Arrhenius reaction rates) this degree of modeling is rarely used when seeking to obtain IB gun chamber pressures, gun tube wave dynamics, and projectile muzzle velocity. Rather, heat release kinetics is regularly used in these IB models [Nusca, 2011]. In addition, these IB models do not extend into the "transitional" ballistics domain (i.e., exterior to the gun tube) and thus do not model muzzle gas efflux and blast. The requirements of the present project precipitated the use of an evolving new capability that extends the application of the ARL's 2D/2-phase IB model into the muzzle environment so that modeling of the blast can naturally follow a simulation that is started with the primer function and proceeds through the events leading to expulsion of the round from the gun [Nusca 2016].

For the present simulations, it is assumed that the propellant used in the M855 ammunition produces (anaerobically) combustion product gases as listed in Table 4-1 (the mixture molecular weight is 33.8 g/g-mole). These results were generated using the Constant Breech Pressure (CBP) model which is a very good approximation for optimized fielded guns and gives the equilibrium composition of gases at muzzle [Kotlar, 1992] (given the proper species database). The CBP gun calculation is the idealized limiting case of interior ballistics, that is, in the CBP gun the chemistry is at equilibrium and the propellant burns at optimum conditions for a given breech pressure. This method is a complete thermochemical state description of the ballistic cycle, the output of which is projectile velocity and equilibrium chemical composition at the muzzle of the gun, modified in-house (ARL) to include variable amounts of condensed carbon (soot). This modification is an alternative to the standard CHEETAH gun calculation performed on the propellant tested here, which predicts no condensed phase products. The formation of soot in the gun propellant products allows a higher concentration of CO_2

relative to CO than that predicted by CHEETAH. In the interest of completeness, the results of a standard CHEETAH run on the M855 propellant (SMP 842) is shown in Appendix B. Although possible given an appropriate chemical kinetics set for the propellant, it was outside the scope of the present effort to model chemical reactions for the gas-phase species in the muzzle blast flow (although see Appendix A for input data necessary to accomplish this). Rather, the assumption of "frozen chemistry" was used so that the gas species expelled from the gun muzzle at the time of shot exit (about 1.13 milliseconds (ms) from gun primer ignition) are then distributed through and mixed with the near field air solely by mean of convection and diffusion.

Table 4-1: *Computed Species and Mole Fractions for Muzzle Exit Efflux, approximately 1.13 milliseconds after primer function. These gas species are mixed with air and combust, producing final products.*

Specie	**O_2**	**N_2**	**H_2**	**H_2O**	**CO**	**CO_2**	**CH_4**	**C_2H_6**	**NH_3**
Mole Fraction	0.0	0.15749	0.00181	0.07039	0.00143	0.56354	0.20488	0.00008	0.00017

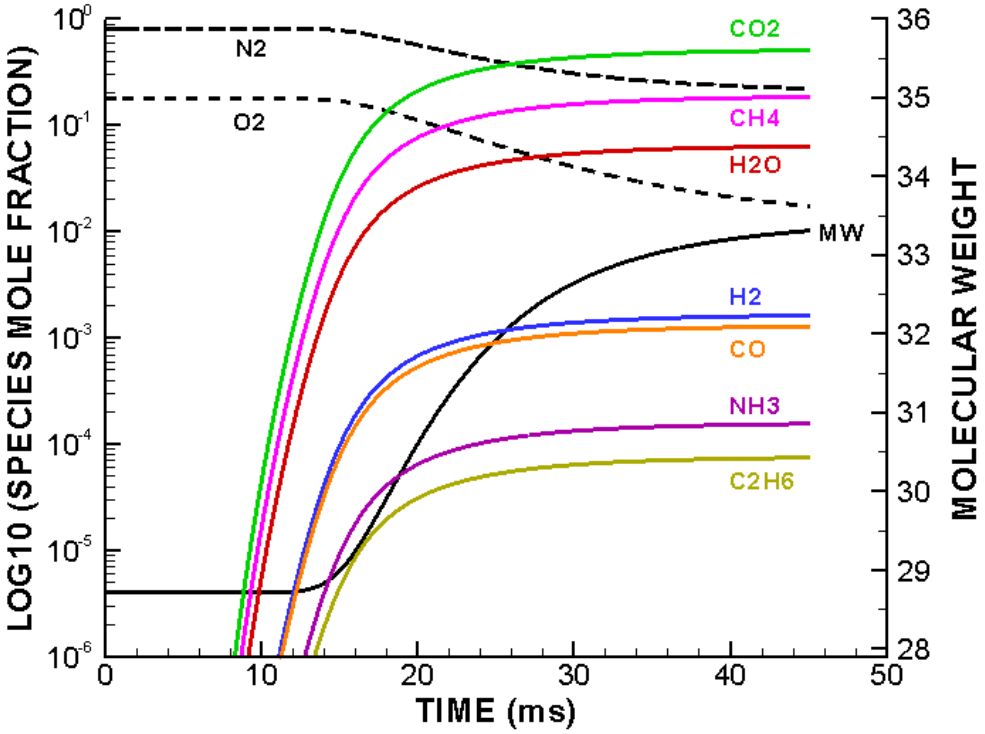

Figure 4-1: *Computed time history mole fractions and mixture molecular weight up to 40 ms for muzzle gas species at the probe location.*

Table 4-2: *Computed Species and Mole Fractions at Probe Location for* ***142 ms*** *after primer function.*

Specie	**O_2**	**N_2**	**H_2**	**H_2O**	**CO**	**CO_2**	**CH_4**	**C_2H_6**	**NH_3**
Mole Fraction	0.18590	0.00768	0.00173	0.06739	0.00137	0.53952	0.19616	0.00008	0.00017

The details of the modeling will be discussed later in this section, but the end results are shown in Figure 4-1 and Table 4-2. Figure 4-1 shows the computed time-dependent species mole fraction histories for about 40 ms following gun primer function (the bullet exits the gun muzzle at 1.13 ms) at a specific location in the near-field gun flow-field termed the "probe location". This location is 15 cm below the gun tube centerline and in-line with the gun muzzle. It closely approximates the actual

location of the instruments used in the gas and particle measurements without extending the computational domain to a breadth that would make the timely execution of the model prohibitive.

As the initial environment outside the gun tube is air (at standard pressure and temperature), the sole gas species for about 8 ms (the time it takes for the chemical cloud to reach the probe) are O_2 and N_2. Driven by the muzzle blast (shock waves) and modeled using convection and diffusion, the other species eventually reach the probe location. Table 4-2 lists the species mole fractions at about 142 ms after primer function when the mixture molecular weight is 34.3 g/g-mole.

Figure 4-2 shows the computational domain for the 5.56mm ammunition (M855) and M4 gun barrel to include 34 cm in front of the muzzle (the gun tube is 46 cm long) and 30 cm around the gun barrel (referenced to the barrel centerline) -- the domain shown in the figure is not plotted to scale (it is stretched in the lateral direction for clarity); as a result, the true curvature of the shock waves is not represented. The boundary conditions prescribed on the edges of the domain are outflow with proper characteristic treatment so the extent of the domain around the gun barrel, which is user-extendable, should not affect the results. The 5.56 mm-diameter bullet (not shown in these views since shot exit is approximately 1.13 ms after primer function) is modeled as a right-cylinder for simplicity and is assumed to fit perfectly into the gun tube; typical blow-by of gun gases is not considered. The plotted color contours are gas pressure (blue to red: low to high) which are used to highlight the muzzle shock waves (and thus ignore the projectile bow shock). High pressure gas (250 psia and above) is evident within the gun barrel for which details of the internal flow field are obscured and low pressures are green-yellow-light blue colors so that relatively low pressure details as in the projectile bow shock are obscured as well; in order to highlight details of the muzzle flow, the selected pressure contour level

range cannot simultaneously show details for both internal and external regions of the gun barrel. Peak efflux from the gun muzzle occurs at about 15 ms after primer ignition (note the two barrel shocks that end in a normal shock near the gun muzzle, Figure 4-3). By 30 ms after primer function the gun tube "blow-down" event is occurring (note the presence of a rarefaction shock traveling into the gun barrel at 30 ms after primer function, Figure 4-4). Similar results and a more detailed description are available [Nusca, 2016].

Figure 4-5 shows the computed color (banded for clarity) mole fraction contours for CO_2 throughout the near-field of the gun tube and correspond to the times of the pressure contour plots of Figure 4-2. The highest concentration of CO_2 is evident near the gun tube muzzle where the pressure is also the highest and the gas velocity is subsonic.

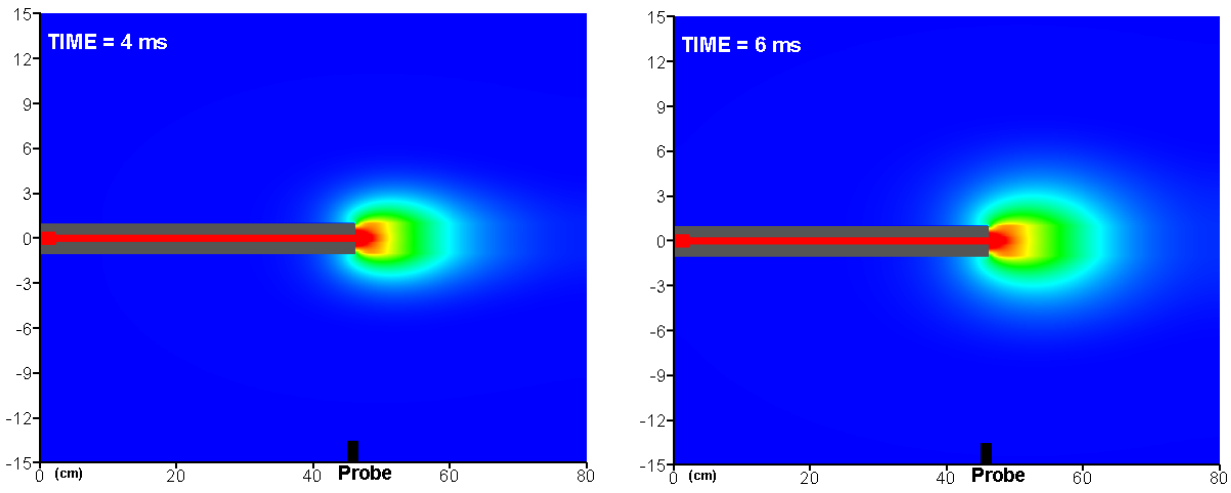

Figure 4-2: *Computed color pressure contours (blue to red: 0 to 250 psia) for 5.56mm (M855) ammunition and M4 gun barrel: 4ms and 6ms after primer ignition (bullet exit at 1.13 ms).*

By 30 ms after primer ignition (see Figures 4-6 and 4-7) the highest concentration of CO_2 should be measured at the probe location since for subsequent times the gun tube flow is reducing due to blow

down (recall Figure 4-4). This corresponds to the results shown in Figure 4-1. The time-dependent behavior of other gas species is similar to that of CO_2.

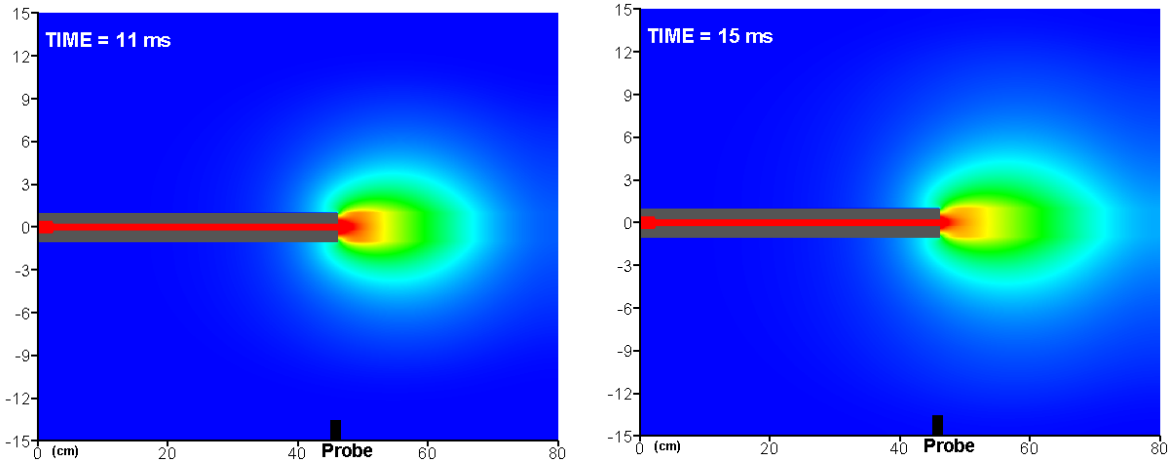

Figure 4-3: *Computed color pressure contours (blue to red: 0 to 250 psia) for 5.56mm (M855) ammunition and M4 gun barrel: 11ms and 15ms after primer ignition (bullet muzzle exit at 1.13 ms).*

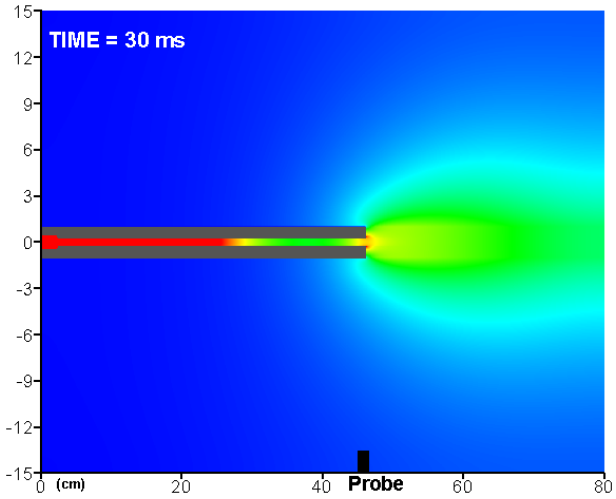

Figure 4-4: *Computed color pressure contours (blue to red: 0 to 250 psia) for 5.56mm (M855) ammunition and M4 gun barrel: 30ms after primer ignition (bullet muzzle exit at 1.13 ms).*

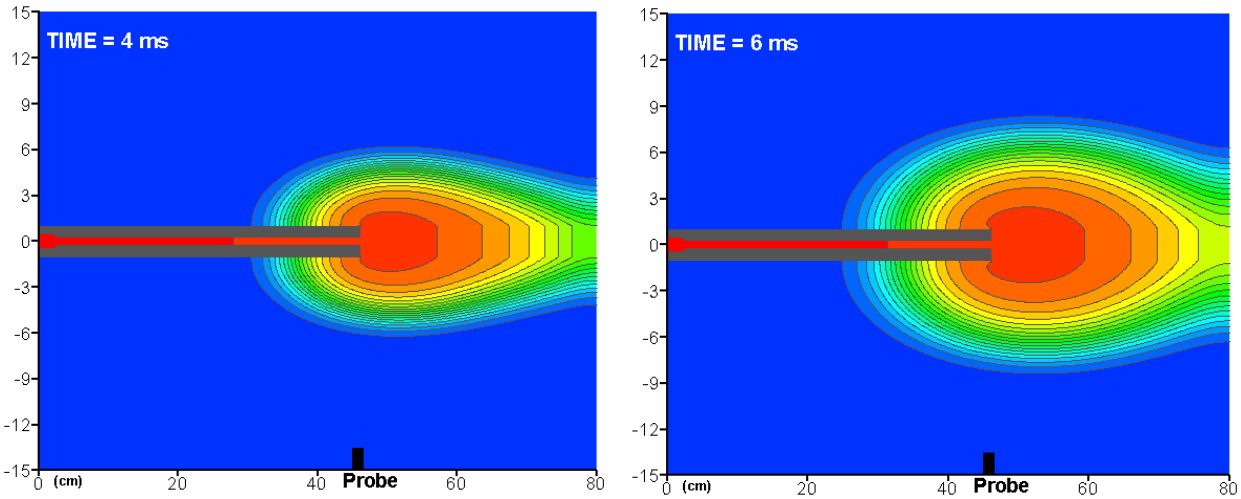

Figure 4-5: *Computed color (banded) mole fraction contours of CO_2 (blue to red:0 to 0.6) for 5.56mm (M855) ammunition and M4 gun barrel: 4ms and 6ms after primer ignition (bullet muzzle exit at 1.13 ms).*

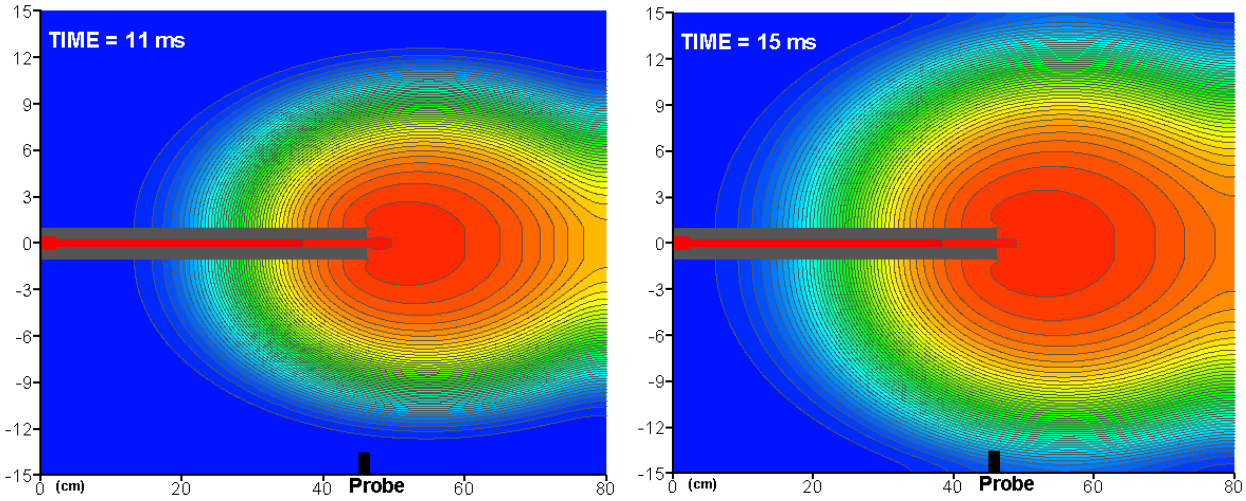

Figure 4-6: *Computed color (banded) mole fraction contours of CO_2 (blue to red:0 to 0.6) for 5.56mm (M855) ammunition and M4 gun barrel: 11ms and 15ms after primer ignition (bullet muzzle exit at 1.13 ms).*

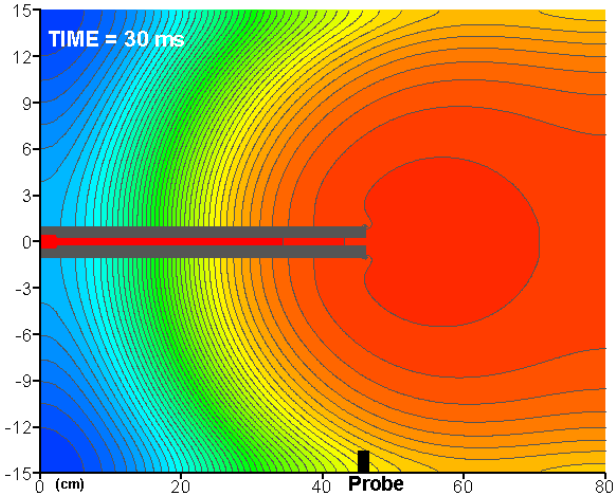

Figure 4-7: *Computed color (banded) mole fraction contours of CO_2 (blue to red:0 to 0.6) for 5.56mm (M855) ammunition and M4 gun barrel: 30ms after primer ignition (bullet muzzle exit at 1.13 ms).*

Calculated emission factors for the simulation employing the NASA-Lewis equilibrium thermochemical code are shown in Table 4-3. MCE's for both simulation methods are shown in Table 4-4. Output of a CHEETAH gun run for the propellant in the M855 round is shown in Appendix B.

Table 4-3: *Calculated Emission Factors for firing of a single round of M855 ammunition (non-salted, SMP-842, gram of emitted species per gram propellant).*

Species	**NASA-Lewis**
CO	0.0075
N_2	0.101
CO_2	0.465
H_2O	0.024
CH_4	0.0615
H_2	trace

Table 4-4: *Modified combustion efficiency (MCE) for firing of M855 ammunition.*

	MCE
Nasa-Lewis Simulation with soot formation M855	0.732
CHEETAH/CHEMKIN Gun Calculation M855	0.998

5. Results of Experiments - Small Caliber Gun Propulsion

a. M4 Carbine Emission Factors – CO_2, CO, and CH_4

Major gaseous carbon species are listed in Table 5-1. Significant levels of incomplete CO oxidation resulted in MCE values less than or equal to 0.5. CH_4 was detected at trace levels. Shot to shot variation was minor as seen by low RSD and RPD values. Slightly less CO oxidation is observed with the M855 "Salted" ammunition than with "unsalted" rounds, although within experimental error the MCE for each type of round are the same. The legacy rounds exhibited less complete CO oxidation than the M855 salted or the M855 unsalted rounds.

Table 5-1: *CO_2, and CO emission factors as well as modified combustion efficiency.*

Compound	855-Salted				855 Unsalted				Legacy			
	n[a]	Average g/kg fuel	Stand. Dev. g/kg fuel	RSD[b] %	n[a]	Average g/kg fuel	Stand. Dev. g/kg fuel	RSD[b] %	n[a]	Average g/kg fuel	Stand. Dev. g/kg fuel	RSD[b] %
CO_2	5	284	44	15	4	300	55	18	1	253	56	22
CO	5	191	17	8.9	4	192	19	9.8	1	208	30	14
		Average Fraction	Stand. Dev. Fraction			Average Fraction	Stand. Dev. Fraction			Fraction	Stand. Dev. Fraction	
MCE[c]	5	0.49	0.056	19	4	0.5	0.064	22	1	0.44	0.080	24

[a] Number of samples collected. [b] RSD = relative standard deviation, calculated when n=3 or more. [c] MCE = modified combustion efficiency ($\Delta CO_2/(\Delta CO_2+\Delta CO+\Delta CH_4)$).

b. M4 Carbine Emission Factors – Particulate Material (PM)

The near equivalence of $PM_{2.5}$ results with PM_{10} results indicate that the majority of the emitted particles are of diameter less than or equal to 2.5 µm, Table 5-2 and Figures 5-1 and 5-2. This is consistent with the sampling chamber work of Wingfors et al. [Wingfors, 2014] who found the aerodynamic size increasing from 0.2 µm at 2 min after firing to 1 µm after 12 min, the increase in size due to particle agglomeration. The PM emission factors for the two different ammunition compositions

(855-Salted versus 855-Unsalted and Legacy) are statistically distinct, ($p<0.004$, $F>3.8$). The relative standard deviation (RSD) and relative percent difference (RPD) are low for these rounds indicating consistency in the emissions as well as the testing and sampling method. The emission factors for PM_{10} are consistent with those measured by Wingfors, et al. [Wingfors, 2014] for total suspended particles (0.029-0.030 g/round), albeit using different methods and different ammunition types.

Table 5-2: *PM emission factors from firing of M4 carbine. g/kg fuel is used because the ammunition includes both propellant and primer.*

PM size	Bullet type	n[a]	Average g/kg fuel	Stand. Dev. g/kg fuel	Average g/round	Stand. Dev. g/round	RSD[b] %	RPD[c] %
$PM_{2.5}$	M855 Salt	3	23	2.3	0.040	0.0040	10.0	
PM_{10}	M855 Salt	3	34	5.3	0.059	0.0091	15.5	
$PM_{2.5}$	M855	2	15		0.025			15.7
PM_{10}	M855	2	17		0.029			5.4
$PM_{2.5}$	Legacy	2	10		0.017			38
PM_{10}	Legacy	2	11		0.020			21

[a] Number of samples collected. [b] RSD = relative standard deviation, calculated when n=3 or more.[c] RPD = relative percent difference, calculated when n=2.

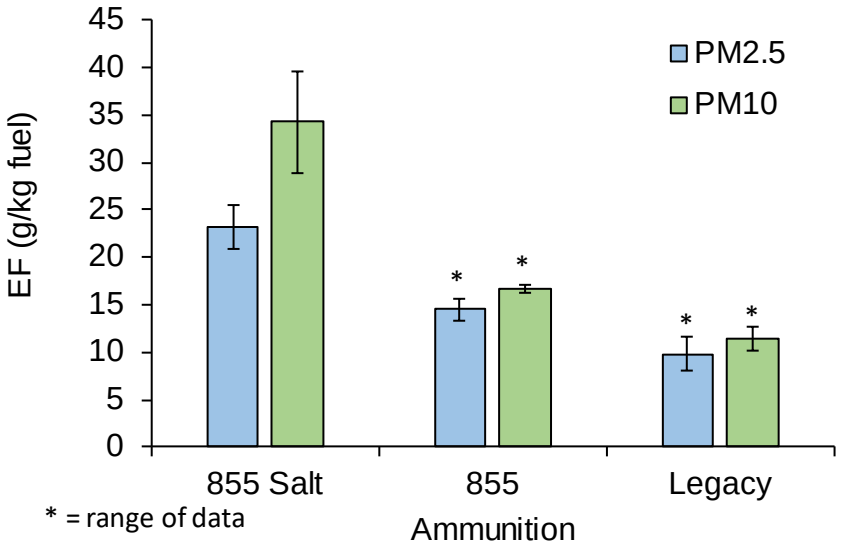

Figure 5-1: *PM emission factors from M4 carbine in g/kg fuel. Error bars represent 1 standard deviation if nothing else stated.*

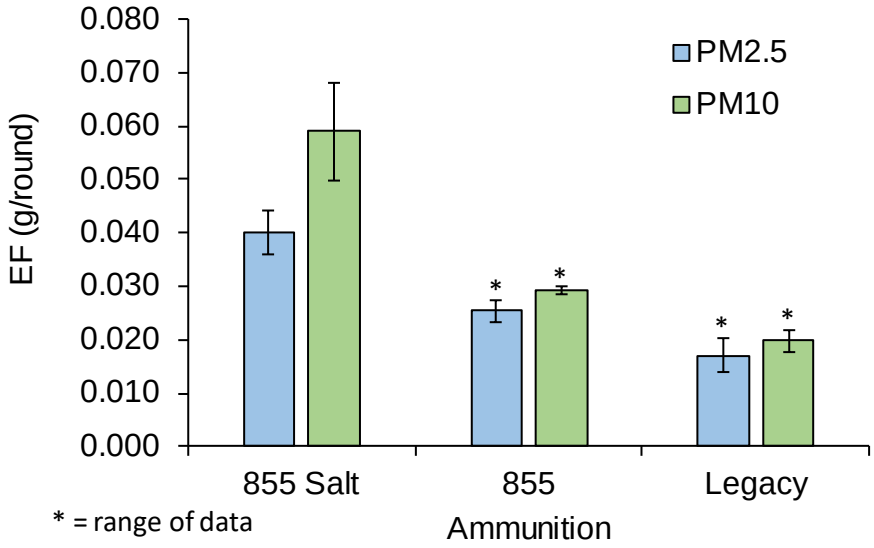

Figure 5-2: *PM emission factors from M4 carbine in g/round. Error bars represent 1 standard deviation if nothing else stated.*

c. M4 Carbine Emission Factors - Elements

Elemental emissions are found in recovered particles. Element emissions are shown in Table 5-3, 5-4, and 5-5, below. All three ammunition types show relatively similar metal emission factors (Figure 5-3) with the exception of K from the salted (KNO_3) ammunition.

Cu exhibits the highest metal emission factor we observed for the gun firings although there is no Cu in the propellants and primers of the three tested bullets. Rather, the bullets (slug) are encased in a Cu jacket which is etched by the rifled barrel to enable the bullet to spin, aiding in accuracy. As the barrel etches the copper jacket, copper is deposited on the barrel interior and, as these results show, emitted from the barrel. In addition, a de-coppering agent (Bi) is added to the propellant to keep the rifle barrel clean. Other elements are also observed in the PM but are not reported in the propellant and primer formulation including Na, Fe, Zn, and K (in the non-salted rounds). It is possible that these elements are alloyed in low amounts in the bullet (slug) casing.

Element emission factors from $PM_{2.5}$ and PM_{10} are quite similar between round types (Figure 5-4) indicating that the majority of particles are of 2.5 μm median diameter or less, as stated above. The metals within the three round types have similar emission factors (Figure 5-3). The Legacy ammunition showed detectable levels of Cl while the 855 ammunition showed no detectable levels of Cl. Rather, the M855 unsalted ammunition showed detectable levels of S, unlike the Legacy ammunition. There is limited overlap in reported metals by Wingfors et al. Their Cu, Pb, and Zn values were 11.4, <7.3, and 3.7 mg/round, respectively, which compare with our average values (Tables 5-3, 5-4, 5-5) of 25.5, 3.4, and 9.7 mg/round. Their Pb values are much lower than measured in this work, consistent with their use of Pb-free rounds.

Table 5-3: *Element emission factors from M4 carbine, M855 Salted ammunition.*

	M855 Salted							
	$PM_{2.5}$				PM_{10}			
Element	**n[a]**	**Average g/kg fuel**	**Stand. Dev. g/kg fuel**	**RSD[b] %**	**n[a]**	**Average g/kg fuel**	**Stand. Dev. g/kg fuel**	**RSD[b] %**
Mg	3	0.28	0.019	6.5	3	0.40	0.11	26
Al[d]	3	0.072	0.028	39	3	0.15	0.05	34
S	3	0.76	0.20	26	3	0.49	0.17	34
K	3	9.07	0.69	7.6	3	9.94	1.74	17
Fe	3	0.17	0.021	12	3	0.27	0.06	24
Cu	3	16.39	1.01	6.2	3	26.35	4.18	16
Zn	3	2.12	0.14	6.8	3	3.02	0.47	16
Bi	3	2.91	0.60	21	3	4.28	1.24	29
Pb	3	5.77	0.42	7.3	3	7.61	0.89	12
Ba	3	0.31	0.039	13	3	0.47	0.11	24
Sb	3	1.56	0.22	14	3	2.17	0.52	24
V	3	0.017	0.002	11	3	0.025	0.007	29
Cl	0	ND[c]			0	ND[c]		
	n[a]	**Average mg/round**	**Stand. Dev. mg/round**		**n[a]**	**Average mg/round**	**Stand. Dev. mg/round**	
Mg	3	0.49	0.03		3	0.70	0.18	
Al[d]	3	0.12	0.05		3	0.25	0.08	
S	3	1.31	0.34		3	0.85	0.29	
K	3	15.65	1.19		3	17.15	3.00	
Fe	3	0.30	0.04		3	0.46	0.11	
Cu	3	28.29	1.75		3	45.47	7.21	
Zn	3	3.66	0.25		3	5.22	0.81	
Bi	3	5.02	1.04		3	7.39	2.13	
Pb	3	9.96	0.73		3	13.14	1.54	
Ba	3	0.53	0.07		3	0.80	0.20	
Sb	3	2.69	0.37		3	3.74	0.90	
V	3	0.029	0.003		3	0.043	0.013	
Cl	0	ND[c]			0	ND[c]		
		Average g/kg element[e]	**Stand. Dev. g/kg element[e]**			**Average g/kg element[e]**	**Stand. Dev. g/kg element[e]**	
Al[d]	3	50.6	19.5		3	102.9	34.7	
S	3	883.7	232.0		3	573.6	197.3	
Pb	3	1672.2	122.6		3	2204.6	259.2	

Ba	3	89.8	11.5	3	136.8	33.3
Sb	3	715.9	99.0	3	993.6	239.7
Bi	3	1484.5	306.9	3	2184.9	630.3

[a] Number of samples collected. [b] RSD = relative standard deviation. [c] ND = not detected. [d] Al values less than three times the uncertainty of the analytical method. [e] Element (Al, S, Pb, Ba, Bi or Sb) in the ammunition.

Metals Pb and Bi (except for Legacy rounds) result in higher emissions than were present in the initial bullet composition (Figure 5-4). This suggests some compositional discrepancies or the presence of residual contamination of the M4 from previous firings.

Table 5-4: *Element emission factors from M4 carbine, M855 ammunition.*

Element	M855 $PM_{2.5}$ n[a]	Average g/kg fuel	RPD[b] %	PM_{10} n[a]	Average g/kg fuel	RPD[b] %
Mg	2	0.22	29	2	0.19	6.4
Al	2	0.086	0.96	2	0.093	21
S[d]	1	0.0005		0	ND[c]	
K	2	0.570	103	2	0.45	91
Fe	2	0.15	4.4	2	0.15	13
Cu	2	15.61	11	2	18.14	10
Zn	2	2.04	11	2	2.09	14
Bi	2	2.85	33	2	2.93	5.6
Pb	2	6.07	7.3	2	5.77	29
Ba	2	0.33	4.7	2	0.33	14
Sb	2	1.55	5.4	2	1.47	17
V	2	0.086	9.6	2	0.020	5.6
Cl	0	ND[c]		0	ND[c]	
	n[a]	Average mg/round		n[a]	Average mg/round	
Mg	2	0.39		2	0.34	
Al	2	0.15		2	0.16	
S[d]	1	0.00082		0	ND[c]	
K	2	1.00		2	0.78	
Fe	2	0.26		2	0.27	
Cu	2	27.25		2	31.67	
Zn	2	3.55		2	3.64	
Bi	2	4.98		2	5.12	
Pb	2	10.60		2	10.07	
Ba	2	0.57		2	0.57	
Sb	2	2.70		2	2.57	
V	2	0.15		2	0.034	
Cl	0	ND[c]		0	ND[c]	
	n[a]	Average g/kg element[e]		n[a]	Average g/kg element[e]	
Al[d]	2	85.4		2	92.5	
S[d]	1	0.55		0	ND[c]	
Pb	2	1765.2		2	1484.6	
Ba	2	440.9		2	1676.4	
Sb	2	333.6		2	441.9	

Bi	2	1444.6	2	317.4	

[a] Number of samples collected. [b] RPD = relative percent difference. [c] ND = not detected. [d] Values less than three times the uncertainty of the analytical method. [e] Element (Al, S, Pb, Ba, Bi or Sb) in the ammunition.

Table 5-5: *Element emission factors from M4 carbine, Legacy ammunition.*

Element	855 $PM_{2.5}$ n[a]	Average g/kg fuel	RPD[b] %	PM_{10} n[a]	Average g/kg fuel	RPD[b] %
Mg	2	0.17	32	2	0.13	24
Al	2	0.077	35	2	0.073	26
S	0	n/c[e]		0	n/c[e]	
K	2	0.099	2.3	2	0.090	2.6
Fe	2	0.50	37	2	0.48	37
Cu	2	12.14	28	2	13.71	29
Zn	2	1.76	29	2	1.80	31
Bi	2	0.074	119	2	0.073	115
Pb	2	4.95	20	2	4.69	26
Ba	2	0.28	28	2	0.28	34
Sb	2	1.30	31	2	1.25	33
V	2	0.014	15	2	0.016	32
Cl	2	0.082	87	2	0.042	58
	n[a]	Average mg/round		n[a]	Average mg/round	
Mg	2	0.29		2	0.22	
Al	2	0.13		2	0.13	
S	0	n/c[e]		0	n/c[e]	
K	2	0.17		2	0.16	
Fe	2	0.87		2	0.83	
Cu	2	21.05		2	23.77	
Zn	2	3.05		2	3.12	
Bi	2	0.13		2	0.13	
Pb	2	8.58		2	8.13	
Ba	2	0.48		2	0.49	
Sb	2	2.25		2	2.17	
V	2	0.025		2	0.027	
Cl	2	0.14		2	0.073	
	n[a]	Average g/kg element[d]		n[a]	Average g/kg element[d]	
Al	2	75.9		2	72.6	
S	0	n/c[e]		0	n/c[e]	
Pb	2	1437.7		2	1363.7	
Ba	2	372.2		2	378.3	
Sb	2	280.2		2	270.1	
Bi	2	37.5		2	37.0	

[a] Number of samples collected with detectable levels. [b] RSD = relative standard deviation. [d] metal (Al, S, Pb, Ba, Bi or Sb) in the full round. [e]n/a=not collected

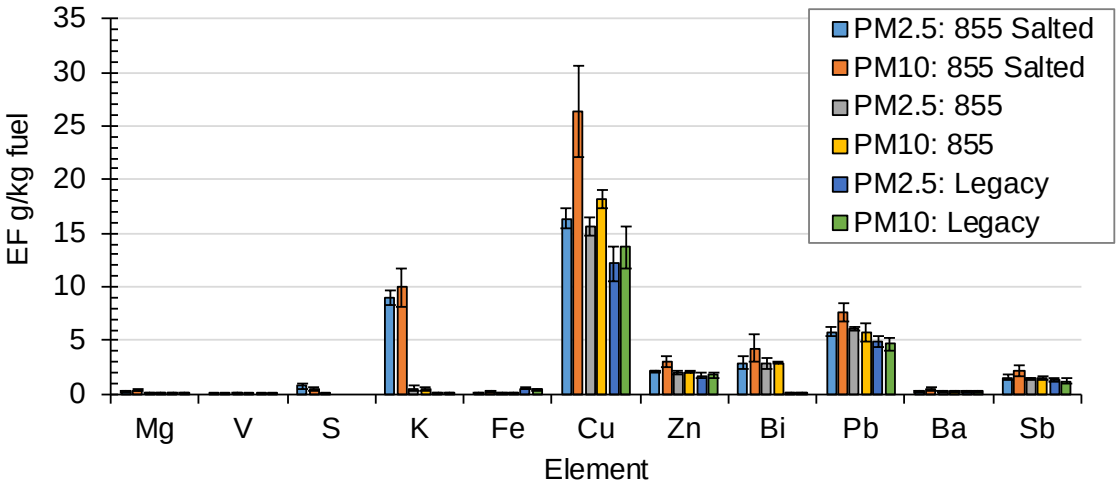

Figure 5-3: *Element emission factors from three different ammunition types fired in the M4 carbine.*

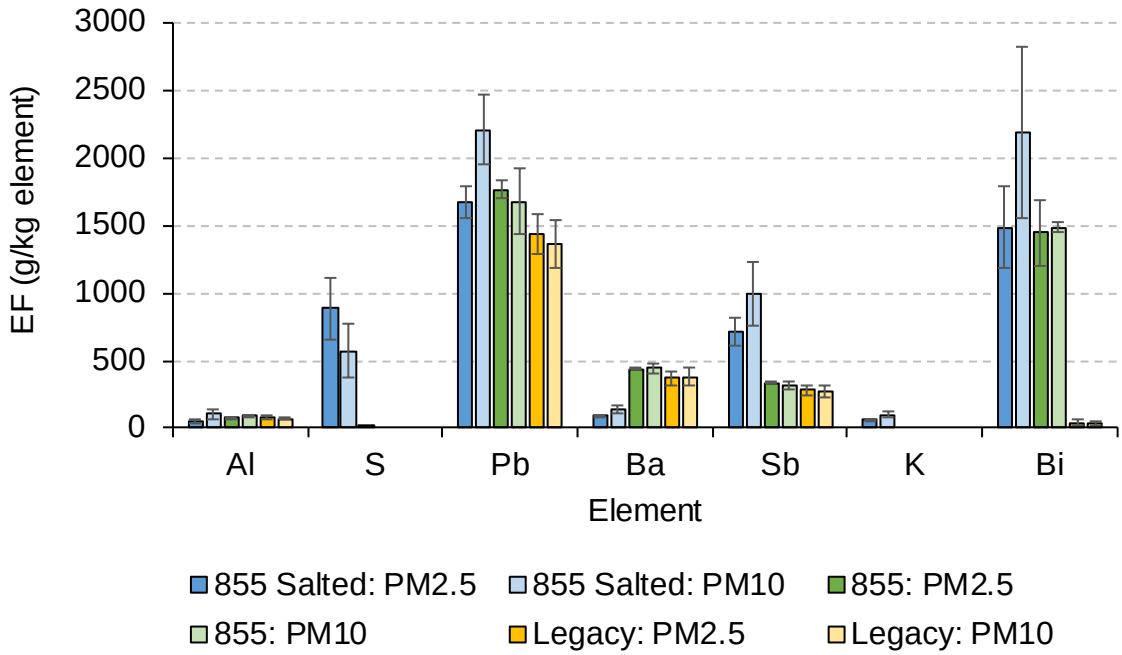

Figure 5-4: *Element emission factors in g/kg element in $PM_{2.5}$ and PM_{10} fractions from firing of M4 carbine.*

d. M4 Carbine Emission Factors -VOCs

VOC data from the three bullet types are shown in Tables 5-6 and 5-7. The sole overlap with data from Wingfors et al. [Wingfors, 2014] is acrolein for which they obtained 8 ±1 µg/round as compared to this work at a 6-bullet average 3.8 µg/round. Some of these VOCs may originate from the acrylic glass (PMMA) cracking from the shockwave, such as methyl methacrylate which showed high levels after the first round (M855 salted): 40 mg/kg fuel compared to less than 5 mg/kg fuel for the rest of the rounds (Figure 5-5). Methylene chloride and trichloroethene followed the same methyl methacrylate level pattern trend, suggesting that these emissions relate to the PMMA cracking as well. Isopropyl alcohol (2-propanol) showed also a pattern with test order (Figure 5-6) although it followed the cleaning of the PMMA box, suggesting that it relates to the glass cleaner that contained isopropanolamine. We have no explanation for the spike in MeCl levels for the initial test.

Table 5-6: *VOC emission factors from firing of M4 carbine.*

	M855			M855 Salted					Legacy	
	n[b]	Average mg/kg	RPD[c] %	n[b]	Average mg/kg	Stand. Dev. mg/kg	RSD[d] %	RPD[c] %	n[b]	mg/kg
Propene	2	16.19	5.5	3	13.6	5.17	38		1	16.19
1,3-Butadiene[a]	2	3.70	8.4	2	3.33			43	1	2.35
Ethanol	2	3.03	24	2	3.67			4.8	1	2.67
Acetonitrile	2	86.79	0.07	3	60.0	19.00	32		1	93.86
Acrolein[a]	2	1.22	12	3	2.90	0.59	20		1	2.06
Acetone	2	0.57	54	1	1.70				0	ND[e]
Trichlorofluoromethane	2	0.76	57	2	0.62			33	1	0.26
2-Propanol	2	2.10	99	2	6.08			145	1	4.22
Acrylonitrile[a]	2	9.52	2.5	3	6.71	2.29	34		1	12.44
Methylene Chloride[a]	2	180.36	51	1	1201				1	13.82
Carbon Disulfide[a]	2	0.57	48	2	1.92			178	1	0.16
2-Butanone (MEK) [a]	2	0.62	12	2	0.39			26	1	0.47
Ethyl Acetate	2	4.08	4.9	2	4.28			16	1	6.80
n-Hexane	2	0.08	12	1	0.16				0	ND
Benzene[a]	2	100.33	1.7	3	93.8	27.01	29		1	119.58
Carbon Tetrachloride[a]	2	0.01	12	1	0.01				0	ND[e]
Trichloroethene	2	9.00	57	3	34.2	52.93	155		1	1.01
Methyl Methacrylate[a]	2	2.17	61	3	13.8	22.61	164		1	0.23
n-Heptane	2	0.10	12	0	ND				0	ND[e]
Toluene[a]	2	7.24	17	3	6.64	2.20	33		1	7.67
2-Hexanone	2	0.11	12	0	ND[e]				0	ND[e]
n-Butyl Acetate	0	ND[e]		1	3.05				0	ND[e]
Tetrachloroethene	2	0.24	105	0	ND[e]				0	ND[e]
Ethylbenzene	2	0.44	12	2	0.41	0.11	27	38	1	0.31
m,p-Xylenes[a]	2	0.70	17	2	0.69	0.21	30	42	1	0.45
Styrene[a]	2	0.47	17	2	0.84	0.41	49	70	0	ND[e]
o-Xylene[a]	2	0.29	15	2	0.29	0.078	27	38	1	0.21
alpha-Pinene	2	1.06	18	2	1.21			100	1	0.17
1,2,4-Trimethylbenzene	2	0.11	27	0	ND[e]				0	ND[e]
d-Limonene	2	1.17	24	2	1.40			130	1	0.16

[a] On EPA's list of hazardous air pollutants. [b] number of samples with detectable levels. [c] RPD = relative percent difference, calculated when n=2.[d] RSD = relative standard deviation, calculated when n=3 or more. [e] ND = not detected

Table 5-7: *VOC emission factors from firing of M4 carbine in per round.*

	M855			M855 Salted				Legacy	
	n[b]	Average µg/round	RPD[c] %	n[b]	Average µg/round	Stand. Dev. µg/round	RSD[d] %	RPD[c] %	n[b]	µg/round
Propene	2	28.27	5.5	3	23.49	8.93	38		1	28.07
1,3-Butadiene[a]	2	6.46	8.4	2	5.74			43	1	4.07
Ethanol	2	5.30	24	2	6.34			4.8	1	4.64
Acetonitrile	2	151.53	0.07	3	103.63	32.80	32		1	162.75
Acrolein[a]	2	2.13	12	3	5.00	1.02	20		1	3.57
Acetone	2	1.00	54	1	2.93				0	ND
Trichlorofluoromethane	2	1.33	57	2	1.08			33	1	0.45
2-Propanol	2	3.67	99	2	10.49			145	1	7.32
Acrylonitrile[a]	2	16.63	2.5	3	11.59	3.95	34		1	21.56
Methylene Chloride[a]	2	314.92	51	1	2072.98				1	23.96
Carbon Disulfide[a]	2	1.00	48	2	3.32			178	1	0.28
2-Butanone (MEK) [a]	2	1.09	12	2	0.67			26	1	0.82
Ethyl Acetate	2	7.12	4.9	2	7.39			16	1	11.80
n-Hexane	2	0.13	12	1	0.28				0	ND
Benzene[a]	2	175.17	1.7	3	161.95	46.62	29		1	207.36
Carbon Tetrachloride[a]	2	0.024	12	1	0.02				0	ND
Trichloroethene	2	15.72	57	3	59.11	91.36	155		1	1.75
Methyl Methacrylate[a]	2	3.78	61	3	23.75	39.02	164		1	0.41
n-Heptane	2	0.17	12	0	ND				0	ND
Toluene[a]	2	12.65	17	3	11.45	3.80	33		1	13.30
2-Hexanone	2	0.20	12	0	ND				0	ND
n-Butyl Acetate	0	ND		1	5.27				0	ND
Tetrachloroethene	2	0.41	105	0	ND				0	ND
Ethylbenzene	2	0.78	12	2	0.71	0.19	27	38	1	0.53
m,p-Xylenes[a]	2	1.22	17	2	1.19	0.36	30	42	1	0.77
Styrene[a]	2	0.83	17	2	1.44	0.71	49	70	0	ND
o-Xylene[a]	2	0.51	15	2	0.50	0.13	27	38	1	0.36
alpha-Pinene	2	1.85	18	2	2.09			100	1	0.30
1,2,4-Trimethylbenzene	2	0.19	27	0	ND				0	ND
d-Limonene	2	2.03	24	2	2.41			130	1	0.27

[a] On EPA's list of hazardous air pollutants. [b] number of samples with detectable levels. [c] RPD = relative percent difference, calculated when n=2.[d] RSD = relative standard deviation, calculated when n=3 or more. [e] ND = not detected

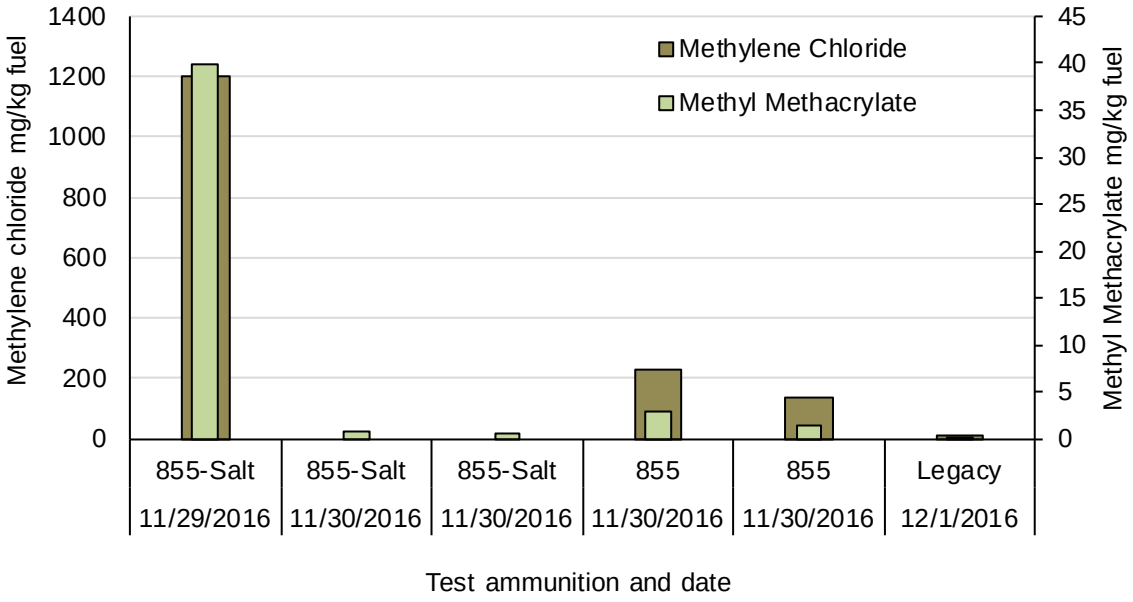

Figure 5-5: *Emission factors of methylene methacrylate and methylene chloride in order of the testing.*

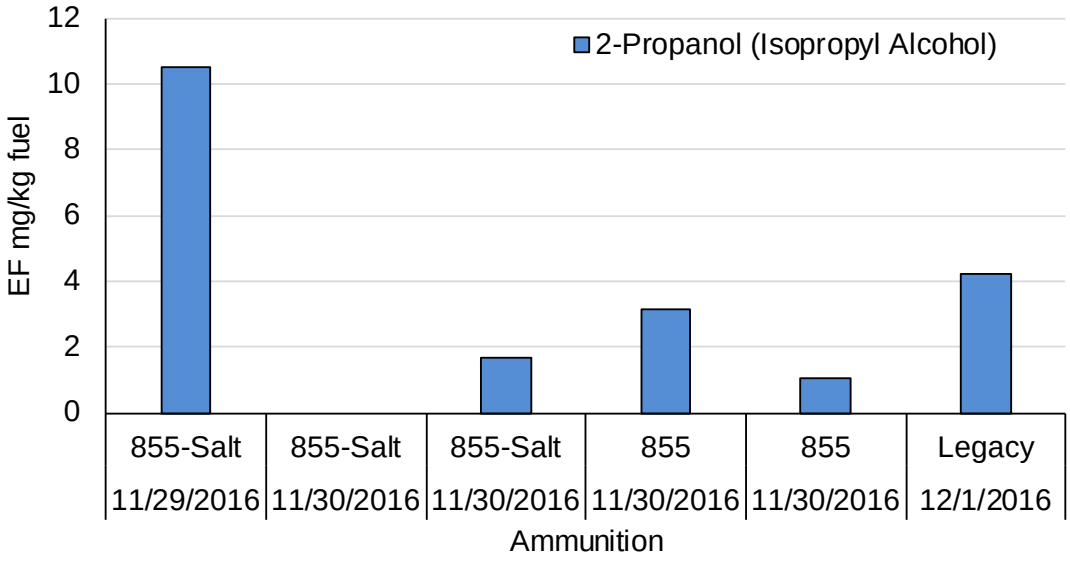

Figure 5-6: *Emission factors of 2-propanol (isopropyl alcohol) in order of the testing.*

e. M4 Carbine Emission Factors - Energetics

None of the target nitroaromatics were above the instrument detection limit and so are reported at the method detection limit, MDL (Table 5-8 and Table 5-9).

Table 5-8: *Energetics method detection limits in mg/kg fuel.*

Method detection limits	**855 Salt MDL mg/kg fuel**	**855 MDL mg/round**	**Legacy MDL mg/round**
1,3,5-Trinitrobenzene	<22.4	<19.8	<15.2
1,3-Dinitrobenzene	<22.4	<19.8	<15.2
2,4,6-Trinitrotoluene	<22.4	<19.8	<15.2
2,4-Dinitrotoluene	<22.4	<19.8	<15.2
2,6-Dinitrotoluene	<22.4	<19.8	<15.2
2-Amino-4,6-Dinitrotoluene	<22.4	<19.8	<15.2
2-Nitrotoluene	<22.4	<19.8	<15.2
3,5-DNA	<22.4	<19.8	<15.2
3-Nitrotoluene	<22.4	<19.8	<15.2
4-Amino-2,6-Dinitrotoluene	<22.4	<19.8	<15.2
4-Nitrotoluene	<22.4	<19.8	<15.2
HMX	<22.4	<19.8	<15.2
Nitrobenzene	<22.4	<19.8	<15.2
Nitroglycerine	<22.4	<19.8	<15.2
PETN	<55.9	<49.4	<38.0
RDX	<22.4	<19.8	<15.2
Tetryl	<22.4	<19.8	<15.2

MDL = Method detection limit.

Table 5-9: *Energetics method detection limits in mg/round.*

Method detection limits	**M855 Salted MDL mg/round**	**M855 MDL mg/round**	**Legacy MDL mg/round**
1,3,5-Trinitrobenzene	<0.039	<0.034	<0.026
1,3-Dinitrobenzene	<0.039	<0.034	<0.026
2,4,6-Trinitrotoluene	<0.039	<0.034	<0.026
2,4-Dinitrotoluene	<0.039	<0.034	<0.026
2,6-Dinitrotoluene	<0.039	<0.034	<0.026
2-Amino-4,6-Dinitrotoluene	<0.039	<0.034	<0.026
2-Nitrotoluene	<0.039	<0.034	<0.026
3,5-DNA	<0.039	<0.034	<0.026
3-Nitrotoluene	<0.039	<0.034	<0.026
4-Amino-2,6-Dinitrotoluene	<0.039	<0.034	<0.026
4-Nitrotoluene	<0.039	<0.034	<0.026
HMX	<0.039	<0.034	<0.026
Nitrobenzene	<0.039	<0.034	<0.026
Nitroglycerine	<0.039	<0.034	<0.026
PETN	<0.096	<0.086	<0.066
RDX	<0.039	<0.034	<0.026
Tetryl	<0.039	<0.034	<0.026

MDL = Method detection limit

f. M4 Carbine Emission Factors - PAHs

Particle plus gas phase PAH emission factors are shown in Figure 5-7 (Sum PAHs) and Tables 5-10 and 5-11 (details). While Figure 5-7 indicates higher Sum PAHs from the Legacy bullet, the limited data (n=5 total points) for these results suggest that these preliminary results remain to be verified. Naphthalene, pyrene, and phenanthrene are the most predominant PAHs across all three bullet types. The most toxic PAH, common for all three bullet types, is benzo(a)pyrene, which accounts for over 55% of the 16-PAH toxic equivalency value.

The PAH results obtained here are often three orders of magnitude higher than particle phase (only) data from Wingfors et al. [Wingfors, 2013] (Table II, p. 286) indicating the predominantly volatile nature of the PAHs.

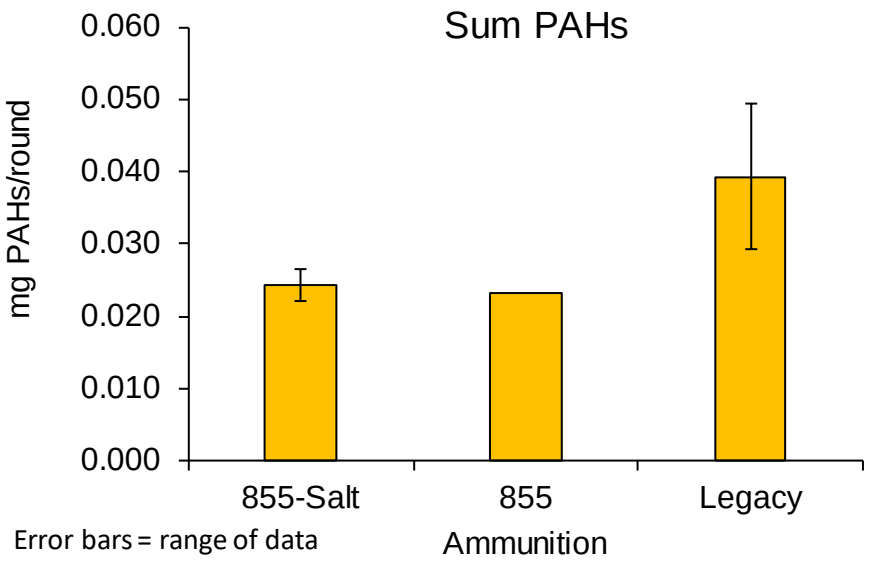

Figure 5-7*. PAH emission factors from firing of M4 carbine.*

Table 5-10: *PAH emission factors from firing of M4 carbine, in mg/kg fuel.*

	M855 Salted, n=2			M855, n=1		Legacy, n=2		
Targets	**Average mg/kg fuel**	**Average mg B[a]P TEQ/kg fuel**	**RPD[c] %**	**mg/kg fuel**	**mg B[a]P TEQ/kg fuel**	**Average mg/kg fuel**	**Average mg B[a]P TEQ/kg fuel**	**RPD %**
Naphthalene	9.22E+00	N/A[b]	25	8.96E+00	N/A[b]	1.59E+01	N/A[b]	42
Acenaphthylene	9.33E-01	N/A[b]	25	8.25E-01	N/A[b]	1.31E+00	N/A[b]	49
Acenaphthene	ND[a]	N/A[b]	N/A[b]	ND[a]	N/A[b]	ND[a]	N/A[b]	N/A[b]
Fluorene	ND[a]	N/A[b]	N/A[b]	ND[a]	N/A[b]	ND[a]	N/A[b]	N/A[b]
Phenanthrene	9.02E-01	4.51E-04	4	8.48E-01	4.24E-04	1.26E+00	6.28E-04	49
Anthracene	1.48E-01	7.38E-05	37	1.34E-01	6.69E-05	1.76E-01	8.79E-05	34
Fluoranthene	4.10E-01	2.05E-02	7	3.68E-01	1.84E-02	5.08E-01	2.54E-02	62
Pyrene	1.07E+00	1.07E-03	4	9.54E-01	9.54E-04	1.62E+00	1.62E-03	99
Benzo(a)anthracene	7.06E-02	3.53E-04	6	6.35E-02	3.17E-04	6.33E-02	3.16E-04	57
Chrysene	1.21E-01	3.62E-03	4	1.16E-01	3.47E-03	1.52E-01	4.57E-03	66
Benzo(b)fluoranthene	1.92E-01	1.92E-02	5	1.58E-01	1.58E-02	2.09E-01	2.09E-02	62
Benzo(k)fluoranthene	8.42E-02	4.21E-03	37	8.07E-02	4.04E-03	9.28E-02	4.64E-03	91
Benzo(a)pyrene	1.36E-01	1.36E-01	6	1.28E-01	1.28E-01	1.34E-01	1.34E-01	64
Indeno(1,2,3-cd)pyrene	2.00E-01	2.00E-02	11	1.54E-01	1.54E-02	1.82E-01	1.82E-02	76
Dibenz(a,h)anthracene	2.73E-02	3.00E-02	88	ND[a]	0.00E+00	ND[a]	ND[a]	N/A[b]
Benzo(ghi)perylene	6.29E-01	1.26E-02	0.04	5.08E-01	1.02E-02	1.09E+00	2.18E-02	114
SUM 16-EPA PAHs	1.41E+01	2.48E-01	18	1.33E+01	1.97E-01	2.27E+01	2.32E-01	51

ND[a] = not detected. N/A[b] = not applicable. [c]RPD = relative percent difference, calculated when n=2. Naphthalene, acenapththylene, acenaphthene and fluorene have not been assigned a toxic equivalent number.

Table 5-11: *PAH emission factors from firing of M4 carbine, in mg/round.*

	M855 Salted, n=2			M855, n=1		Legacy, n=2		
Targets	**Average mg/round**	**Average mg B[a]P TEQ/round**	**RPD[c] %**	**mg/round**	**mg B[a]P TEQ/round**	**Average mg/round**	**Average mg B[a]P TEQ/round**	**RPD[c] %**
Naphthalene	1.59E-02	N/A[b]	25	1.56E-02	N/A[b]	2.75E-02	N/A[b]	42
Acenaphthylene	1.61E-03	N/A[b]	25	1.44E-03	N/A[b]	2.27E-03	N/A[b]	49
Acenaphthene	ND[a]	N/A[b]	N/A[b]	ND[a]	N/A[b]	ND[a]	N/A[b]	N/A[b]
Fluorene	ND[a]	N/A[b]	N/A[b]	ND[a]	N/A[b]	ND[a]	N/A[b]	N/A[b]
Phenanthrene	1.56E-03	7.78E-07	4	1.48E-03	7.40E-07	2.18E-03	1.09E-06	49
Anthracene	2.55E-04	1.27E-07	37	2.33E-04	1.17E-07	3.05E-04	1.52E-07	34
Fluoranthene	7.08E-04	3.54E-05	7	6.43E-04	3.22E-05	8.82E-04	4.41E-05	62
Pyrene	1.84E-03	1.84E-06	4	1.67E-03	1.67E-06	2.81E-03	2.81E-06	99
Benzo(a)anthracene	1.22E-04	6.09E-07	6	1.11E-04	5.54E-07	1.10E-04	5.49E-07	57
Chrysene	2.08E-04	6.24E-06	4	2.02E-04	6.05E-06	2.64E-04	7.92E-06	66
Benzo(b)fluoranthene	3.31E-04	3.31E-05	5	2.76E-04	2.76E-05	3.62E-04	3.62E-05	62
Benzo(k)fluoranthene	1.45E-04	7.27E-06	37	1.41E-04	7.05E-06	1.61E-04	8.04E-06	91
Benzo(a)pyrene	2.35E-04	2.35E-04	6	2.23E-04	2.23E-04	2.33E-04	2.33E-04	64
Indeno(1,2,3-cd)pyrene	3.46E-04	3.46E-05	11	2.70E-04	2.70E-05	3.16E-04	3.16E-05	76
Dibenz(a,h)anthracene	4.70E-05	5.17E-05	88	ND[a]	ND[a]	ND[a]	ND[a]	N/A[b]
Benzo(ghi)perylene	1.08E-03	2.17E-05	0.04	8.88E-04	1.78E-05	1.89E-03	3.79E-05	114
SUM 16-EPA PAHs	2.44E-02	4.29E-04	18	2.32E-02	3.44E-04	3.93E-02	4.03E-04	51

ND[a] = not detected. N/A[b] = not applicable. [c]RPD = relative percent difference, calculated when n=2. Naphthalene, acenapththylene, acenaphthene and fluorene have not been assigned a toxic equivalent number.

a. M4 Carbine Particle – Size Distributions

The initial normalized mass weighted size distribution of the emissions is shown in Figure 5-8. The size distribution was similar for all three ammunition types, with a mass median diameter ranging of 0.389 ± 0.109 µm for the M855 Salted, 0.330 ± 0.124 µm for the M855, and 0.575 ± 0.130 µm for the Legacy ammunitions. These differences in size distribution between ammunition types were not statistically significant.

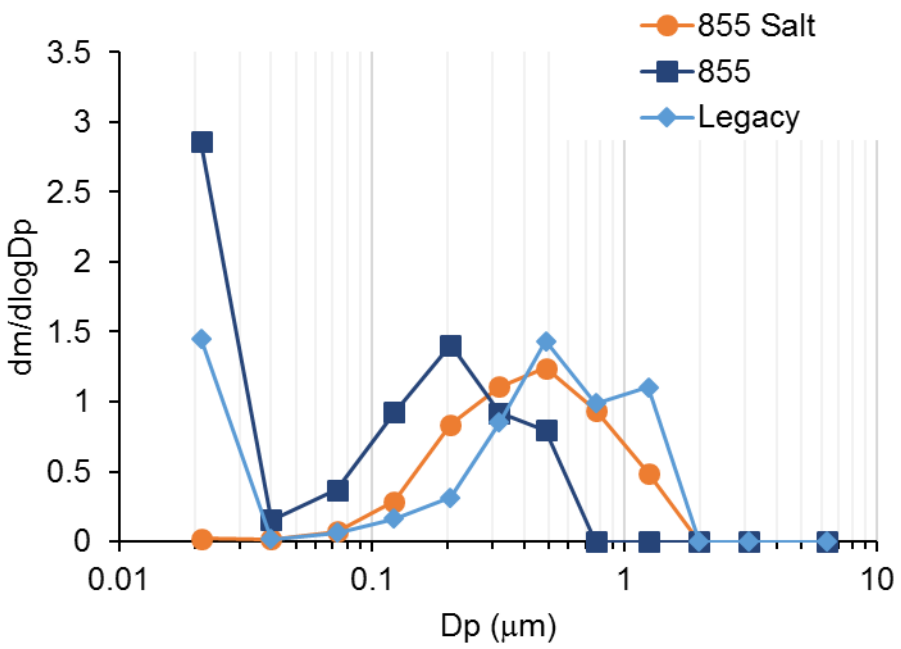

Figure 5-8: *Representative initial mass normalized mass weighted PM size distributions from M4 carbine for different ammunition types.*

The initial size distribution evolved rapidly over the first few seconds as the particles aggregated causing a shift towards larger diameter particles (Figure 5-9). Initially, the mass distribution has a median diameter of approximately 96 nm and all the particles present are smaller than 2.5 µm. Over the first minute the particles agglomerate rapidly and the median diameter shifts to 766 nm after 30 seconds, with a sizeable fraction of particles larger than 1 µm. This agglomeration process explains the slightly larger PM10 emission factors versus PM2.5 emission factors despite the initial particle distributions all being significantly smaller than 10 µm in diameter.

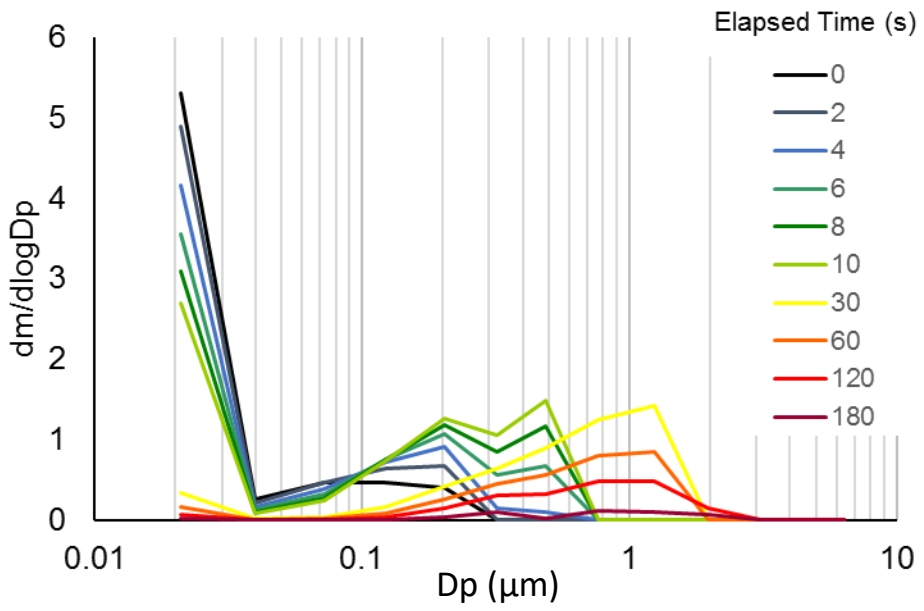

Figure 5-9*. Mass normalized mass weighted PM size distributions from M4 carbine for M855 ammunition over the first 3 minutes after the blast.*

The color ratio is the ratio of the incandesce signal for each particle in the range from 580 to 710 nm to that of the incandescence in the wavelength range from 330 to 550 nm. A larger color ratio indicates a shift towards longer wavelengths in the incandescence spectrum, which is caused by a lower temperature at which the particle incandesces which denotes a differing particle composition. The color ratio of incandescing particles emitted from gun blasts with M855 ammunition and M855 salted ammunition is shown in Figure 5-10. The color ratio had a bimodal distribution that varied between ammunition types, indicating that two different incandescing particle types were present in the emissions. The smaller mode of the color ratio is consistent with that for carbonaceous soot and the larger mode may be associated with a metal oxide. These results suggest that the SP2 color ratio may be used to distinguish between particles of different composition, although further study is needed to identify the composition of these particles.

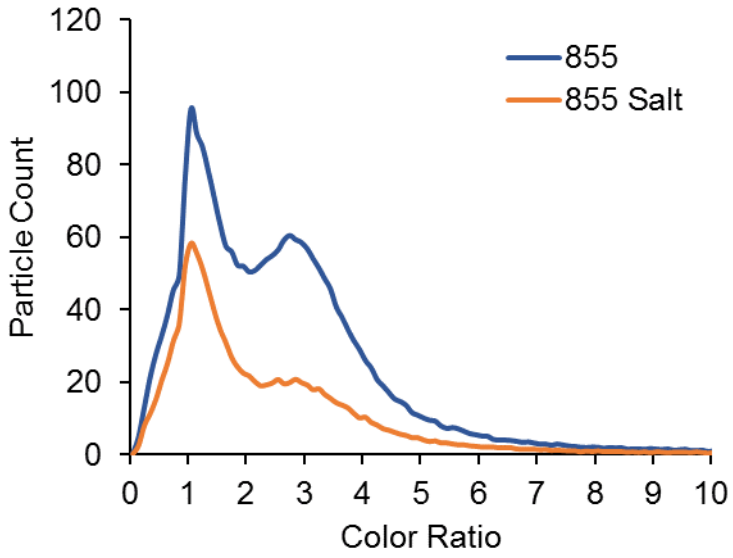

Figure 5-10. *Color ratio for incandescing particles in the emissions from M4 carbine for M855 and M855 salted ammunition types.*

6. Discussion - Small Caliber Gun Propulsion

Table 6-1 shows measured and calculated Modified Combustion Efficiency for the M855 ammunition fired by the M4 carbine. The Nasa-Lewis simulation and the CHEETAH-CHEMKIN simulation overpredict the MCE for the gun firing event.

Table 6-1: *Modified Combustion Efficiency (MCE) for firing of M855 ammunition in the M4 rifle based on results reported here.*

	MCE
M855 Salted (experiment)	0.49 (0.056)
M855 (experiment)	0.5 (0.064)
M855 Legacy (experiment)	0.44 (0.080)
Nasa-Lewis Simulation with soot formation M855	0.732
CHEETAH/CHEMKIN Gun Calculation M855	0.998

Although the NASA-Lewis simulation results in a MCE closer to the measured results, the code overpredicts CO_2 at the muzzle. The prediction of zero condensed species by CHEETAH does not match with high speed images of the event (see Figures 1-1, 3-5), or measurements of particulates. The NASA-Lewis simulation allows for variable amounts of condensed carbon, but over predicts measured CH_4 and CO_2 concentrations. It should be noted that the temperature used in the CHEMKIN kinetic calculation to predict CO oxidation was 1000K, and heat dissipation was not accounted for during the kinetic calculation. We believe that an improved simulation will take better account of particle production during interior ballistics, and that a much lower temperature for afterburn of muzzle gases may lower the calculated MCE. Finally, future testing should include detailed measurement of HCN gas. HCN is expected to be present at levels of approximately 1 milligram per gram of propellant burned [Kirchner, 1993; Wingfors, 2014].

Solid Chemical Explosives

7. Background – Detonations of Solid Chemical Explosives

Our approach to predicting the products from open detonation (OD) of neat and of metallized solid chemical explosives is based on time evolution of the energy release processes. This has been studied by thousands of researchers over the last 150 years [Rankine, 1870; Kistiakowski, 1941, Mader 2008], yet because of the high rate at which energy release occurs, many aspects of the process remain under investigation [Glumac, 2013]. Energy release following initiation of solid chemical explosives may be approximated to occur in stages [McNesby, 2010]. The first stage of energy release includes detonation of the solid explosive,

in which an exothermic chemical reaction is propagated by a compressive shock wave, and the subsequent anaerobic expansion of the products of the chemical reaction [Kinney, 1985]. The second stage of energy release occurs when the products of the first stage

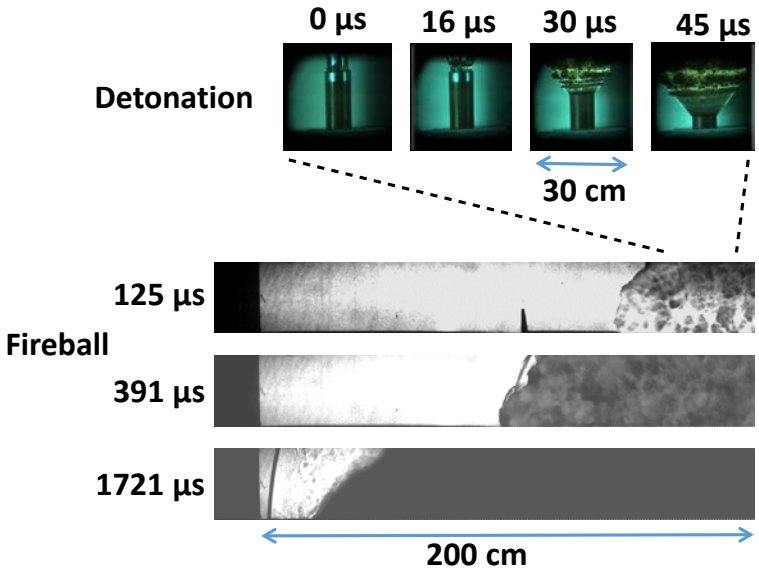

Figure 7-1: *A composite image sequence (2 different experiments) showing stages of energy release following initiation of 2.2 kilograms of the solid explosive TNT. The air shock may be seen detaching from the detonation product species in the last two images.*

burn in surrounding air (called afterburn, or fireball) [Kuhl, 1998]. The power of the second stage is dependent on chemical species produced in the first stage. The power in each stage is dependent upon the initial chemical formulation, although the first stage of energy release in most solid explosives is more powerful than the second stage [Kim, 2004]. Figure 7-1 is a set of images, taken by the authors, depicting energy release following initiation of 2.2 kilograms of solid TNT (trinitrotoluene, $C_7H_5N_3O_6$). This image sequence was created using high-speed cameras and high-brightness illumination techniques [McNesby, 2005]. In solid TNT, the rate at which the detonation propagates is approximately 7 millimeters (mm) per microsecond (µs). In the first stage, near the peak of the compressive shock wave, the reacting TNT has a density slightly higher than bulk (1.7 g per cm^3), a peak temperature near 3300K, and a pressure near 20

GigaPascals (GPa). In the second stage, the fireball radial expansion rate varies as a function of time, from 7 mm per μs at very early times to sonic velocity (0.35 mm per μs) at later times [Meyer, 2007].

a. Prediction of Product Species - Detonations of Solid Explosives

As shown in Figure 7-1, when the detonation has completed, the detonation product gases are hot, dense, and expanding. As the gases expand and cool, chemical reactions occur between the initial detonation products, reaching an equilibrium composition at each temperature [Johansson, 1970]. The chemistry occurring in the initial expansion is anaerobic. As the gases continue to expand and cool, their composition becomes fixed. For simulation purposes, this is the end of the first stage of energy release. As the hot gases of fixed composition continue to expand, they mix with air, and if they are fuel-rich and hot enough, afterburning (fireball) begins [Frost, 2002]. Combustion chemistry occurring during afterburning determines the magnitude of second stage of energy release.

The approach we employ to predict final products of detonation/explosion attempts to simulate, and link, the two stages of energy release described above. For this we use equilibrium chemical calculations to predict anaerobic detonation product species (first stage) followed by finite rate chemical kinetics to calculate air combustion of these detonation products (second stage). The initial chemical species produced during detonation and anaerobic expansion and their relative amounts, density, and temperature are predicted by the equilibrium simulation computer code CHEETAH [LLNL, 2010]. As mentioned above, we approximate the end of the first stage of energy release as the density and temperature at which chemical species

stop changing (i.e., “freeze out”). For most energetic materials this occurs near a temperature of 1800K. To predict the second stage of energy release (aerobic combustion), we use the CHEMKIN chemical kinetic simulation code, marketed by Reaction Design, Inc. The CHEMKIN simulation code uses finite rate chemical kinetics to predict rates of combustion, species evolution, temperature, and energy release. In order to use this simulation, it is necessary to have initial temperature and pressure, type of combustion system (e.g., premixed, well-stirred reactor, opposed flow, etc.), chemical species, and individual chemical reactions and their rates (the reaction mechanism) [Glassman,1987]. In the work described here, the chemical species used in the input to CHEMKIN are those predicted by CHEETAH at species freeze out. The time evolution of chemical species and temperature is simulated as a function of initial temperature in a homogeneous mixture of 1% to 50% detonation products with the balance air. The reaction mechanism is based on the GRI-mech kinetic database [Smith, 2004], and is supplemented by the chemical combustion mechanisms found on the LLNL (Lawrence Livermore National Laboratory) explosives handbook, the SNL (Sandia National Laboratory) website [Appel, 2000], and through published articles in the peer reviewed literature [Spadaccini, 1994]. It should be noted that a more complete picture is provided by incorporating flow dynamics, turbulence, and multiphase combustion (i.e., combustion of solid particles) [Davini, 1996]. The inclusion of these enhancements is beyond the scope of the present work.

8. Materials - Detonations of Solid Chemical Explosives

a. Composition

Two types of detonable solid chemical explosives were tested:

- TNT (trinitrotoluene)
- TNT with Mg:B additives at 80:4:16 mass ratio

TNT was selected as the base solid chemical explosive because it has a large negative oxygen balance. At the end of stage one energy release as described above, the explosive products consist of approximately 30% by mole fraction of graphitic carbon [LLNL, 2010]. The Mg:B metal additive was chosen because it consists of a metal (Mg) known to react rapidly in explosive formulations, and a semi-metal (B) known to partially react in explosive formulations [McNesby, 2010]. Table 8-1 lists composition, by mass, for each detonative material tested, including the explosive train (excluding RP-80 detonator). The RP-80 detonator (Teledyne-RISI) is an exploding bridgewire (EBW) device, and uses 80 mg of PETN as an initiator, and 123 mg RDX as an output explosive. According to the manufacturer, it does not contain lead azide.

Table 8-1: *Detonation composition in mass per charge (includes detonation train components, excluding detonator).*

Test Item		TNT g/charge	TNT MgB g/charge
TNT		640	565
PMMA centering device		18.9	18.9
Pentolite		5.0	6.0
Comp B:	TNT	67	67
	RDX	103	103
	Wax	17	17
Boron		N/A	70.5
Magnesium		N/A	70.5

N/A = not applicable (not in the composition).

9. Methods - Detonations of Solid Chemical Explosives

a. TNT Test Series

For the TNT test series to measure emission factors, TNT right circular cylinders, each weighing approximately 660 grams, were exploded in the US Army Research Laboratory Detonation Science Facility indoor blast chamber at the Aberdeen Proving Ground in Maryland. In order to obtain assurance of a detonation, each explosion was imaged using a high speed framing camera (2.5 million frames per second, Cordin Co. Model 570) and wavelength-resolved emission spectra were recorded for each event for the duration of the framing camera recording time [Princeton Instruments PI-Max-4]. By measuring the rate at which the imaged detonation front travelled through the solid explosive [McNesby, 2016], it was determined that the reaction front travelled faster than the sound speed in solid TNT, and at the velocity found in the literature, satisfying the main criterion for a detonation [Cooper, 1996]. Figure 9-1a shows the explosive assembly to include an RP-80 detonator (not shown, Teledyne-RISI), a 0.5 inch X 0.75 inch pentolite initiator pellet (50% TNT, 50% PETN, $C_5H_8N_4O_{12}$) in a

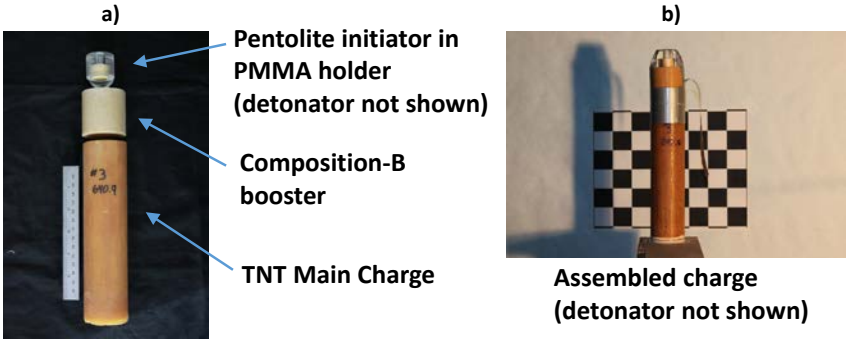

Figure 9-1: a) *a photo of the components of the TNT charge used in the tests.* ***b)*** *The assembled charge. The detonator (RISI RP-80) is not shown.*

polymethylmethacrylate (PMMA) holder (into which the detonator is inserted), a 2 inch X 2 inch Comp-B booster (40% TNT, 60 % RDX, $C_3H_6N_6O_6$), and the main TNT charge (2 inch by 8 inch right circular cylinder, labelled #3 in Figure 9-1a). Figure 9-1b) shows the assembled explosive charge prior to initiation. Because an emission spectrum of the event was being recorded, no exterior illumination was used. Figure 9-2 a-h shows the cigarette-like

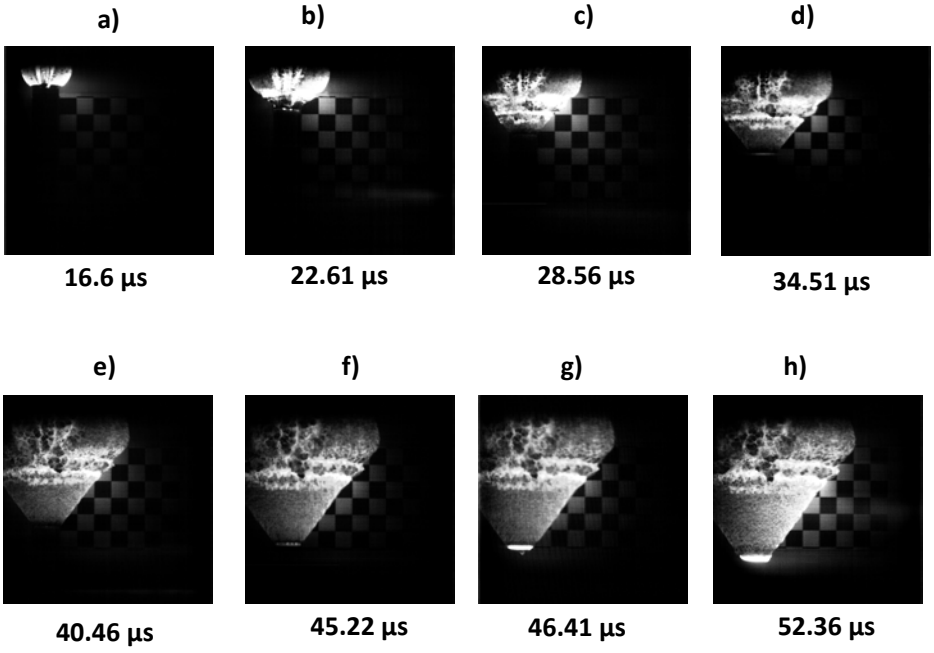

Figure 9-2: *Sequential images (self-illuminating) of the reaction front following initiation of the TNT charge shown in Figure 9-1. The measured velocity of the reaction front was 7 mm per microsecond, consistent with the detonation velocity in neat TNT [Cooper, 1996].*

progression of the reaction front following initiation of the explosive charge. The images are self-illuminating. The brightest region in images 9-2 g)-h) are from air ionization as the detonation pushed out the bottom end of the cylindrical explosive charge [Davis, 2006].

b. TNT:Mg:B Test Series

Figure 9-3 shows a photo of the explosive assembly to include an RP-80 detonator (not shown, Teledyne-RISI), a 0.5 inch X 0.75 inch pentolite initiator pellet (50% TNT, 50% PETN, $C_5H_8N_4O_{12}$) in a PMMA holder (into which the detonator is inserted), a 2 inch X 2 inch Comp-B booster (40% TNT, 60 % RDX, $C_3H_6N_6O_6$), and the main TNT:Mg:B charge (80:4:16 by weight). Because an emission spectrum of the event was being recorded (not shown in this report), no exterior illumination was used for imaging the explosives cylinder during function. Figure 9-4 a-g shows the cigarette-like progression of the reaction front following initiation of the explosive charge. The images are self-illuminating.

Figure 9-3: *A photo of the components of the TNT:Mg:B charge used in the tests. The black color of the main charge is caused by the boron additive.*

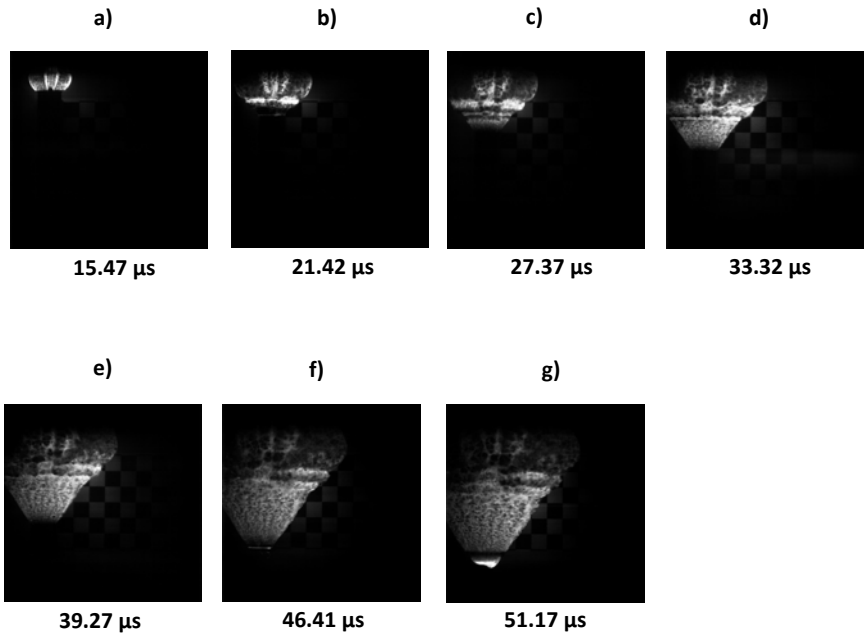

Figure 9-4: *The cigarette-like progression of the reaction front following initiation of the TNT:Mg:B (80:4:16 by weight) explosive charge. The images are self-illuminating.*

c. Target Analytes and Collected Target Analytes – Detonations of Solid Explosives

The target analytes for detonations of solid explosives are listed in Table 9-1. CO_2 and CO were successfully measured continuously through all tests. The total number of target analyte samples collected for each type of detonation are shown in Table 9-2.

Table 9-1: *Target analytes for detonations of solid explosives.*

Analyte	Instrument/Method	Frequency
CO_2	Non-dispersive infrared	Continuous
CO	Electrochemical cell	Continuous
$PM_{2.5}$[a]	Impactor, Teflon filter	Batch
PM_{10}[b]	Impactor, Teflon filter	Batch
Nitrocellulose	Glass fiber filter	Batch
Nitroaromatics	Glass fiber filter	Batch
PAHs	Glass fiber filter and PUF[c]	Batch
Elements	Teflon filter from $PM_{2.5}$ batch filter	Batch
VOCs	SUMMA Canister	Batch
PM Size distribution	Electrical Low Pressure Impactor	Continuous & Batch
PM Composition/Size	Single Particle Soot Photometer	Continuous & Batch

[a]Fine particles in the ambient air with particles less than or equal to 2.5 µm in diameter. [b]Fine particles in the ambient air with particles less than or equal to 10 µm in diameter.

Table 9-2: *Collected Target Analytes for the solid explosives TNT and TNT:Mg:B.*

Analyte	TNT	TNT MgB	Total
$PM_{2.5}$	3	3	6
PM_{10}	2	2	4
Nitroaromatics	2	3	5
Elements	5	5	10
VOCs	2	2	4
PAHs	2	3	5
PM Size	2	2	4
PM Size/Composition	3	3	6

d. Samplers and Analytical

The sampling equipment for analysis of detonations of solid explosives was the same used for analysis of M4 gun firings (see section 3).

e. Test Chamber

Detonations of solid chemical explosives took place within the small blast chamber at the ARL Detonation Science Experimental Facility in Aberdeen MD. The blast chamber is a squashed sphere, 4.9 m tall and 4.9 m in diameter. The chamber is equipped with a stack attached to the ceiling, open to atmosphere, to prevent overpressure. Following explosive initiation, a second vent was opened and the bulk of product gases exhausted to the outside via a separate roof port, typically a 15-20 minute process. The charges were 50 mm x 200 mm right circular cylinders. Each type of charge (neat TNT and TNT:Mg:B), and the explosive train, are described in detail in sections 9a and 9b. Detonator initiation was by a RISI FS-43 control unit, with time gating provided by a Cordin Company Model 454 time delay generator. The charges

were initiated in two configurations, depending upon whether imaging was being used to verify detonation of the solid chemical explosive, or whether species emission was being measured.

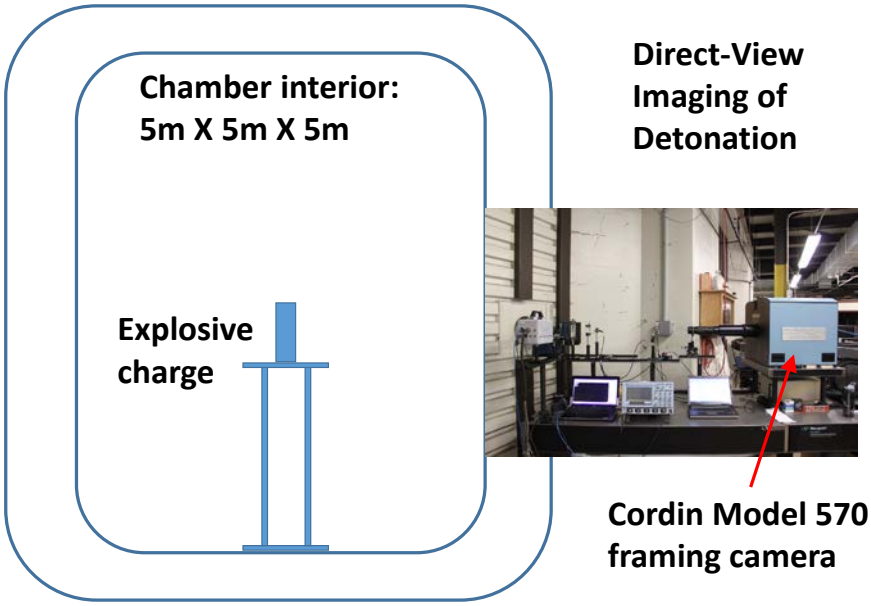

Figure 9-5: *A schematic of the charge placement within the ARL small blast chamber for testing when the Cordin Model 570 high-speed framing camera was used to verify detonation of the solid chemical explosive.*

For verification of detonation, the solid chemical explosive assembly sat on a wooden platform approximately 1.2 m from the blast chamber floor, and detonation and explosion imaged indirectly via a 20-inch square first-surface mirror through one of the chamber optical ports. This was done to maximize time before ground shock reflections disturb the detonation product expansion. A schematic of the charge within the blast chamber and position of the Cordin Model 570 digital framing camera is shown in Figure 9-5. The photo of a TNT charge

assembly, positioned on the wooden platform within the ARL small blast chamber is shown in Figure 9-6.

Figure 9-6: *The TNT charge assembly (minus detonator), positioned on the wooden platform within the ARL small blast chamber (also see Figure 9-5). This configuration was used for high-speed imaging of the detonation and explosion.*

For emission sampling of gases and particles, the explosive charge was placed on the deck (floor) of the ARL small blast chamber, to minimize wood combustion products being sampled. A schematic of the charge on the deck of the ARL small blast chamber, and the relative position of the gas and particle sampling apparatus is shown in Figure 9-7.

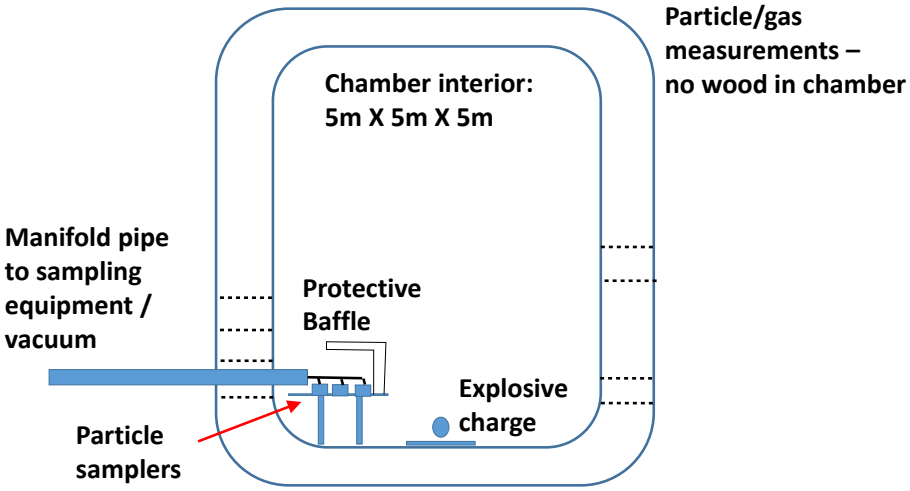

Figure 9-7: *A schematic of the charge assembly and gas and particle emission apparatus during gas and particle emission measurement.*

Figure 9-8 shows a photograph of a TNT:Mg:B explosive assembly, positioned on the deck of the blast chamber, prior to gas and particle emission measurement.

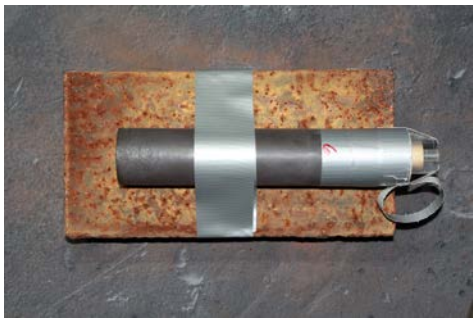

Figure 9-8: *A photograph of a TNT:Mg:B explosive assembly, positioned on the deck of the blast chamber, prior to initiation and subsequent gas and particle emission measurement.*

Emission sampling of gases and particles was accomplished via an extractive probe set through the blast chamber wall. Additionally, $PM_{2.5}$ and PM_{10} were collected inside the chamber in tandem with a second set of CO_2 and CO sensors. The sampling apparatus for emissions from detonations of solid chemical explosions is shown in Figure 9-9.

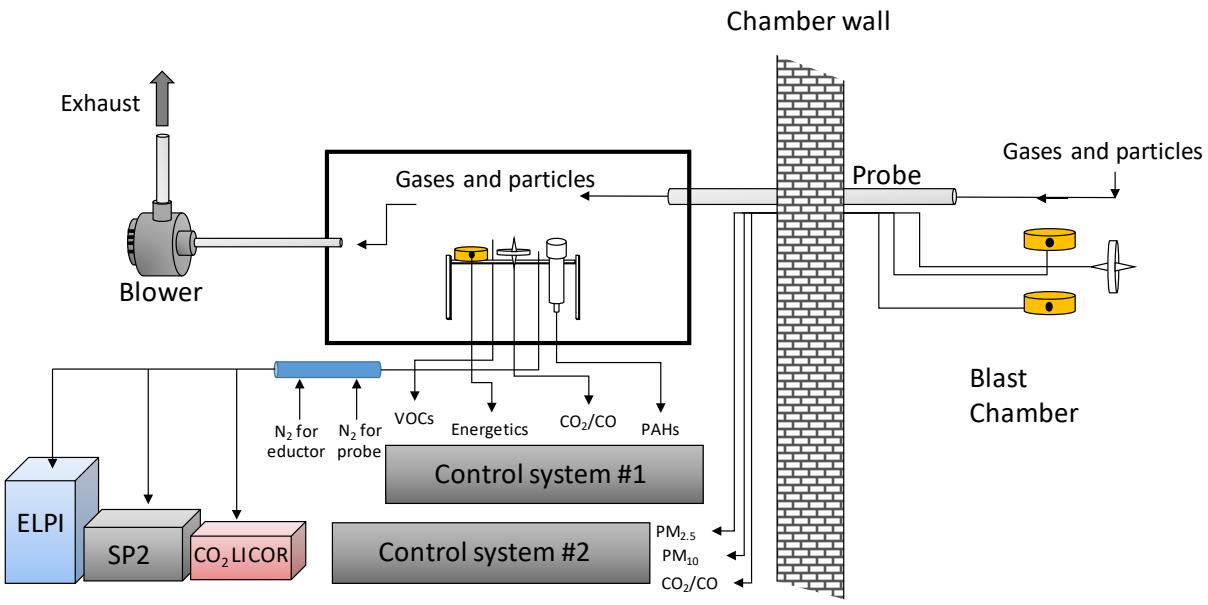

Figure 9-9: *The sampling apparatus for emissions from detonations of solid chemical explosions.*

Figure 9-10 shows a photograph of the sampling apparatus interior to the blast chamber, and a detail of this apparatus, showing the particle sample canisters and the interior CO_2 and CO sensors. Figure 9-11 is a photo of the sampling and control electronics exterior to the blast chamber.

a) **b)**

***Figure 9-10**: **a)** The sampling apparatus interior to the blast chamber. **b)** a detail of the interior sampling apparatus, showing the particle sample canisters and the interior CO_2 and CO sensors.*

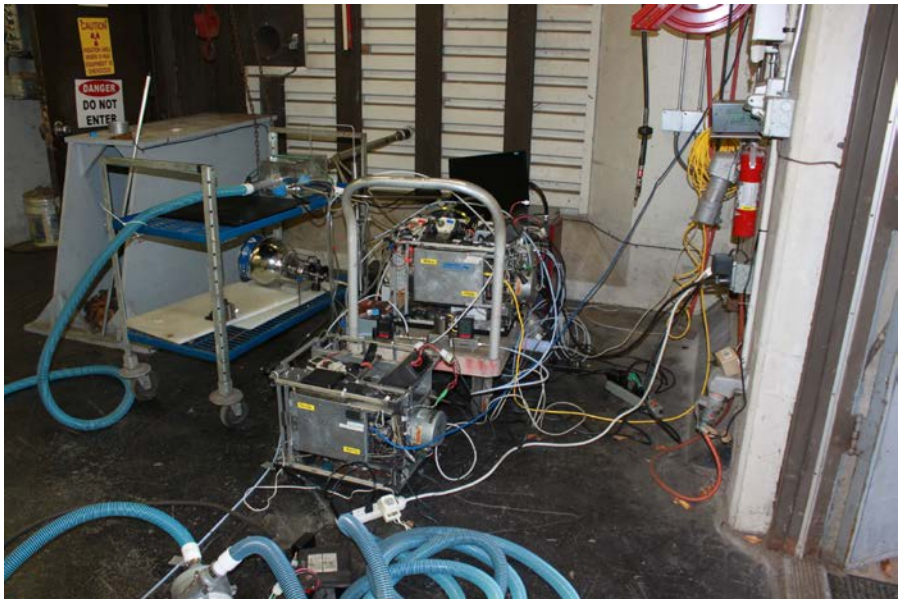

***Figure 9-11:** A photo of the sampling and control electronics, and plumbing for sample extraction, exterior to the ARL small blast chamber.*

10.Results of Simulations - Detonations of Solid Chemical Explosives

a. Prediction of Detonation Product Species of TNT – CHEETAH

As mentioned previously, the approach we employ to calculate products of TNT detonation/explosion uses CHEETAH and CHEMKIN to mimic the stages of energy release of the actual event (see Figure 7-1). The output of CHEETAH is used to simulate the first stage of TNT energy release (i.e., the detonation), and determines the input to CHEMKIN, which is used to simulate the second stage of TNT energy release (i.e., the fireball). The chemical equilibrium calculator CHEETAH (V6.0, note later versions are available) predicts the composition, density, and temperature of the initial products of the detonation prior to expansion (The "Chapman-Jouguet point"- for TNT, T= 3400K, P= 20 GPa), and the changing chemical composition for the anaerobic expansion of the detonation product gases [Cooper, 1996]. At some time after detonation, the composition of the expanding gases becomes fixed. For TNT this temperature and composition is called "freeze out", and occurs near 1800K at a pressure of 1 atmosphere. Because TNT does not contain enough oxygen to fully oxidize the carbon in the molecule, the detonation products are a fuel source [Kim, 2004]. When they mix with ambient air, an aerobic combustion reaction may occur that produces the yellow fireball associated with TNT detonation/explosion. CHEETAH will also predict the species that result when the original explosive is burned in excess air. Using CHEETAH, it is possible to predict the composition of chemical species produced when TNT detonates, TNT products expand, and TNT products burn in excess air. The balanced chemical equation for the full detonation and combustion of TNT in excess air is:

$$4\ C_7H_5N_3O_6 + 21\ O_2 = 6\ N_2 + 28\ CO_2 + 10\ H_20 \qquad \Delta H = -15\ kJ/gram \qquad \textbf{Eq. 10-1}$$

Table 10-1 shows the predicted evolution of the most prevalent (99.9% accounting) detonation products (solid and gaseous) of TNT from the C-J point (3240K, 20 GPa), to freeze out (1800K, 1 atm), as predicted by CHEETAH. The full combustion data is based on the reaction stoichiometry as shown in equation 10-1.

Table 10-1: *Detonation products for TNT at different stages of energy release, as predicted by CHEETAH 6.0.*

C-J point (3240K, 20 GPa)		Freeze Out (1800K, 1 Atm)		Full Combustion	
Species	**Mole Fraction**	**Species**	**Mole Fraction**	**Species**	**Mole Fraction**
C(gr[a])	.4311	CO	.2578	CO_2	.636
H_20	.1827	C (gr[a])	.2575	H_2O	.227
CO_2	.1516	N_2	.1549	N_2	.136
N_2	.1036	CO_2	.1426		
CHNO	.07937	H_20	.08459		
CO	.03361	CH_4	.06878		
NH_3	.01306	H_2	.02635		
CH_4	.001841	NH_3	.003647		
H_2	.001748	C_2H_6	.001561		
C_2H_4	.0005828	C_2H_4	.001193		
CH_3OH	.0003933	CHNO	.0007385		
NO	.00008430	CH_2O_2	.00009456		
C_2H_6	.00008216	CH_3OH	.00007871		
CH_2O_2	.00007333	HCN	.00007650		
H	.00001951	C_2H_2	.00004298		

gr[a]=graphite

b. Inclusion of Finite-rate Chemical Kinetics for TNT afterburn – CHEMKIN

The final chemical species actually produced by exploding TNT may not be those of full combustion [Glassman, 1987]. The final species may depend on charge confinement, available oxygen, ambient temperature, initial detonation product temperature, etc. To begin to account for these variations we use finite rate chemical kinetics to calculate air combustion of TNT detonation products when these products are mixed with ambient air at varying mixture ratios. The CHEMKIN chemical kinetic simulation code, marketed by Reaction Design Inc., is used to predict the time evolution of gas-phase chemical species in the afterburn, or fireball. The initial

chemical species and their relative amounts in the CHEMKIN calculation are those predicted by CHEETAH at freeze out (see Table 10-1). The evolution of the gas phase combustion is simulated as a function of initial temperature in a homogeneous mixture of from 1% to 50% TNT detonation products at atmospheric pressure, with the remainder air. As noted above, a more accurate chemical kinetic simulation is provided by incorporating flow dynamics, turbulence, and multiphase combustion [Kuo, 2012] (i.e., combustion of solid particles). The inclusion of these enhancements is beyond the scope of the present work.

c. Chemical Kinetic Mechanism Reduction

To perform the kinetic calculation, a chemical reaction mechanism [McNesby, 2010] was compiled that includes known reaction parameters (rate constants, activation energies) for the combustion of all species predicted by CHEETAH at freeze out for TNT detonation. This mechanism is based on the GRI-mech kinetic database, and is supplemented by the chemical combustion mechanisms found in the LLNL (Lawrence Livermore National Laboratory) explosives handbook, the SNL (Sandia National Laboratory) website, and through published articles in the peer reviewed literature [Smith, 2004]. The initial mechanism for combustion of all species predicted at freeze out for TNT contained 2032 reactions and 249 species [McNesby, 2010]. This initial chemical kinetic mechanism is too large to allow simulations over a range of input conditions, and for future inclusion of flow dynamics to include incomplete mixing. Therefore, four reduced mechanisms were compiled, with between 20 and 34 species and up to 88 reactions [Montgomery, 2006; Tomlin, 1997].

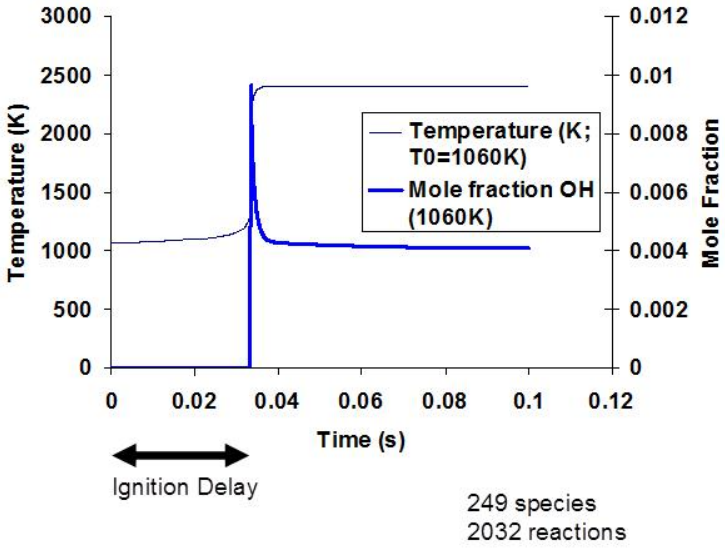

Figure 10-1: *A CHEMKIN calculation for the onset of ignition (the fireball) for the detonation products of TNT. The full reaction mechanism was used, homogeneous mixing with air (1:1 by volume), initial temperature of 1060K.*

These reduced mechanisms were compared to results of the full mechanism for ignition delay (the time it takes for the fireball to begin burning after detonation) and peak OH radical concentrations (OH is a main flame propagation radical species - see Figures 10-1 and 10-2). The reduced mechanism that produced results most consistent with those of the full mechanism was selected for the full set of calculations presented here. Although the reduced mechanism was not mandatory for the homogeneous reactor calculations we believe that it will be needed for calculations that simulate any degree of incomplete mixing [Menon 2003]. The reduced mechanism (CHEMKIN format) for combustion of TNT detonation products is provided in Appendix A.

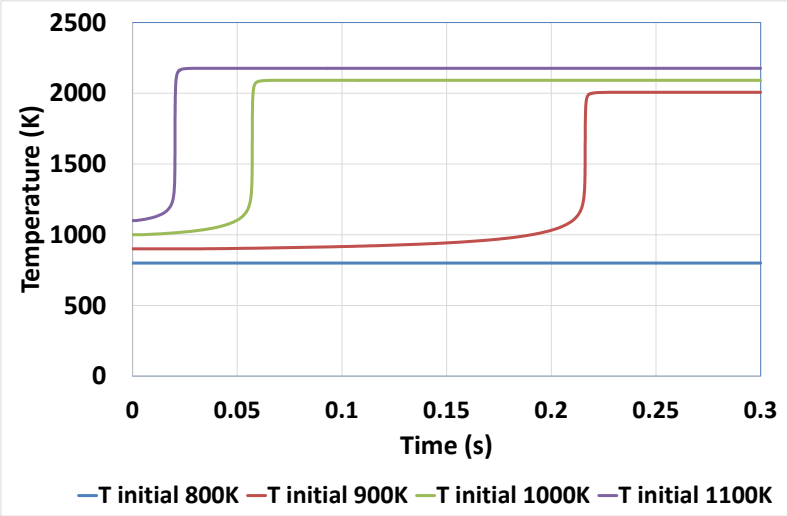

Figure 10-2: *The temperature dependence of the onset of afterburning (ignition delay) for a 1:1 by volume mixture of TNT detonation products (freeze out) and air.*

Figure 10-2 shows the temperature dependence of the ignition delay for onset of afterburn, or fireball. Note that for a temperature below 900K, the afterburn does not occur. In this case, the species present after explosion would be those predicted by CHEETAH at freeze out.

d. Combustion of Detonation Products of TNT – Results of CHEMKIN Simulations

The model homogeneous reaction vessel used by us in CHEMKIN does not include heat dissipation. Therefore, if the initial temperature is high enough, the gas phase reaction proceeds until one or more reactants is consumed. Figure 10-3 shows a bar graph of the most common gas phase species predicted by CHEMKIN before and after the afterburn (fireball) of TNT detonation products in a 1:1 mixture with air. As expected, combustion occurring in this "nascent" fireball (simulating the beginning of the second stage of energy release) further oxidizes CO and hydrocarbons to CO_2 and H_2O. In this case (the 1:1 mixture), the reactant limiting the duration of the afterburn is oxygen from ambient air.

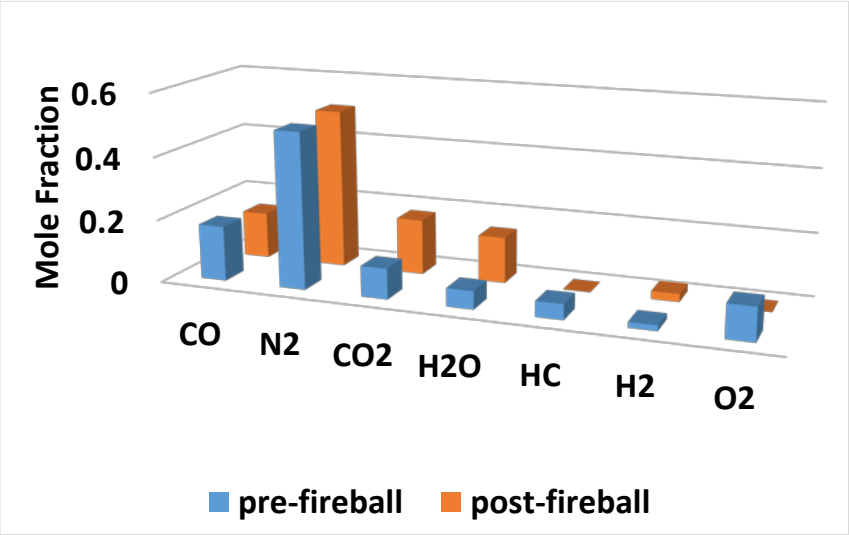

Figure 10-3: *Results of a CHEMKIN calculation of a homogeneous reactor containing a 1:1 by volume mixture of TNT detonation products and air. Initial temperature was 1060K. Pre-fireball are concentrations before combustion begins.*

Figure 10-4 shows a bar graph of the most common gas phase species predicted by CHEMKIN before and after the afterburn (fireball) of TNT detonation products in a 100 parts air:1 part TNT detonation product mixture. This simulation more closely mimics full combustion. The excess O_2 fully oxidizes CO, hydrocarbons, and H_2 to CO_2 and H_2O. In Figure 10-4, neither O_2 or N_2 mole fractions are shown. Because this figure depicts combustion of small amounts of TNT detonation products in excess air, N_2 and O_2 mole fractions are omitted because their amounts change minutely relative to actual concentration, and because their inclusion would make the mole fractions of detonation product species indistinguishable from each other in Figure 10-4.

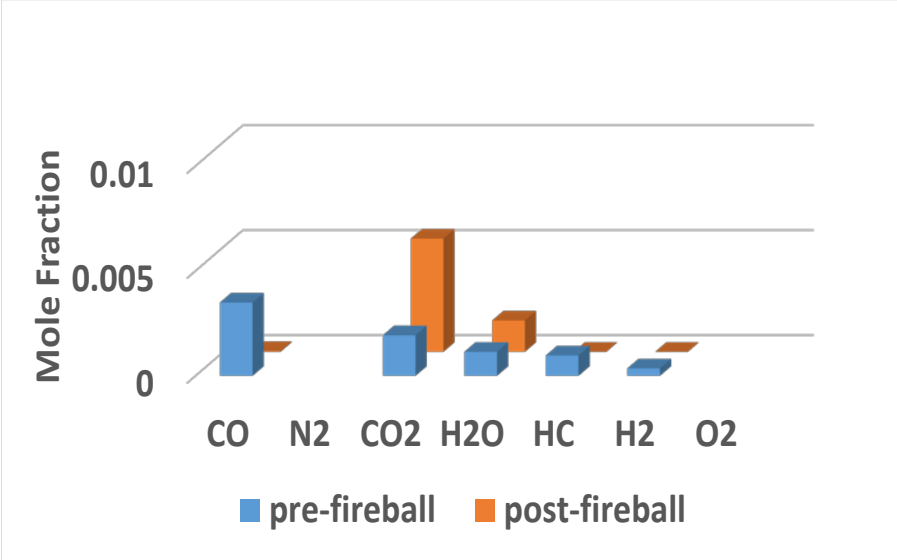

Figure 10-4: *Results of a CHEMKIN calculation of a homogeneous reactor containing a 100:1 by volume mixture of air and TNT detonation products, respectively. Initial temperature was 1000K.* N_2 *and* O_2 *are not reported on this graph (see text).*

e. Predicted Emission Factors for TNT Detonations

A comparison of emission factors, calculated using CHEETAH and CHEMKIN for detonation/explosions of TNT, based upon simulations described above, is shown in Table 10-2. The simulation of the 100:1 TNT detonation product:air emission factor is very similar to the full combustion emission factor, with the exception that the full combustion simulated emission factor (based on stoichiometry shown in equation 10-1) assumes all initial carbon is oxidized to CO_2.

Table 10-2: *Predicted Emission Factors for explosions of neat TNT (gram of emitted species per gram TNT).*

Species	CHEETAH	CHEMKIN 1:1 air	CHEMKIN 100:1 air	Full Combustion
C-graphite	0.13	0.13	0.13	
CO	0.304	0.255	0.005	
N_2	0.182	0.184	0.184	0.184
CO_2	0.264	0.476	1.17	1.36
H_2O	0.064	0.162	0.172	0.176
CH_4	0.0464	trace	trace	
H_2	0.00224	0.00311	trace	

$MCE = \Delta C_{CO2} / (\Delta C_{CO2} + \Delta C_{CO} + \Delta C_{CH4} + \Delta C_{PC}) = 0.866$

f. Prediction of Detonation Product Species of TNT:B:Mg – CHEETAH

As mentioned previously, the approach we employ to calculate products of TNT (neat, 100%) and TNT:Mg:B (80%-4%-16% by weight) detonation/explosion uses CHEETAH and CHEMKIN to mimic the stages of energy release of the actual event (see Figure 7-1). The output of CHEETAH determines the input to CHEMKIN. The chemical equilibrium calculator CHEETAH (V6.0, note later versions are available) predicts the composition, density, and temperature of the initial products of the detonation prior to expansion (The "Chapman-Jouguet point"- for TNT:Mg:B (inactive), T= 2975K, P= 7.4 GPa), and the changing chemical composition for the anaerobic expansion of the detonation product gases [Cooper, 1996].

For TNT:B:Mg, the CHEETAH calculation offers predictions for B active and for B inactive. For B active calculations, enthalpy of formation of B oxidation products are considered in the calculation (e.g., ΔH for B_2O_3, HOBO, etc.[Dreizin, 1999]). For B inactive,

[Yeh, 996] B is considered to be inert. The Mg in the explosive formulation is considered to be reactive in all CHEETAH calculations described here. As described previously for TNT, at some time after detonation, the composition of the expanding gases becomes fixed (freeze out). Because the TNT:B:Mg formulation does not contain enough oxygen to fully oxidize the carbon, B, and Mg in the formulation, the detonation products are a fuel source [Kim, 2004]. When they mix with ambient air, an aerobic reaction may occur, producing a fireball. As for neat TNT, using CHEETAH, it is possible to predict the composition of chemical species produced when the TNT:B:Mg formulation detonates, and products expand to a fixed composition. The balanced chemical equation for the detonation and combustion of TNT:Mg:B (B inactive) in oxygen is:

$$4\ C_7H_5N_3O_6 + B + 2Mg + 22\ O_2 = 6\ N_2 + 28\ CO_2 + 10\ H_20 + B + 2MgO \quad \textbf{Eq. 10-2}$$

For B active, the balanced chemical equation is:

$$4\ C_7H_5N_3O_6 + 2B + Mg + 23\ O_2 = 6\ N_2 + 28\ CO_2 + 10\ H_20 + B_2O_3 + MgO \quad \textbf{Eq. 10-3}$$

Tables 10-3 and 10-5 show the predicted evolution of the most prevalent (99.9% accounting) detonation products (solid and gaseous) of TNT:Mg:B from the C-J point (3514K, 16.9 GPa, B inert) to freeze out (1800K, 1 atm), for B inactive and B active, respectively. Also shown are the product mole fractions based upon equations 10-2 and 10-3, respectively.

Table 10-3: *Detonation products for TNT:B:Mg (80:4:16 by weight, B inactive) at different stages of energy release, as well as products based on reaction stoichiometry (Eq. 10-2).*

C-J point (3514K, 16.9 Pa)		Freeze Out (1800K, 1 Atm)		Full Combustion	
Species	**Mole Fraction**	**Species**	**Mole Fraction**	**Species**	**Mole Fraction**
C(gr[a])	.3354	CO	.3131	CO_2	.47
H_20	.1204	C (gr[a])	.1365	H_2O	.169
CO_2	.06704	N_2	.1130	N_2	.101
N_2	.08052	CO_2	.01948	MgO	.079
CHNO	.04457	H_20	.01488	B	.178
CO	.05129	CH_4	.05785		
NH_3	.01240	H_2	.05299		
CH_4	.004711	NH_3	.0009868		
H_2	.004455	C_2H_6	.0006369		
C_2H_4	.002061	C_2H_4	.001167		
CH_3OH	.0005025	CHNO	.0001106		
NO	.00007832	CH_2O_2	trace		
C_2H_6	.0002948	CH_3OH	trace		
CH_2O_2	.0001280	HCN	.0007358		
H	.00005574	C_2H_2	.0001708		
MgO (s[b])	.08492	MgO (s[b])	.08875		
B (s)	.1909	B (s[b])	.1995		

gr[a]=graphite; s[b]=solid

Table 10-4: *Calculated Emission Factors (gram of emitted species per gram TNT:Mg:B) and MCE, for neat TNT:Mg:B (80:4:16 by weight), B inactive.*

Species	CHEMKIN 100:1 air	Full Combustion
C (gr[a])	0.076	
CO	0.00026	
N_2		0.184
CO_2	0.803	1.36
B	0.1	0.1
MgO	0.165	0.166
H_2O	0.165	0.198
CH_4	trace	
H_2	trace	

gr[a] = graphite

$$MCE = \Delta C_{CO2} \; / \; (\Delta C_{CO2} + \Delta C_{CO} + \Delta C_{CH4} + \Delta C_{PC}) = 0.74$$

Table 10-5: *Detonation products for TNT:Mg:B (80:4:16 by weight, B active) at different stages of energy release, as well as products based on reaction stoichiometry (Eq. 10-3).*

C-J point (3746K, 16.9 GPa)		Freeze Out (1800K, 1 Atm)		Full Combustion	
Species	**Mole Fraction**	**Species**	**Mole Fraction**	**Species**	**Mole Fraction**
C(gr[a])	.03955	CO	.3642	CO_2	.519
H_20	.03643	C (gr[a])	.1538	H_2O	.185
CO_2	.002121	N_2	.01385	N_2	.111
N_2	.1102	CO_2	.0002987	B_2O_3	.098
CHNO	.01013	H_20	.0005218	MgO	.087
CO	.02226	CH_4	.009040		
NH_3	.02917	H_2	.1690		
HOBO	.007589	HCN	.001039		
C_2H_2	.001033	C_2H_2	.0007332		
NO	.00007832	HOBO	.0001096		
CH_4	.03052	NH_3	trace		
H_2	.02056	C_2H_6	trace		
C_2H_4	.01633	C_2H_4	.0001953		
CH_3OH	.0005025	CHNO	trace		
C_2H_6	.003131	CH_2O_2	trace		
CH_2O_2	.0001280	CH_3OH	trace		
H	.00005574	HCN	.001039		
MgO (s[b])	.08492	C_2H_2	.0007332		
B (s[b])	.1909	MgO (s[b])	.08849		
C (l[c])	.4588	BN (s[b])	.1985		
B_2O_3 (l[c])	.1099	B_2O_3 (l[c])	.0001562		
MgO (l[c])	.1012				

gr[a]=graphite; s[b]=solid; l[c]=liquid

Tables 10-4 and 10-6 show emission factors (EF's) and modified combustion effiency (MCE's) based upon CHEMKIN input derived from Table 10-5.

Table 10-6: *Calculated Emission Factors (gram of emitted species per gram TNT:Mg:B) and MCE, for TNT:Mg:B (80:4:16 by weight), B active.*

Species	CHEMKIN 100:1 air	Full Combustion
C (gr[a])	0.086	
CO	0.00014	
N_2		0.184
CO_2	0.768	1.36
B		
MgO	0.165	0.166
H_2O	0.158	0.198
CH_4	trace	
H_2	trace	
BN	0.23	
B_2O_3		0.644

gr[a]=graphite

$$MCE = \Delta C_{CO2} / (\Delta C_{CO2} + \Delta C_{CO} + \Delta C_{CH4} + \Delta C_{PC}) = 0.71$$

11. Results of Experiments - Detonations of Solid Chemical Explosives

a. Emissions of CO_2, CO, and CH_4

Major gaseous carbon species are listed in Table 11-1 for explosions of neat TNT and for the TNT:Mg:B explosive formulation (80:4:16 by weight). For each explosive tested, initial C oxidation to CO_2 was near complete. Shot to shot variation was minor as seen by low RSD and RPD values.

Table 11-1: *CO_2, CO, and CH_4 emission factors as well as modified combustion efficiency.*

Compound	TNT			TNT MgB		
	n[a]	Average g/kg fuel	RPD[b] %	n[a]	Average g/kg fuel	RPD[b] %
CO_2	2	1,314	0.65	2	1,117	1.5
CO	2	17	32	1	15	16
CH_4	2	ND[c]	N/A[d]	2	0.16	N/A[d]
		Average Fraction			**Average Fraction**	
MCE[e]	2	0.980	0.66	2	0.979	0.35

[a] Number of samples collected. [b] RPD = relative percent difference, calculated when n=2. [c] ND = not detected. [d] N/A = not applicable. [e] MCE = modified combustion efficiency ($\Delta CO_2/(\Delta CO_2+\Delta CO+\Delta CH_4)$).

b. Solid Chemical Explosives Emission Factors – Particulate Matter (PM)

PM emission factors for the detonations are shown in Table 11-2 and Figure 11-1. RSD and RPD values below 23% indicate excellent test to test precision. The PM_{10} values found here for TNT, 61 g/kg, compare with previous values determined by an aerostat-lofted instrument package in the field (130 g/kg NEW, [Aurell, 2011]) and laboratory scale (BangBox) studies 73 g/kg [Mitchell, 1998]. Field values were most certainly elevated due to TNT detonation on the surface of a fine, sandy soil resulting in considerable entrainment of background particles. The addition of Mg:B powder to the TNT increases the PM emissions by a factor of 8 and 3 for $PM_{2.5}$ and PM_{10}, respectively.

Table 11-2: *PM emission factors from small detonations of TNT and TNT-MgB.*

PM size	Ordnance	n[a]	Average g/kg fuel	Stand. Dev. g/kg fuel	RSD[b] %	RPD[c] %
$PM_{2.5}$	TNT	2	22	0.48	2.2	
PM_{10}	TNT	2	61			23
$PM_{2.5}$	TNT MgB	3	166	89	53	
PM_{10}	TNT MgB	2	204			23

[a] Number of samples collected. [b] RSD = relative standard deviation, calculated when n=3 or more. [c] RPD = relative percent difference, calculated when n=2.

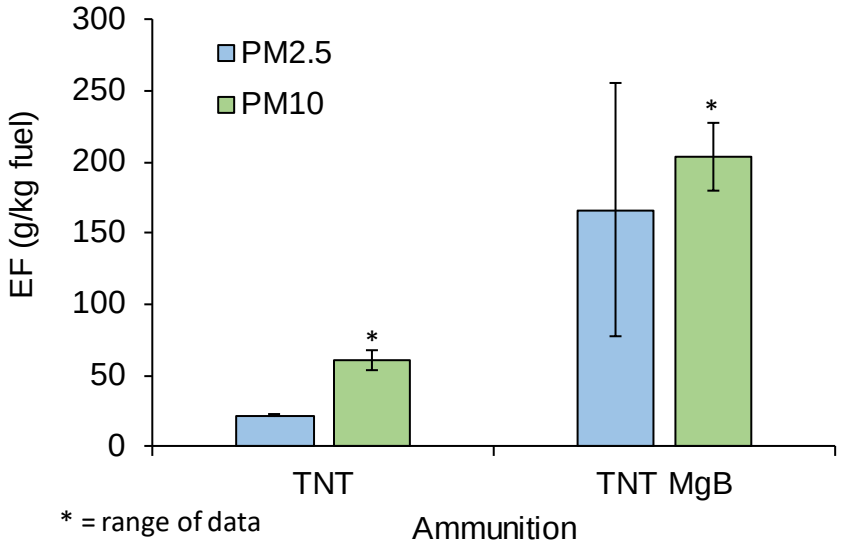

Figure 11-1: *PM emission factors from TNT and TNT:Mg:B. Error bars represent 1 standard deviation if nothing else stated.*

c. Solid Chemical Explosives Emission Factors - Elements

Elemental emissions were found in collected particles. Boron (B) was the most abundant element in particles from explosions of TNT:Mg:B (64.18±34.35 g/kg fuel) and considerably

larger than for explosions of neat TNT (0.199±0.007 g/kg fuel), see Figure 11-2 and Tables 11-3 and 11-4. The levels of magnesium (Mg) were also higher in the TNT:Mg:B plumes (5.20±2.48 g/kg fuel) than from the TNT plumes (0.034±0.014 g/kg fuel). Although, these Mg levels were low in most of the samples with levels less than three times the uncertainty of the analytical method. One of the three TNT tests was conducted after the TNT/Mg/B tests as a control to test for potential residual contamination of the facility. The levels of B and Mg in the last TNT plume sample were approximately 15 times higher than in the two TNT plumes conducted prior to the TNT/Mg/B tests, indicating contamination of chamber wall by previous tests. Iron (Fe) levels were relatively high in all samples, most likely originating from the walls of the detonation chamber. This is most likely also true of other elements found in the collected plume samples.

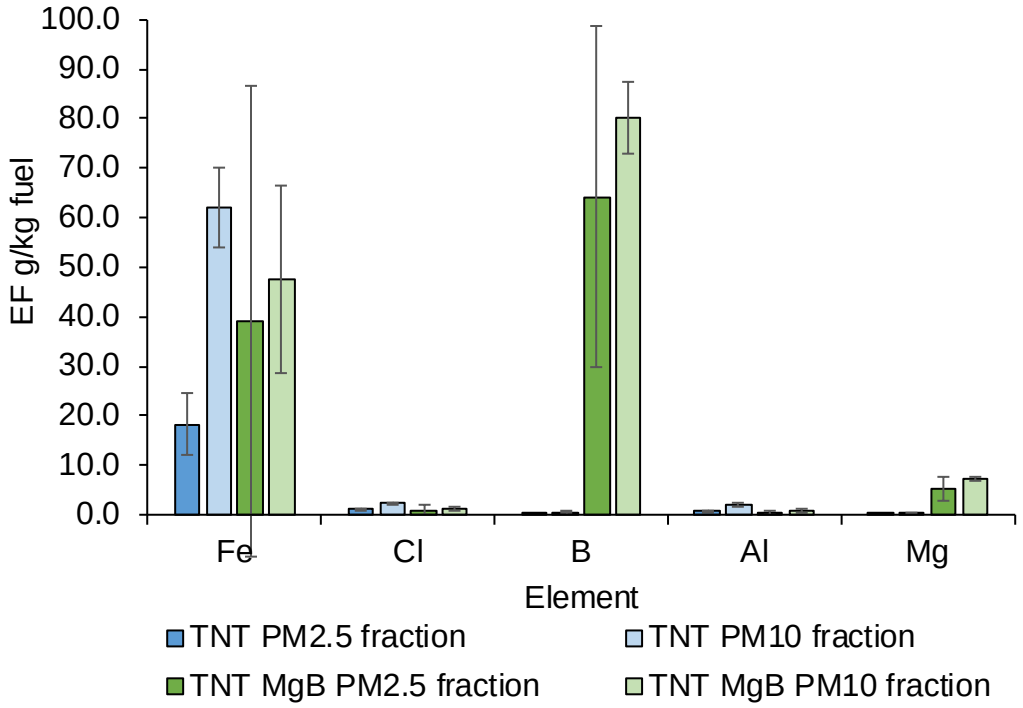

Figure 11-2: *Element emission factors from detonation of TNT and TNT:Mg:B.*

Table 11-3: *TNT element emission factors.*

Metal	$PM_{2.5}$				PM_{10}		
	n[a]	Average g/kg fuel	Stand. Dev. g/kg fuel	RSD[b] %	n[a]	Average g/kg fuel	RPD[c] %
Fe	3	18.261	6.197	34	2	62.134	26
Cl	3	1.248	0.105	8.4	2	2.542	7.6
B	2	0.199		7.1	2	0.503	95
Al	3	0.750	0.198	26	2[d]	2.09	49
Cu	3	0.256	0.137	54	2	0.315	29
Mg	2[d]	0.034		86	2[e]	0.205	106
Mn	3	0.221	0.030	14	2	0.589	33
Zn	3	0.167	0.010	6.1	2	0.304	28
Ba	3	0.0482	0.0241	50	2	0.126	54
Ni	3	0.0460	0.0141	31	2	0.138	27
Sb	3	0.0427	0.0215	50	2	0.048	11
Cr	3	0.0345	0.0089	26	2	0.110	15
Pb	3	0.0197	0.0039	20	2	0.028	32
Bi	3	0.0114	0.0061	53	2[d]	0.015	79

[a] Number of samples collected. [b] RSD = relative standard deviation, calculated when n=3 or more. [c] RPD = relative percent difference, calculated when n=2. [d] Some values were less than three times the uncertainty of the analytical method. [e] All values were less than three times the uncertainty of the analytical method.

Table 11-4: *TNT:Mg:B element emission factors.*

Element	$PM_{2.5}$ n[a]	Average g/kg fuel	Stand. Dev. g/kg fuel	RSD[b] %	PM_{10} n[a]	Average g/kg fuel	RPD[c] %
Fe	3	39.101	47.345	121	2	47.496	80
Cl	3	1.001	0.924	92	2	1.242	61
B	3	64.180	34.350	54	2	80.051	18
Al	3[d]	0.394	0.300	76	2[e]	0.84	68
Cu	3	0.169	0.135	80	2	0.243	40
Mg	3[d]	5.197	2.483	48	2[e]	7.331	11
Mn	3	0.321	0.364	113	2	0.421	72
Zn	3	0.197	0.142	72	2	0.271	30
Ba	3	0.1040	0.0872	84	2	0.113	69
Ni	3	0.0751	0.0833	111	2	0.105	67
Sb	3	0.0253	0.0159	63	2	0.038	57
Cr	3	0.0710	0.0892	126	2	0.084	94
Pb	3	0.0182	0.0126	69	2	0.027	4.0
Bi	2	0.0037		22[c]	2	0.002	113
		Average	**Stand. Dev**			**Average**	
		g/kg element in fuel				**g/kg element in fuel**	
B	3	822.0	439.9	54	2	235.1	18
Mg	3[d]	66.6	31.8	48	2[e]	141.4	11

[a] Number of samples collected. [b] RSD = relative standard deviation, calculated when n=3 or more. [c] RPD = relative percent difference, calculated when n=2. [d] Some values were less than three times the uncertainty of the analytical method. [e] All values were less than three times the uncertainty of the analytical method.

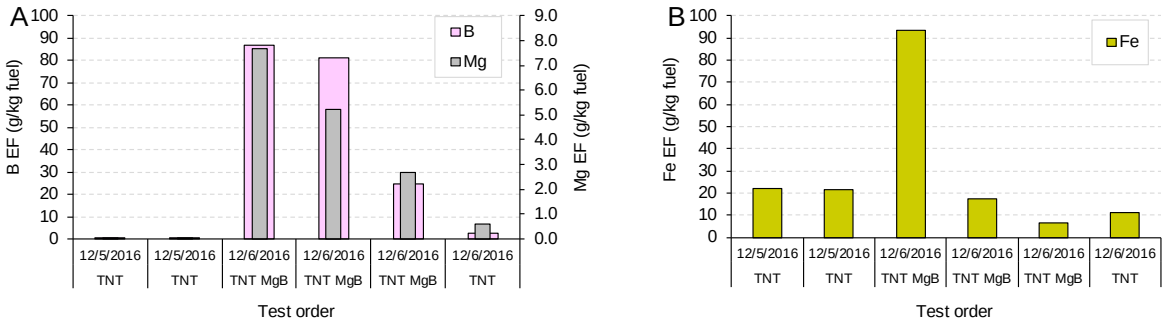

Figure 11-3: *Boron, Magnesium (graph A), and Fe (graph B) emission factors in test order.*

d. Solid Chemical Explosives Emission Factors VOCs

The most abundant VOC was methyl methacrylate followed by chloromethane and benzene from both TNT and TNT:Mg:B (80:4:16 by weight). The methyl methacrylate originates most probably from the PMMA centering device for the TNT cylinders. The benzene value from TNT (23.84 mg/kg fuel) was lower than previously found from open detonation of TNT sampled from an aerostat based sampling package (220 mg/kg fuel [Aurell, 2011]) and from an airplane (96 mg/kg fuel [AMCCOM, 1992]) during open detonations but higher than from Bangbox testing of TNT (4.07 mg/kg [AP, 2009]). A VOC analysis on a TNT (only) test after the TNT MgB testing was not done due to an insufficient number of canisters. Future tests should incorporate these test checks to ensure that observed reductions in VOCs (e.g., ethanol) are due to formulation changes rather than facility wall contamination from prior projects.

Table 11-5: *VOC emission factors from small scale detonations of TNT and TNT:Mg:B (80:4:16 by weight).*

	TNT			TNT MgB		
	n[b]	Average mg/kg fuel	RPD[c] %	n[b]	Average mg/kg fuel	RPD[c] %
Chloromethane[a]	2	35.44	1.4	2	27.35	33
Vinyl Chloride[a]	2	11.84	46	2	9.56	21
1,3-Butadiene[a]	2	3.96	72	2	4.10	3.5
Bromomethane[a]	2	1.39	26	1	0.69	
Chloroethane[a]	2	0.94	22	1	0.71	
Ethanol	1	22.10		0	ND[d]	
Acetonitrile	2	18.13	33	2	12.71	31
Acrolein[a]	2	52.41	30	2	42.06	33
Acetone	1	23.14		0	ND[d]	
Trichlorofluoromethane	1	0.11		1	0.10	
Acrylonitrile[a]	2	8.01	47	2	5.71	32
1,1-Dichloroethene	2	0.53	18	0	ND[d]	
3-Chloro-1-propene (Allyl Chloride) [a]	2	3.92	39	2	2.09	21
Carbon Disulfide[a]	2	5.57	115	0	ND[d]	
Vinyl Acetate[a]	2	2.63	30	0	ND[d]	
2-Butanone[a] (MEK)	2	2.08	17	2	1.81	19
Chloroform[a]	2	0.81	17	1	0.74	
Tetrahydrofuran (THF)	2	0.60	28	0	ND[d]	
Benzene[a]	2	23.84	30	2	17.88	21
Carbon Tetrachloride[a]	2	0.58	12	1	0.50	
Trichloroethene	1	0.36		1	0.34	
Methyl Methacrylate[a]	2	1,597	17	2	1,675	14
2-Hexanone	2	0.48	30	0	ND[d]	
Chlorobenzene[a]	2	1.93	48	2	1.34	27
Styrene[a]	1	5.88		2	4.48	168
Benzyl Chloride[a]	2	0.69	55	1	0.47	

[a] On EPA's list of hazardous air pollutants. [b] number of samples with detectable levels. [c] RPD = relative percent difference, calculated when n=2. [d] ND = not detected.

e. Solid Chemical Explosives Emission Factors - Energetics

Detectable levels of HMX and RDX were found from both TNT and TNT:Mg:B. TNT:Mg:B also showed detectable levels of the base explosive TNT – indicating some of the

material did not react. Previous bangbox [AP-42, 2009] studies showed no detectable levels of energetics from TNT while TNT and dinitrotoluene (DNT) were found in the plumes of open detonation of TNT [AP-42, 2009]. It is also conceivable that some of the detected RDX/HMX came from the chamber walls.

***Table 11-6**: Energetics emission factors from small scale detonations of TNT and TNT:Mg:B (80:4:16 by weight).*

	TNT mg/kg fuel	**TNT MgB mg/kg fuel**
1,3,5-Trinitrobenzene	<5.61	<4.47
1,3-Dinitrobenzene	<5.61	<4.47
2,4,6-Trinitrotoluene	<5.61	2.97 (35%)[a]
2,4-Dinitrotoluene	<5.61	<4.47
2,6-Dinitrotoluene	<5.61	<4.47
2-Amino-4,6-Dinitrotoluene	<5.61	<4.47
2-Nitrotoluene	<5.61	<4.47
3,5-DNA	<5.61	<4.47
3-Nitrotoluene	<5.61	<4.47
4-Amino-2,6-Dinitrotoluene	<5.61	<4.47
4-Nitrotoluene	<5.61	<4.47
HMX	20.95 (46%)[a]	6.19 (56%)[a]
Nitrobenzene	<5.61	<4.47
Nitroglycering	<5.61	<4.47
PETN	<14.03	<11.17
RDX	46.35 (42%)[a]	9.79±4.18[b] (43%)[c]
Tetryl	<5.61	<4.47

[a] Relative percent difference
[b] 1 standard deviation
[c] Relative standard deviation

f. Solid Chemical Explosives Emission Factors - PAH's

Fourteen of the sixteen EPA PAHs were detected (Table 11-6). No statistical difference was found between TNT and TNT:Mg:B ($p=0.14$, $F = 0.4$), although the statistical analysis is based on only two replicates for the TNT (three or more replicates are preferred). The TNT emission

factors for PAH's in this study were on average 3.4 and 2.5 times lower than previously found emission factors from open detonation of TNT sampled using an aerostat [Aurell, 2011] and airplane [AMCCOM, 1992], respectively. This may be due to the significant difference in charge size (~0.8 kg here versus 45 kg with the aerostat [CFR App. J, 2014]).

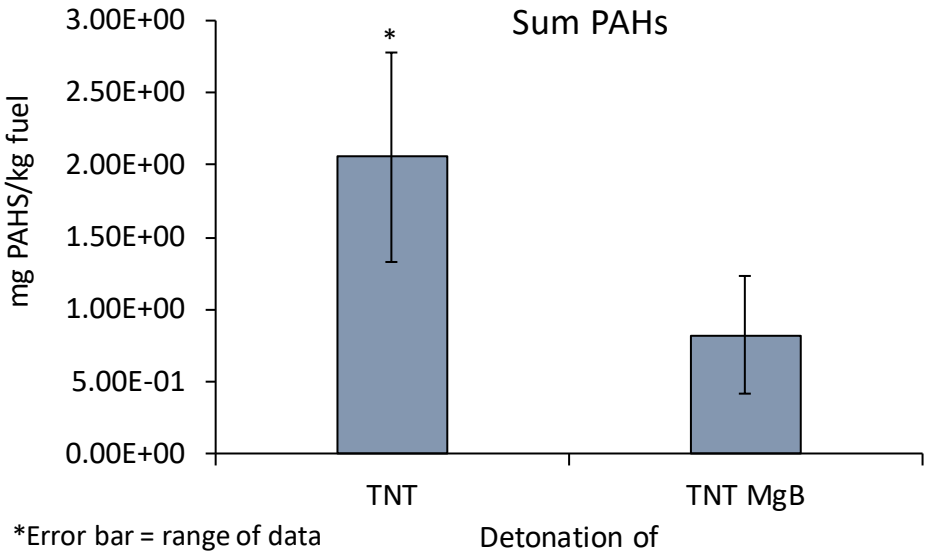

Figure 11-4: *PAH emission factors from detonation of TNT and TNT:Mg:B. Error bars represents 1 Stand. Dev.*

Table 11-7: *PAH emission factors from small scale detonations of TNT and TNT:Mg:B (80:4:16 by weight).*

	TNT			TNT/Mg/B				
	n=2	**n=2**	**RPD**	**n=3**	**STDV**	**n=3**	**STDV**	**RSD**
Targets	**mg/kg fuel**	**mg B[a]P TEQ/kg fuel**	**%**	**mg/kg fuel**		**mg B[a]P TEQ/kg fuel**		**%**
Naphthalene	1.08E+00	N/A[b]	68	4.88E-01	2.64E-01	N/A[b]	N/A[b]	54
Acenaphthylene	5.17E-02	N/A[b]	104	1.30E-02	5.65E-03	N/A[b]	N/A	43
Acenaphthene	ND[a]	N/A[b]	N/A[b]	ND[a]	N/A[b]	N/A[b]	N/A[b]	N/A[b]
Fluorene	ND[a]	N/A[b]	N/A[b]	ND[a]	N/A[b]	N/A[b]	N/A[b]	N/A[b]
Phenanthrene	3.97E-01	1.99E-04	93	1.59E-01	6.79E-02	7.97E-05	3.39E-05	43
Anthracene	3.97E-02	1.98E-05	13	1.10E-02	4.67E-03	5.50E-06	2.33E-06	42
Fluoranthene	1.54E-01	7.72E-03	72	4.50E-02	2.06E-02	2.25E-03	1.03E-03	46
Pyrene	1.05E-01	1.05E-04	66	2.41E-02	1.16E-02	2.41E-05	1.16E-05	48
Benzo(a)anthracene	2.97E-02	1.49E-04	50	7.24E-03	3.16E-03	3.62E-05	1.58E-05	44
Chrysene	6.74E-02	2.02E-03	62	1.95E-02	1.09E-02	5.85E-04	3.27E-04	56
Benzo(b)fluoranthene	4.14E-02	4.14E-03	46	2.39E-02	6.16E-03	2.39E-03	6.16E-04	26
Benzo(k)fluoranthene	3.17E-02	1.59E-03	57	6.80E-03	3.51E-03	3.40E-04	1.75E-04	52
Benzo(a)pyrene	1.46E-02	1.46E-02	18	ND	N/A	ND	N/A	N/A
Indeno(1,2,3-cd)pyrene	1.95E-02	1.95E-03	8	1.01E-02	3.42E-03	1.01E-03	3.42E-04	34
Dibenz(a,h)anthracene	5.06E-03[c]	2.78E-03[c]	N/A[b]	4.50E-03	3.21E-03	4.95E-03	3.53E-03	71
Benzo(ghi)perylene	2.12E-02	4.25E-04	3	8.86E-03	2.61E-03	1.77E-04	5.22E-05	29
SUM 16-EPA PAHs	2.06E+00	3.57E-02	70	8.22E-01	4.06E-01	1.18E-02	6.12E-03	49

[a] ***ND = not detected.*** [b] ***N/A= not applicable. Naphthalene, acenapththylene, acenaphthene and fluorene have not been assigned a toxic equivalent number.*** [c] ***n=1***

g. Solid Chemical Explosives Emission Factors – Particle Size Distributions

The initial normalized mass weighted size distribution of the emissions from detonations are shown in Figure 11-5. The mass weighted particle size distributions for both detonations extended above the range of the ELPI, which was limited to particles less than 6 µm. The number distributions (Figure 11-6) were within the instrument range and exhibited a lognormal shape. The TNT detonation exhibited a bimodal distribution with the first peak appearing below the range of the ELPI (< 0.02 µm) and a second peak at 0.63 µm. The TNT:Mg:B detonation exhibited a trimodal distribution with a peak at approximately 0.04 µm, 0.11 µm, and at 0.53 µm. The larger size modes dominate the mass distribution and result in a mass median diameter of 4.3 µm for the TNT:Mg:B detonation and 1.4 µm for the TNT detonation. These mass weighted particle size distribution are consistent with the filter results showing larger PM_{10} emission factors as compared to $PM_{2.5}$.

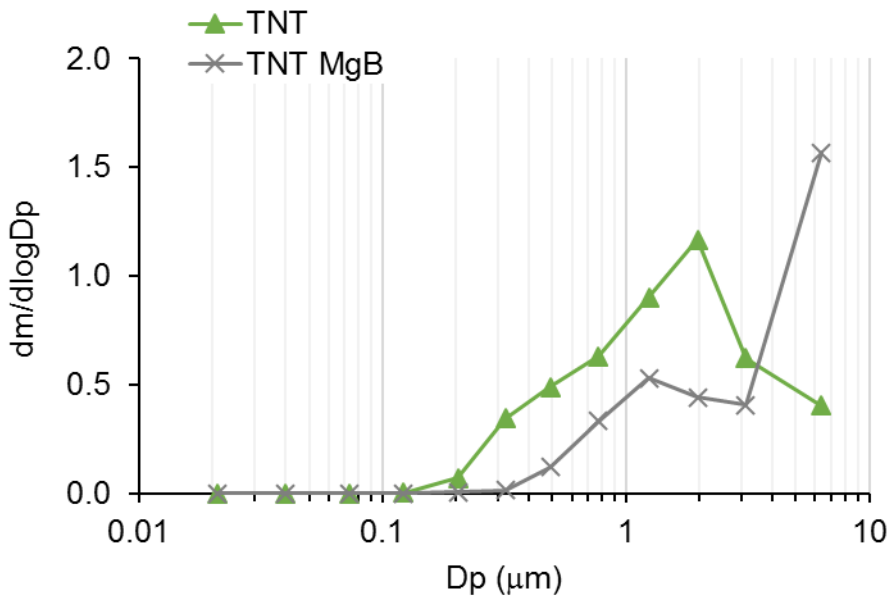

Figure 11-5: *Representative initial mass normalized mass weighted PM size distributions for detonations.*

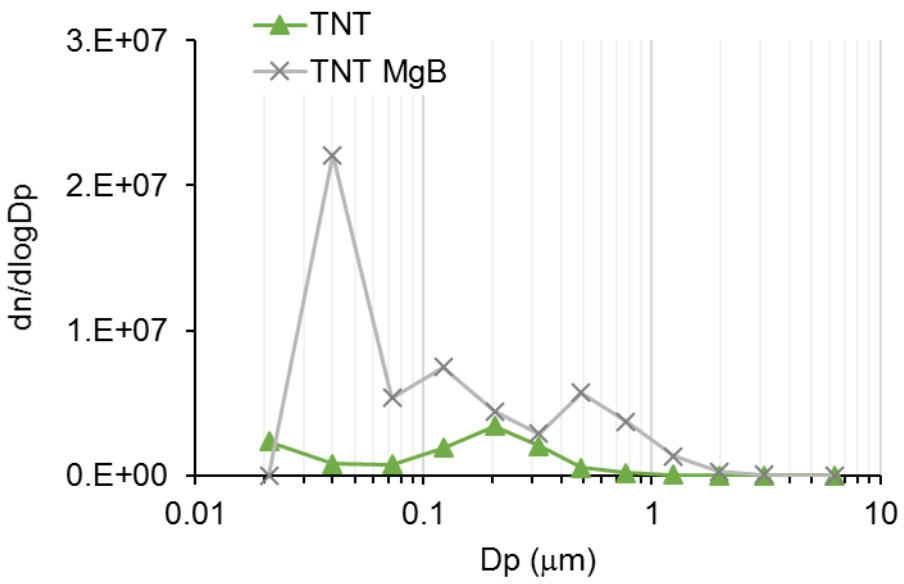

Figure 11-6: *Normalized number weighted PM size distributions corresponding to mass weighted size distributions in the figure above.*

The initial size distribution evolved over the first minute as the particles aggregated causing a shift towards larger diameter particles (Figure 11-7). The smaller size modes decreased in number concentration as the larger size modes increased until eventually the aerosol was just a single large mode.

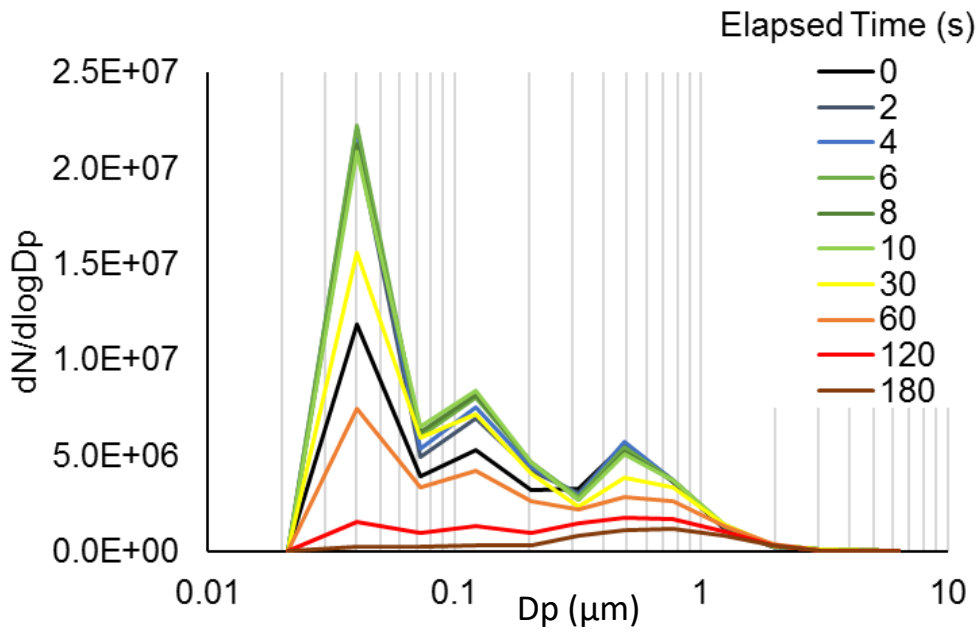

Figure 11-7: *PM number distributions from TNT:Mg:B detonation over the first 3 minutes after the blast.*

The color ratio of incandescing particles emitted from detonations is shown in Figure 11-8. The color ratio for TNT detonations had a bimodal distribution, indicating that two different incandescing particle types were present in the emissions. The TNT:Mg:B detonation had a single mode distribution. As with the gun blasts, these results suggest that the SP2 color ratio may be used for some emissions to distinguish between particles of different composition, although further study is needed.

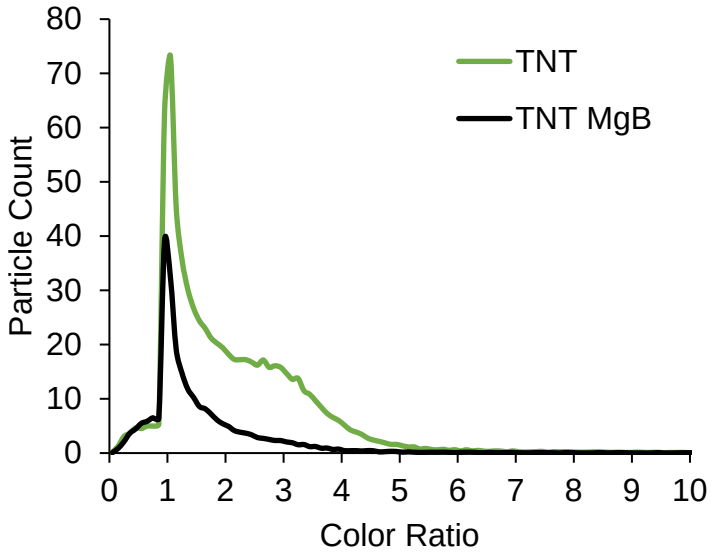

Figure 11-8: *Color ratio for incandescing particles in the emissions from TNT and TNT:Mg:B detonations.*

12. Discussion - Detonations of Solid Chemical Explosives

Tables 12-1 and 12-2 summarize simulation and measurement of emission factors (EF's) and modified combustion efficiency's (MCE's) for detonation/explosions of TNT and TNT:Mg:B (80:4:16 by weight). In general, there is reasonable agreement between experiment and simulation values for MCE (approximately 14% to 27%), with the largest error for the B active simulation. We believe the main source of error between simulation and experiment, for the present work, is our inability to include heterogeneous combustion (i.e., burning of particles) in the CHEMKIN calculations. Since the CHEETAH calculations predict up to 0.35 mole fraction graphitic carbon for detonations of TNT, this is a source of non-reactive carbon, lowering the simulated MCE relative to the measured value.

Table 12-1: *Modified Combustion Efficiency (MCE) for detonation / explosion of TNT and TNT:Mg:B (80:4:16 by weight) with B inactive and active, simulated and measured.*

	MCE
TNT	0.98 (0.66)
TNT/Mg/B	0.979 (0.35)
TNT simulation	0.866
TNT/Mg/B (B inactive) simulation	0.74
TNT/Mg/B (B active) simulation	0.71

Table 12-2: *Emission Factors for detonation / explosion of TNT and TNT:Mg:B (80:4:16 by weight) with B inactive and active, simulated and measured.*

Compound	TNT			TNT MgB			TNT simulated	TNT/Mg/B simulated B inactive	TNT/Mg/B Simulated B active
	n[a]	Average g/kg fuel	RPD[b] %	n[a]	Average g/kg fuel	RPD[b] %	g/kg fuel	g/kg fuel	g/kg fuel
CO_2	2	1,314	0.65	2	1,117	1.5	1,170	803	860
CO	2	17	32	1	15	16	5	.26	.14
CH_4	2	ND[c]	N/A[d]	2	0.16	N/A[d]	trace	trace	trace

[a] Number of samples collected. [b] RPD = relative percent difference, calculated when n=2. [c] ND = not detected. [d] N/A = not applicable. [e] MCE = modified combustion efficiency ($\Delta CO_2/(\Delta CO_2+\Delta CO+\Delta CH_4)$).

This is also evident in the measured and predicted emission factors for CO_2. If the CHEMKIN calculations included heterogeneous combustion (i.e., if particle combustion was included) we believe that the CHEMKIN simulation will provide a good estimate of the afterburn occurring in the blast chamber.

13. Conclusions/Recommendations/Implications for Future Research

This work has demonstrated simulation approaches and experimental methodologies for comprehensive estimation and sampling of emissions from metal-based energetics under conditions that simulate potential warfighter exposure. Simulations used an approach based on verified stages of energy release. Tests firing an M4 carbine and detonating metallized TNT charges examined the effect of propellant and explosive formulations on emissions. Emphasis was placed on a comprehensive array of samplers to determine emission characterization, repeatability, and an

ability to discern effects of changing metal formulations. Measurement technologies were successful, resulting in high precision between replicates and comparable values with the limited available field data. Where available, measured emission factors compared well with simulation and previous studies, either by this group or elsewhere. Emission factors determined from this work can be used in activity models to determine warfighter exposure.

a. M4

Emissions from the M4 carbine firing M855 ammunition exhibited average CO concentrations around 1500 ppm after firing, suggesting that inhalation studies on firing ranges may be warranted. Emitted particles had mass median diameters between 0.389 and 0.575 µm, a respirable particle size. With particle agglomeration, these sizes increase but are still less than 2 µm after 120 s. Three different round types were tested; differences in PM emission factors could be observed due to the low relative standard deviation (10%), indicating the precision of the method. PM was highest from the 855 Salted round, likely due to incomplete secondary combustion in the muzzle blast, caused by addition of K to scavenge combustion radicals. Cu was the metal observed in highest concentration for all three round formulations; it originated from the copper jacket on the bullet. More than 100% of the Pb in the propellant formulations was observed to be emitted for all three round types. This could be due to contributions by the copper-jacketed lead slug, and to combined error of sampling and the determination of the formula composition. The same issue was observed for Bi on all but the legacy rounds. The methodology for sampling volatile organic compounds successfully detected residual gases from the initial fracturing of the PMMA M4 carbine chamber and the glass cleaner used to clean the box interior between shots. No residual energetics were detected at levels typically less than 19.8 mg/round.

Simulations of emission factors provided reasonable results, and in all cases differed from experimental measurements by a maximum of a factor of two. For the NASA-Lewis based simulation, predicted MCE differed from measured MCE by approximately 30% (0.732 predicted versus 0.5 measured for salted rounds). We believe that improved estimates of emission factors for chemical species during M4 weapon firing will result from the combination of accurate flow dynamics, improved IB thermodynamic calculations, with incorporation of a chemical kinetic mechanism to simulate muzzle flash. We believe this report makes a reasonable case to continue this effort along those lines, combining experimental evidence with modeling predictions.

b. TNT

Emissions from the TNT detonations indicated combustion efficiencies of about 98%. Comparison of PM emission factors show that our laboratory results, while consistent with others, are half that of our field values, likely due to detonations in the field entraining sandy soil. The addition of Mg:B to the TNT formulations significantly increased the $PM_{2.5}$ emission by a factor of 8. As expected, Pb emission factors are unaffected by the presence of Mg:B; emission factors only differed by 4% - in fact, lead may be coming from blast chamber walls, as there was no lead in the explosive train, including the RP-80 detonator. The sensitivity of the VOC sampling was again observed through detection of PMMA from the TNT cylinder centering device. Residual TNT, HMX, and RDX were detected.

The simulation of emission factors using a combination of thermodynamic calculations for detonation (CHEETAH) and chemical kinetics (CHEMKIN) for afterburn produced results in

reasonable agreement with experimental measurement (0.865 predicted vs 0.997 measured). We believe this shows that the approach of using observed stages of energy release during and following detonation of solid explosives as a guide to simulation is acceptable when full computational flow dynamics with detailed finite rate chemistry is not available. It is worth noting that performing the experiments in a blast chamber is advantageous as the transit of the shock wave back and forth within the chamber, following detonation, provides mixing approximating the homogeneous reactor used in the chemical kinetic calculations. Finally, the need to incorporate finite rate chemical kinetics for heterogeneous mixtures would be a welcome addition to any future effort.

c. Recommendations/Implications for Future Research

- The high levels of CO and respirable PM emitted from the M4 carbine warrant additional sampling and analysis on outdoor and indoor range environments.
- The sampling methods should be extended to assess emissions from the carbine breech due to its proximity to the user and greater inhalation likelihood
- The analytical methods employed were sufficiently sensitive to detect residual chemicals unrelated to the test formulations. Care should be taken to document cleaning formulas and prior testing formulations. Time series background analyses should be done prior to test formulation changes to determine potential residual carry over. Indoor results should be compared with outdoor range results to verify carry over and wall effects.
- Ground-deposited residuals should be sampled concurrently with emissions to assess potential range contamination issues.

- Compositional analyses of the formulations should be determined prior to testing to ensure that trace variations in components are properly accounted.
- Finite rate chemical kinetics should be incorporated with improved estimates of temperature and the inclusion of heat loss.
- Investigations of NASA-Lewis (NASA-Glenn) simulations with soot production during the interior ballistics (IB) cycle should be expanded.

14. Literature Cited

[AMCCOM, 1988] U.S. Army, Development of methodology and technology for identifying and quantifying emission products from open burning and open detonation thermal treatment methods, in: Proceedings of the Technical Steering Committee Symposium, 6–8 July 1988, Salt Lake City, UT. U.S. Army, AMMCOM, Rock Island, IL 61299-6000, 1988.

[AMCCOM, 1992] U.S. Army, Development of Methodology and Techniques for Identifying and Quantifying Products from Open Burning and Open Detonation Thermal Treatment Methods-Field Test Series A, B and C, vol. 1, Test Summary, U.S. Army, AMCCOM, Rock Island, IL 61299-6000, January 1992; U.S. Army, AMCCOM, Development of Methodology and Techniques for Identifying and Quantifying Products from Open Burning and Open Detonation Thermal Treatment Methods-Bang Box Test Series, Vol. 1, Test Summary Rock Island, IL 61299-6000, January 1992.

[AP-42, 2009] AP-42 Draft Chapter 16. Emission factors for demilitarization processes: open burning and open air detonation. 2009

[Appel, 2000] J. Appel, H. Bockhorn, M.Y. Frenklach, Hydrocarbons Combust. Flame 121 (2000) 122–136.

[Aurell, 2011] Aurell, J.; Gullett, B.K.; Pressley, C.; Tabor, D.; Gribble, R. Aerostat-lofted instrument and sampling method for determination of emissions from open area sources. Chemosphere. 85:806-811; 2011

[Burling, 2010] Burling, I.R.; Yokelson, R.J.; Griffith, D.W.T.; Johnson, T.J.; Veres, P.;Roberts, J.M.; Warneke, C.; Urbanski, S.P.; Reardon, J.; Weise, D.R.; Hao, W.M.; de Gouw, J. Laboratory measurements of trace gas emissions from biomass burning of fuel types from the southeastern and southwestern United States. Atmos Chem Phys. 10:11115-11130; 2010

[Center for Chemical Process Safety, 2006] Safe Design and Operation of Process Vents and Emission Control Systems: Appendix A; by Center for Chemical Process Safety; Copyright 2006; John Wiley & Sons, Inc.

[CFR AppJ, 2014] 40 CRF Part 50, Appendix J. Reference method for determination of particulate matter as PM10 in the Atmopshere. 1987. https://www.gpo.gov/fdsys/pkg/CFR-2014-title40-vol2/pdf/CFR-2014-title40-vol2-part50-appJ.pdf Accessed November 22, 2016

[CFR AppL, 2014] 40 CFR Part 50, Appendix L. Reference method for the determination of particulate matter as PM2.5 in the Atmosphere. 1987. https://www.gpo.gov/fdsys/pkg/CFR-2014-title40-vol2/pdf/CFR-2014-title40-vol2-part50-appL.pdf Accessed November 22, 2016

[Cooper, 1996] P.W. Cooper, Explosives Engineering (Wiley-VCH Inc., New York, 1996).

[Davini, 1996] P. Davini, P. Ghetti, L. Bonfanti, G. De Michele, “Investigation of the combustion of particles of coal”; Fuel; Volume 75, Issue 9, July 1996, Pages 1083-1088.

[Davis, 2006] W. C. Davis, T. R. Salyer, S. I. Jackson, and T. D. Aslam, "Explosive driven shock waves in argon," in Proceedings of the 13th International Detonation Symposium (The Office of Naval Research, U.S. Navy, 2006), pp. 1035–1044.

[Dreizin, 1999] E. L. Dreizin, D. G. Keil, W. Felder, and E. P. Vicenzi, "Phase changes in boron ignition and combustion," Combust. Flame 119, 272–290 (1999).

[Einfeld, 1990] Einfeld, W., D. J. Morrison, and B. V. Mokler, 1990. "An Experimental Study to Determine Gaseous and Particulate Products From Small-scale TNT Detonations and Propellant Burns," Report No. SAND90-0605, Sandia National Laboratories, Albuquerque, NM 87185.

[Einfeld, 1996] W. Einfeld, D. J. Morrison, S. E. Mullins, 1996; "Instrumentation Advances in Emissions Characterization from Propellant/ Explosive Combustion"; Report No. SAND96-0772C, Sandia National Laboratories, Albuquerque, NM 87185

[EPA, 1989] U.S. EPA Method 3A. Determination of oxygen and carbon dioxide concentrations in emissions from stationary sources (instrumental analyzer procedure). 1989. http://www.epa.gov/ttn/emc/promgate/m-03a.pdf Accessed May 5, 2014

[EPA, 2007] "The Plain English Guide to the Clean Air Act", United States Environmental Protection Agency, Office of Air Quality Standards and Planning, Research Triangle Park, NC; Publication No. EPA-456/K-07-001; April 2007

[EPA-25C, 2016] U.S. EPA Method 25C. Determination of nonmethane organic compounds (NMOC) in landfill gases. http://www.epa.gov/ttn/emc/promgate/m-25c.pdf Accessed May 11, 2016.

[EPA-GC/MS, 1999] U.S. EPA Compendium Method TO-15. Determination of volatile organic compounds (VOCs) in air collected in specially-prepared canisters and analyzed by gas chromatography/mass spectrometry (GC/MS). 1999. http://www.epa.gov/ttnamti1/files/ambient/airtox/to-15r.pdf Accessed November 10, 2015.

[EPA-HPLC, 2006] U.S. EPA Method 8330B. Nitroaromatics, nitramines, and nitrate esters by high performance liquid chromatograph (HPLC). 2006. https://www.epa.gov/sites/production/files/2015-07/documents/epa-8330b.pdf Accessed July 18, 2016.

[EPA-ICP, 1999] U.S. EPA Compendium Method IO-3.4. Determination of metals in ambient particulate matter using inductively coupled plasma (ICP) spectroscopy. 1999. http://www.epa.gov/ttn/amtic/files/ambient/inorganic/mthd-3-4.pdf Accessed May 5, 2014.

[EPA-nitrate, 1993] U.S. EPA Method 353.2. Determination of Nitrate-Nitrite Nitrogen by automated colorimetry. 1993. https://www.epa.gov/sites/production/files/2015-08/documents/method_353-2_1993.pdf Acessed July 18, 2016.

[EPA-TO-9A] U.S. EPA Compendium Method TO-9A. Determination of polychlorinated, polybrominated and brominated/chlorinated dibenzo-p-dioxins and dibenzofurans in ambient air. 1999. http://www.epa.gov/ttnamti1/files/ambient/airtox/to-9arr.pdf Accessed November 21, 2012.

[EPA-XRF, 1999] U.S. EPA Compendium Method IO-3.3. Determination of metals in ambient particulate matter using X-Ray Fluorescence (XRF) Spectroscopy. 1999. http://www.epa.gov/ttnamti1/files/ambient/inorganic/mthd-3-3.pdf Accessed May 5, 2014

[Frost, 2002] D. L. Frost, S. Goroshin, J. Levin, R. Ripley, and F. Zhang, "Critical conditions for ignition of metal particles in a condensed explosive," in Proceedings of 12th International Detonation Symposium, San Diego, CA (Office of Naval Research, Arlington, VA, 2002), pp. 693–701.

[Glassman, 1987] I. Glassman, Combustion, second ed., Academic Press,San Diego, 1987, pp. 360–375.

[Glumac, 2013] N. Glumac, "Early time spectroscopic measurements during high-explosive detonation breakout into air," Shock Waves; 23, 131–138 (2013).

[Gordan, 1994] Gordan, S.; McBride, B. J. "Computer Program for Calculation of Complex Chemical Equilibrium Compositions and Applications"; reference publication 1311; National Aeronautics and Space Administration: Nasa-Glenn, Cleveland, OH, October 1994.

[Kotlar, 1992] A.J. Kotlar, "The Thermodynamics of Interior Ballistics and Propellant Performance," Proceedings, 29th JANNAF Combustion Meeting, CPIA Publication 593, October 1992.

[Horst, 2006] Horst, A. W.; Nusca, M. J., "The Charge Designer's Workbench: A Range of Interior Ballistic Modeling Tools" ARL-TR-3796; U.S. Army Research Laboratory: Aberdeen Proving Ground, MD, May 2006.

[Johansson, 1970] C. H. Johansson, P. A. Persson (Eds.), Detonics of High Explosives, Academic Press Inc., New York 1970.

[Johnson, 1992] Johnson, M., Development of Methodology and Techniques for Identifying and Quantifying Products from Open Burning and Open Detonation Thermal Treatment Methods – Field Test Series A, B and C, Volume 1 (Test Summary), U.S. Army, Contract DAAD09-87-D-0008, 1992.

[Jones, 1965] R. N. Jones, H. P. Hitchcock and D. R. Villegas; "Engineering Design Handbook Ballistics Series - Interior Ballistics Of Guns", AMCP 706-150; Headquarters, U.S.Army Materiel Command, February 1965

[Kim, 2004] K. Kim, Thermobarics: Promises, Challenges and Recommendations, 7th Joint Classified Bombs/Warheads and Ballistics Symposium, Monterey, CA, August 9 – 12, 2004.

[Kinney, 1985] G. F. Kinney and K. J. Graham, Explosive Shocks in Air, 2nd ed. (Springer-Verlag, Berlin, 1985).

[Kirchner, 1993] Donald B. Kirchner, Joel C. Gaydos, And Mario C. Battigelli; Combustion Products Of Propellants And Ammunition in *Occupational Health: The Soldier and the Industrial Base* ; Office of the Surgeon General, U.S. Dept. of the Army ; Aberdeen Proving Grounds, Md. : U.S. Army Environmental Hygiene Agency ; Bethesda, Md. : Uniformed Services University of the Health Sciences ; Washington, DC : For sale by the Supt. of Docs., U.S. G.P.O., 1993.

[Kistiakowski, 1941] G.B. Kistiakowski, E.B. Wilson, "The prediction of detonation velocities of solid explosives" OSRD No. 69, Serial No. 6 (January 17, 1941).

[Kuhl, 1998] A. L. Kuhl, J. Forbes, J. Chandler, A. K. Oppenheim, R. Spektor, and R.E. Ferguson, "Confined combustion of TNT explosion products in air," in Proceedings of the 8th International Colloquium on Dust Explosions, Schaumberg, IL, 21–25 September 1998.

[Kuo, 2012] K.K. Kuo and R. Acharya; Ignition and Combustion of Single Energetic Solid Particles; Copyright © 2012 John Wiley & Sons, Inc.

[Larsen and Larsen, 1998] Larsen, J.C.; Larsen, P.B. Chemical carcinogens. In: Air pollution and health. Cambridge, UK: The Royal Society of Chemistry:33-56; 1998.

[LLNL, 2010] CHEETAH 6.0 Users Manual, LLNL-SM-416166, Copyright 2010, Lawrence Livermore National Security, All Rights Reserved.

[Lockheed, 1997] Lockheed Martin Energy Systems, Inc., Detonation Summary Report for the Nevada Test Sit, Volume I, Summary Report and Appendices A, B, C, & D, Radian International LLC, Oak Ridge, NT, August 1997.

[Mader, 2008] C. L. Mader, Numerical Modeling of Explosives and Propellants, 3rd ed.; (CRC Press, Boca Raton, FL, 2008).

[Mayer, 1965] "A Compilation of Air Pollutant Emission Factors for Combustion Processes, Gasoline Evaporation, and Selected Industrial Processes", by Martin Mayer; U.S. Department of Health Education and Welfare, Public Health Service, Division or Air Pollution, Cincinnati, Ohio, May 1965.

[McBride, 2016] McBride, B.J., and Gordon, S., "Computer Program for Calculation of Complex Chemical Equilibrium Compositions and Applications, II. User's Manual and Program Description," NASA RP 1311, 1996.

[McNesby, 2005] K. L. McNesby, B. E. Homan, and R. E. Lottero, "High brightness imaging for real time measurement of shock, particle, and combustion fronts produced by enhanced blast explosives," U.S. Army Research Laboratory (ARL), ARL-TR-3411, January 2005.

[McNesby, 2010] K. L. McNesby, B. E. Homan, J. J. Ritter, Z. Quine, R. Z. Ehlers, and B. A. McAndrew, "Afterburn ignition delay and shock augmentation in fuel rich solid explosives," Propellants, Explos., Pyrotech. 35(1), 57–65 (2010).

[McNesby, 2016] K.L. McNesby, B.E. Homan, R.A. Benjamin, V. M. Boyle, J.M. Densmore, and M.M. Biss; "Quantitative imaging of explosions with high-speed cameras"; Review of Scientific Instruments 87, 051301 (2016).

[Menon 2003] S. Menon, V. Sankaran, and C. Stone; "Subgrid Combustion Modeling for the Next Generation National Combustion Code"; NASA publication NASA/CR—2003-212202 (2003).
[Meyer, 2007] R. Meyer, J. Kohler, I.A. Homburg, "Explosives, 6th Edition", John Wiley & Sons, 2007 Wiley-VCH Verlag GmbH & Co.

[Mitchell, 1998] W.J. Mitchell, J.C. Suggs, Emission factors for the disposal of energetic materials by open burning and open detonation (OB/OD), EPA Report-EPA/600/R-98/103, 1998.

[Montgomery, 1999] C.J. Montgomery, M.A. Cremer, M.P. Heap,J.-Y. Chen, C.K. Westbrook, and L.Q. Maurice; "Reduced Chemical Kinetic Mechanisms For hydrocarbon Fuels"; LLNL Report UCRL-JC-136815; published in proceedings of 35th American Institute of Aeronautics and Astronautics/Association for the Study of Medical Education/American Society for Engineering Education Society of Automotive Engineers Joint Propulsion Conference and Exhibit, Los Angeles, CA, June 20-24, 1999.

[NAWCWD, 2008] Naval Air Warfare Center Weapons Division, Phase 1 Open Detonation Environmental Fate Factor Test Report, Vol. I, URS Corp., Oak Ridge, TN, March 2008.

[Nusca, 2011] Nusca, M.J., "Recent Upgrades to the ARL-NGEN3 Computational Interior Ballistics Model," ARL-TR-5613, U.S. Army Research Laboratory, Aberdeen Proving Ground, MD, August 2011.

[Nusca, 2016] Nusca, M., McNesby, K., Biss M.; "Muzzle Pressure Management," in Disruptive Energetics and Propulsion Technologies: FY15 Annual Report, Ciezak-Jenkins, J. ed., ARL-SR-0325, February 2016.

[NYT, 1948] "DONORA SMOG HELD NEAR CATASTROPHE; Expert Asserts Slightly Higher Concentration Would Have Depopulated Community", The New York Times, December 25, 1948.

[O'Brien, 2003] Robert **J.** O'Brien and Mark **D.** Wade; Air Emissions Inventory Guidance Document for Stationary Sources at Air Force Installations (Revised December 2003); IERA-RS-BR-SR-1999-0001

[Radke, 1988] Radke, L. F., D. A. Hegg, J. H. Lyons, C. A. Brock, and P. V. Hobbs, Airborne measurements on smokes from biomass burning, in Aerosols and Climate, edited by P. V. Hobbs and M. P. McCormick, pp. 411 –422, A. Deepak, Hampton, Va., 1988.

[Rankine, 1870] Rankine, W. J. M. (1870). "On the thermodynamic theory of waves of finite longitudinal disturbances". Philosophical Transactions of the Royal Society of London. 160: 277–288.

[Sandia, 2000] U.S. Army Defense Ammunition Center, Executive Summary of Phase II Demonstrations: The Low-Pressure Rocket Motor Burns in X-Tunnel, Sandia SAND2000-8202, January 2000.

[Schmidt, 2009] Schmidt, J.R., and Nusca, M.J., "Progress Toward a Multi-Dimensional Representation of the 5.56-mm Interior Ballistics," ARL-TR-4903, U.S. Army Research Laboratory, Aberdeen Proving Ground, MD, August 2009.

[Schmidt, 2012] J.R. Schmidt, A.J. Kotlar, and P.J. Conroy, "Interior Ballistics-Based Thermochemical Calculations to Predict Combustion Products of Phosphorus Containing Small-Caliber Ammo"; ARL-TR-6215, September 2012.

[Sinha, 2003] Sinha, P., Hobbs, P. V., Yokelson, R. J., Bertschi, I. T., Blake, D. R., Simpson, I. J., Gao, S., Kirchstetter, T. W., and Novakov,T.: "Emissions of trace gases and particles from savanna fires in southern Africa", J. Geophys. Res., 108, 8487, doi:10.1029/2002JD002325, 2003.

[Smith, 2004] Smith, G. P., Golden, D. M., Frenklach, M., Moriarty, N. W.,Eiteneer, B., Goldenberg, M., Bowman, T., Hanson, R. K., Song, S., Gardiner, Jr., W. C., Lissianski, V.V., and Qin, Z., http://www.me.berkeley.edu/gri_mech/

[Spadaccini, 1994] Spadaccini, L.J. and Colket, M.B., III, Prog. Energy Combust. Sci., 20, 431 (1994).

[Spicer, 2006] "A Field Program To Identify Tri Chemicals And Determine Emission Factors From Dod Munitions Activities (CP 1197)"; Chester W. Spicer, Michael W. Holdren, Anthony S. Wisbith,Kenneth A. Cowen, Bertram T. Jobson, Jan Satola, Raj Mangaraj, Michael Alexander, and Darrell W. Joseph, William R. Bolt and James C. Bach, Arthur J. Sedlacek, III, Randall J. Cramer, Jason Szabo; Final Report of Project CP 1197 to the Department of Defense Strategic Environmental Research and Development Program (SERDP), January, 2006

[Tomlin, 1997] A.S. Tomlin, T. Tur´anyi, and M.J. Pilling. Mathematical Tools for the Construction, Investigation and Reduction of Combustion Mechanisms. In Low Temperature Combustion and Autoignition, volume 35 of Comprehensive Chemical Kinetics, pages 293.437. Elsevier, 1997.

[Tucker, 1941] "Smoke Prevention in St. Louis" by Raymond R. Tucker; Ind. Eng. Chem., 1941, 33 (7), pp 836–839.

[Urbinato, 1994] David Urbinato, "London's Historic 'Pea-Soupers,'" EPA Journal, Summer 1994, www.epa.gov/history/topics/perspect/london.htm.

[Ward, 1993] Ward, D. E., and L. F. Radke, Emissions measurements from vegetation fires: A comparative evaluation of methods and results, in Fire in the

Environment: The Ecological, Atmospheric, and Climatic Importance of Vegetation Fires, edited by P. J. Crutzen and J. G. Goldammer, pp. 53–76, John Wiley, New York, 1993.

[Wilkinson, 2004] A. Wilkinson, SALW Ammunition Destruction-Environmental Releases from Open Burning and Open Detonation Events, United Nations Development Pro-gram, South Eastern Europe Clearinghouse for the Control of Small Arms and Light Weapons Guidance Document, May 2004.

[Windex, 2017] http://www.whatsinsidescjohnson.com/us/en/brands/windex/windex-Original-Glass-Cleaner]

[Wingfors, 2014] Wingfors, H.; Svensson, K.; Hagglund, L.; Hedenstierna, S.; Magnusson, R. Emission Factors for Gases and Particle-Bound Substances Produced by Firing Lead-Free Small-Caliber Ammunition. J Occup Environ Hyg. 11:282-291; 2014

[Yeh, 1996] C. L.Yeh and K. K.Kuo, “Ignition and combustion of boron particles,” Prog. Energy Combust. Sci. 22, 511–541 (1996).

Appendix A

Reduced chemical mechanism (CHEMKIN format) for combustion of the anaerobic deonation products of TNT at freeze out (1800K):

```
ELEMENTS
O  H  C  N
END
SPECIES
H2
H
O
O2
OH
H2O
HO2
H2O2
C
CH
CH2
CH2*
CH3
CH4
CO
CO2
HCO
CH2O
CH2OH
CH3O
CH3OH
C2H2
C2H3
C2H4
C2H5
C2H6
HCCO
CH2CO
C2H3O
N2
CH3O2
CH3OCH3
CH3OCH2
N
NO
A4
!C(B)
END
```

```
REACTIONS                                   A            b         Ea
 H+O2 = O+OH                                8.300E+13    0.000  14413.00
 O+H2 = H+OH                                5.000E+04    2.670   6290.00
 OH+H2 = H+H2O                              2.160E+08    1.510   3430.00
 OH+OH = O+H2O                              3.570E+04    2.400  -2110.00
 H+H+M = H2+M                               1.000E+18   -1.000      0.00
   H2/0.0/ H2O/0.0/ CH4/2.0/ CO2/0.0/ C2H6/3.00/
 H+H+H2O = H2+H2O                           6.000E+19   -1.250      0.00
 H+OH+M = H2O+M                             2.200E+22   -2.000      0.00
   H2/0.73/ H2O/3.65/ CH4/2.0/ C2H6/3.0/
 H+O2+M = HO2+M                             2.800E+18   -0.860      0.00
   O2/0.0/ H2O/0.0/ CO/0.75/ CO2/1.5/ C2H6/1.5/ N2/0.0/
 H+O2+H2O = HO2+H2O                         9.380E+18   -0.760      0.00
 H+O2+N2 = HO2+N2                           3.750E+20   -1.720      0.00
 OH+OH(+M) = H2O2(+M)                       7.400E+13   -0.370      0.00
      LOW  /  2.300E+18   -0.900  -1700.00/
      TROE/  0.7346   94.00  1756.00  5182.00 /
   H2/2.0/ H2O/6.0/ CH4/2.0/ CO/1.5/ CO2/2.0/ C2H6/3.0/
 HO2+H = O+H2O                              3.970E+12    0.000    671.00
 HO2+H = O2+H2                              2.800E+13    0.000   1068.00
 HO2+H = OH+OH                              1.340E+14    0.000    635.00
 HO2+O = OH+O2                              2.000E+13    0.000      0.00
 HO2+OH = O2+H2O                            2.900E+13    0.000   -500.00
 HO2+HO2 = O2+H2O2                          1.300E+11    0.000  -1630.00
  DUPLICATE
 HO2+HO2 = O2+H2O2                          4.200E+14    0.000  12000.00
  DUPLICATE
 H2O2+OH = HO2+H2O                          5.800E+14    0.000   9560.00
 CO+O+M = CO2+M                             6.020E+14    0.000   3000.00
  H2/2.0/ O2/6.0/ H2O/6.0/ CH4/2.0/ CO/1.5/ CO2/3.5/ C2H6/3.0/
 CO+OH = CO2+H                              4.760E+07    1.228     70.00
 CO+O2 = CO2+O                              2.500E+12    0.000  47800.00
 CO+HO2 = CO2+OH                            1.500E+14    0.000  23600.00
 C+O2 = CO+O                                5.800E+13    0.000    576.00
 CH+H = C+H2                                1.100E+14    0.000      0.00
 CH+H2 = CH2+H                              1.107E+08    1.790   1670.00
 CH+O2 = HCO+O                              3.300E+13    0.000      0.00
 HCO+H = CO+H2                              7.340E+13    0.000      0.00
 HCO+OH = CO+H2O                            5.000E+13    0.000      0.00
 HCO+M = CO+H+M                             1.870E+17   -1.000  17000.00
    H2/2.0/ H2O/12.0/ CH4/2.0/ CO/1.5/ CO2/2.0/ C2H6/3.0/
 HCO+O2 = CO+HO2                            7.600E+12    0.000    400.00
 CH2+O = HCO+H                              8.000E+13    0.000      0.00
 CH2+OH = CH2O+H                            2.000E+13    0.000      0.00
 CH2+O2 = CO2+H+H                           1.320E+13    0.000   1500.00
 CH2*+N2 = CH2+N2                         1.500E+13    0.000    600.00
 CH2*+O2 = H+OH+CO                        2.800E+13    0.000      0.00
 CH2*+O2 = CO+H2O                         1.200E+13    0.000      0.00
 CH2*+CO = CH2+CO                         9.000E+12    0.000      0.00
 CH2*+CO2 = CH2O+CO                       1.400E+13    0.000      0.00
 CH2O+H(+M) = CH3O(+M)                      5.400E+11    0.454   2600.00
      LOW  /  2.200E+30   -4.800   5560.00/
```

```
     TROE/  0.7580   94.00  1555.00  4200.00 /
   H2/2.0/ H2O/6.0/ CH4/2.0/ CO/1.5/ CO2/2.0/ C2H6/3.0/
CH2O+H = HCO+H2                          2.300E+10    1.050   3275.00
CH2O+O = HCO+OH                          3.900E+13    0.000   3540.00
CH2O+OH = HCO+H2O                        3.430E+09    1.180   -447.00
CH3+H(+M) = CH4(+M)                      1.270E+16   -0.630    383.00
     LOW  /  2.477E+33   -4.760   2440.00/
     TROE/  0.7830   74.00  2941.00  6964.00 /
   H2/2.0/ H2O/6.0/ CH4/2.0/ CO/1.5/ CO2/2.0/ C2H6/3.0/
CH3+O = CH2O+H                           8.430E+13    0.000      0.00
CH3+OH(+M) = CH3OH(+M)                   6.300E+13    0.000      0.00
     LOW  /  2.700E+38   -6.300   3100.00/
     TROE/  0.2105   83.50  5398.00  8370.00 /
   H2/2.0/ H2O/6.0/ CH4/2.0/ CO/1.5/ CO2/2.0/ C2H6/3.0/
CH3+OH = CH2+H2O                         5.600E+07    1.600   5420.00
CH3+OH = CH2*+H2O                        2.501E+13    0.000      0.00
CH3+O2 = O+CH3O                          2.675E+13    0.000  28800.00
CH3+O2 = OH+CH2O                         3.600E+10    0.000   8940.00
CH3+HO2 = CH4+O2                         1.000E+12    0.000      0.00
CH3+HO2 = CH3O+OH                        2.000E+13    0.000      0.00
CH3+HCO = CH4+CO                         2.648E+13    0.000      0.00
CH3+CH2O = CH4+HCO                       3.320E+03    2.810   5860.00
CH3+CH2 = C2H4+H                         4.000E+13    0.000      0.00
CH3+CH3(+M) = C2H6(+M)                   2.120E+16   -0.970    620.00
     LOW  /  1.770E+50   -9.670   6220.00/
     TROE/  0.5325  151.00  1038.00  4970.00 /
H2/2.0/ H2O/6.0/ CH4/2.0/ CO/1.5/ CO2/2.0/ C2H6/3.0/
CH3+CH3 = H+C2H5                         4.990E+12    0.100  10600.00
CH2OH+O2 = CH2O+HO2                      1.800E+13    0.000    900.00
CH4+H = CH3+H2                           6.600E+08    1.620  10840.00
CH4+O = CH3+OH                           1.020E+09    1.500   8600.00
CH4+OH = CH3+H2O                         1.000E+08    1.600   3120.00
CH3OH+H = CH2OH+H2                       1.700E+07    2.100   4870.00
CH3OH+CH3 = CH3O+CH4                     1.000E+07    1.500   9940.00
HCCO+O = H+CO+CO                         1.000E+14    0.000      0.00
C2H2+H(+M) = C2H3(+M)                    5.600E+12    0.000   2400.00
     LOW  /  3.800E+40   -7.270   7220.00/
     TROE/  0.7507   98.50  1302.00  4167.00 /
   H2/2.0/ H2O/6.0/ CH4/2.0/ CO/1.5/ CO2/2.0/ C2H6/3.0/
C2H2+O = HCCO+H                          1.020E+07    2.000   1900.00
C2H2+O = CH2+CO                          1.020E+07    2.000   1900.00
CH2CO+H = HCCO+H2                        5.000E+13    0.000   8000.00
CH2CO+H = CH3+CO                         1.130E+13    0.000   3428.00
CH2CO+OH = HCCO+H2O                      7.500E+12    0.000   2000.00
C2H3+H = C2H2+H2                         3.000E+13    0.000      0.00
C2H3+O2 = C2H3O+O                        1.24E+13   -0.120   1696.0
C2H4+H(+M) = C2H5(+M)                    1.080E+12    0.454   1820.00
     LOW  /  1.200E+42   -7.620   6970.00/
     TROE/  0.9753  210.00   984.00  4374.00 /
   H2/2.0/ H2O/6.0/ CH4/2.0/ CO/1.5/ CO2/2.0/ C2H6/3.0/
C2H4+H = C2H3+H2                         1.325E+06    2.530  12240.00
C2H4+O = CH3+HCO                         1.920E+07    1.830    220.00
```

```
 C2H4+OH = C2H3+H2O                      3.600E+06    2.000   2500.00
 C2H5+O = CH3+CH2O                       1.320E+14    0.000      0.00
 C2H5+O2 = C2H4+HO2                      8.400E+11    0.000   3875.00
 C2H6+H = C2H5+H2                        1.150E+08    1.900   7530.00
 C2H6+O = C2H5+OH                        8.980E+07    1.920   5690.00
 C2H6+OH = C2H5+H2O                      3.540E+06    2.120    870.00
 CH2CO + H = C2H3O               5.40E+11    0.454 1820.0
CH3OCH3       =       CH3+CH3O              1.380E+52 -10.85  9.664E+04
                                            rev /  3.000E+13    .00
0.000E+00 /
CH3OCH3+OH      =      CH3OCH2+H2O            1.402E+08   1.61 -3.500E+01
                                            rev /  1.544E+08   1.31
2.303E+04 /
CH3O2+m         =        CH3+O2+m             3.450E+17   -.12  2.707E+04
                                            rev /  1.410E+16    .00 -
1.100E+03 /
CH3O2+CH3         =       CH3O+CH3O             1.900E+12    .00 -
1.200E+03
                                            rev /  2.000E+10    .00
0.000E+00 /
N+NO<=>N2+O                             2.700E+13     .000     355.00
N+CO2<=>NO+CO                           3.000E+12     .000   11300.00

END
```

Appendix B

CHEETAH 6.0 output for a standard gun run using the double base propellant in M855 ammunition. Additives not in the CHEETAH database have been replaced by urea:

THE COMPOSITION

Name	% weight	% mol	% volume	Formula
nitrocellulose-13	82.700	70.358	81.432	$C_6H_{7.37}N_{2.64}O_{10.29}$
nitroglycerin	13.400	14.112	13.750	$C_3H_5N_3O_9$
urea	3.900	15.531	4.818	CH_4N_2O

Gas phase species	moles / kg of propellant
CO	1.443e+001
H_2O	1.040e+001
CO_2	5.562e+000
N_2	5.403e+000
H_2	3.096e+000
OH	1.0930e-001
H	7.802e-002
NO	1.862e-002
NH_3	6.47e-003

CHO	5.825e-003
HCOOH	4.878e-003
HCN	3.054e-003
CH_2O	2.250e-003
O_2	1.935e-003
HNCO	1.758e-003
O	1.661e-003
NH_2	5.690e-004
HNO	1.513e-004
H_2O_2	1.018e-004